UNIVERSITY OF OKLAHOMA

GRADUATE COLLEGE

COULOMB STRESS ANALYSIS OF THE SITES HOSTING THE THREE LARGEST RECORDED EARTHQUAKES IN OKLAHOMA HISTORY: PAWNEE, OK AND PRAGUE, OK

A THESIS

SUBMITTED TO THE GRADUATE FACULTY

in partial fulfillment of the requirements for the

Degree of

MASTER OF SCIENCE

By

Emily Taylor Hencey

Norman, Oklahoma

2025

Downloaded from SHAREOK. Persistent Handle URL: https://hdl.handle.net/11244/341131

COULOMB STRESS ANALYSIS OF THE SITES HOSTING THE THREE LARGEST RECORDED EARTHQUAKES IN OKLAHOMA HISTORY: PAWNEE, OK AND PRAGUE, OK

A THESIS APPROVED FOR THE

SCHOOL OF GEOSCIENCES

BY THE COMMITTEE CONSISTING OF

Dr. Brett M. Carpenter, Chair

Dr. Jacob I. Walter

Dr. Hao Hu

© Copyright by Emily Taylor Hencey 2025
All Rights Reserved.

ACKNOWLEDGEMENTS

I would like to express my heartfelt gratitude to Dr. Brett M. Carpenter and my committee members for their unwavering support and belief in me throughout my journey at OU. I truly could not have accomplished this without each of you, and I appreciate your endless guidance during my research. Specifically, thank you to Dr. Jake Walter for getting me all the needed data catalogs from OGS and providing me with feedback and guidance throughout the seismicity and Coulomb processes in this study.

Thank you to Dr. Todd Fagin at the University of Oklahoma for assisting me in the startup process for my ArcGIS Pro maps for Pawnee, OK. Your guidance in the setup process for making data points and lines, finding coordinates, layouts, etc. was vital to the success of this project.

Natalie Kongable has been the best office mate, co-TA, roommate, and friend I could have ever asked for during my time at OU. From the very beginning, she has been a constant source of support, encouragement, and laughter. Whether it was driving me to the office when my car wouldn't start or staying up late with me to help brainstorm ideas for my research, Natalie was always there, offering her time and expertise without hesitation. Her kindness, patience, and willingness to help at every turn played a pivotal role in my success throughout this journey.

To my beloved pets: my frogs, Peat and Moss, who have been with me from the very beginning, accompanying me from undergrad in Texas to graduate school in Oklahoma. They were truly part of the supportive community that helped me along the way. Countless hours were spent with them by my side. And, of course, my sweet dogs, Noble and Roxy, who sat beside me, eagerly begging for pets as I worked, making the process a little easier and a lot more joyful.

To my grandpa Dave, I know you would have loved to read my thesis and discuss my research with me. You instilled in me a love for rocks and a fascination with how the Earth works, and I hope the work I accomplished at OU would make you proud. I wouldn't be the scientist I am today without the passion for geology that you nurtured in me from a young age. You have been in my thoughts throughout my science career, and I look forward to discussing it all one day when we meet again. In your honor, I have dedicated the NE trending fault zone I have mapped to you as a token of my appreciation for everything you taught me.

Thank you to my parents for their endless encouragement throughout my journey as a scientist. From the moment I expressed my desire to pursue a B.S. in Geophysics, they have supported me wholeheartedly, and that support never wavered as I worked to obtain my master's. They have been so supportive during my time in graduate school. While I can never fully express my gratitude for everything they have done for me, I hope dedicating my thesis to them conveys a small fraction of my appreciation. I love you both!

Lastly, thank you to my amazing fiancé, Brice, for his unwavering support throughout this entire journey. Words can hardly express how grateful I am for everything he has done for me. From the late nights of writing and data analysis to the moments of self-doubt, Brice has been a constant source of encouragement and positivity. His belief in me and my work has been a steady anchor throughout my graduate school experience. I am beyond grateful for his unwavering presence and love, and I cannot wait to see where the next chapter of my science journey takes us—together. I know that whatever comes next, his support will continue to inspire and motivate me every day.

To mom and dad: thanks for always supporting my dream of becoming a scientist.

To my fiancé Brice: thank you for always being my rock and my best friend.

Table of Contents

ACKNOWLEDGEMENTS iv

LIST OF FIGURES ix

LIST OF TABLES xvii

LIST OF EQUATIONS xviii

ABSTRACT xix

INTRODUCTION 1

1.1: Seismicity 1

1.2: Inducing and Triggering Earthquake Activity 6

1.3: Coulomb Stress Changes 7

1.4: Pawnee Triple Junction 10

1.5: Prague, OK 12

GEOLOGICAL BACKGROUND AND HISTORY OF RECENT SEISMICITY 14

2.1: Geological Background 14

2.2: Seismic History in Oklahoma 15

2.3: Seismic History of the PTJ 17

2.4: Seismic History of Prague 24

METHODOLOGY 28

3.1 Data Collection 28

3.2 Fault Mapping 38

3.3 Field Work 44

3.4 Fault Slip Potential 45

3.5 Stress Change Mapping 47

RESULTS 52

4.1: Pawnee Triple Junction 52

4.1.1: Fault Mapping 52

4.1.2: Fault Slip Potential 2.0 54

4.1.3: Coulomb Modeling Results 59

4.2 Prague, OK 74

4.2.1: Dip Calculations 74

4.2.2: Fault Slip Potential 2.0 74

4.2.3: Coulomb Modeling Results 79

DISCUSSION 87

5.1 Pawnee County Triple Junction 87
5.2: Prague, OK 95
5.3: Coulomb Stress Change 104
5.4: Inducing and Triggering Earthquake Activity 105
CONCLUSIONS, MODEL LIMITATIONS, AND FUTURE WORK 107
6.1 Pawnee Triple Junction 107
6.2 Prague, OK 109
6.3: Future Work 110
REFERENCES 112

LIST OF FIGURES

Figure 1: Map of Oklahoma with starred locations for the Pawnee and Prague, OK earthquake sites (modified from Johnson, 2008).....10

Figure 2: ArcGIS Pro map of the PTJ showing the locations of the SWF, SLF, WF, and NEFZ. SWF and WF were identified using the Oklahoma Geological Survey fault map, while the SLF and NEFZ were mapped by Emily Hencey based on Park et al. 2022 seismicity data in ArcGIS Pro. Purple star is the hypocenter of the 2016 M_w 5.8 rupture along the SLF. 11

Figure 3: Fault map of Prague, OK with the hypocenters of the 2011 and 2024 ruptures shown in the light and dark purple stars. The top star is the 2024 event and the bottom star is the 2011 event. Faults are from the Oklahoma Geological Survey. 13

Figure 4: Cross-sectional view of the area just west of the SLF showing the basement rock composition (Johnson, 2008). This cross section is a good representation for all three sites since they are all located in similar areas of Oklahoma and all have the same geological rock composition within them. 15

Figure 5: Seismicity data in Oklahoma from the early late 1800s/early 1900s to 2014. The black stars represent events M_w 4.0 and greater (Hough and Page, 2015). 16

Figure 6: USGS focal mechanism beachball of the 2016 M_w 5.8 rupture on the Sooner Lake Fault with seismicity maps of a) seismicity prior to the mainshock (August 11, 2013, to September 1, 2016) and b) seismicity after the mainshock (September 3, 2016, to May 15, 2023). Purple star = hypocenter of the M_w 5.8 earthquake along the Sooner Lake Fault in 2016.....19

Figure 7: Locations of the two hypothesized foreshocks on top of the seismicity data leading up to the main rupture in 2016. that caused the 2016 M_w 5.8 rupture along the SLF. Dark purple star = Chen 2017 hypothesis, white star = Walter 2017 hypothesis. Seismicity dates range from August 11, 2013, to September 1, 2016. 21

Figure 8: ArcGIS Pro map of the PTJ showing the locations of the SWF, SLF, WF, and NEFZ. SWF and WF were identified using the Oklahoma Geological Survey fault map, while the SLF and NEFZ were

mapped by Emily Hencey based on Park et al. 2022 seismicity data in ArcGIS Pro. Top photo shows the OGS fault map with the dashed line being the OOF (Chen et al., 2017) (extension of the Labette fault). Bottom photo shows Hencey fault map with the NEFZ. 22

Figure 9: ArcGIS Pro map of the Prague, OK site showing the locations of the 2011 Prague, OK Mainshock along the Meeker-Prague Fault on November 6, 2011, and the 2024 Prague, OK mainshock along the Wilzetta Fault System on February 3, 2024. Overlain this map is the focal mechanism beach balls for each main shock with the year labelled below each one..... 25

Figure 10: Map of locations for the aftershocks from the 2011 and 2024 Prague, OK earthquakes. Dark purple = 2011 aftershock data, light purple = 2024 aftershock data. Seismicity dates range from November 6, 2011, to April 20, 2013, and February 3, 2024, to February 24, 2025. 27

Figure 11: ArcGIS Pro map of the PTJ showing locations of the SWF, SLF, WF, and NEFZ. SWF and WF were identified from the Oklahoma Geological Survey fault map, while the SLF and NEFZ were mapped by Emily Hencey using the Park et al. (2022) seismicity data (white dots) in ArcGIS Pro. Seismicity Dates range from January 1, 2013, to December 31, 2019. 29

Figure 12: ArcGIS Pro map of the PTJ showing locations of the SWF, SLF, WF, and NEFZ. SWF and WF were identified from the Oklahoma Geological Survey fault map, while the SLF and NEFZ were mapped by Emily Hencey using the OGS seismicity data (purple dots) in ArcGIS Pro. Seismicity dates range from November 8, 2013, to May 15, 2023. 30

Figure 13: Seismicity data over the OGS fault map in Prague, OK. Purple stars represent the two major ruptures in this location including the 2011 M_w 5.7 event (light purple star) and 2024 M_w 5.1 event (dark purple star). Seismicity dates range from June 29, 2010, to February 24, 2025. 31

Figure 14: Aftershock location seismicity data from OGS across the Prague, OK fault site from November 6, 2011, to April 20, 2013. 34

Figure 15: Excel plot showing where the aftershocks from the 2011 Prague earthquake break off. The x axis shows the days since the 2011 mainshock while the y axis shows the amount of cumulative

earthquakes. day 0 indicates that those events occurred on the day of the mainshock rupture on November 6, 2011.The increase after 4,000 days is the 2024 earthquake and its aftershocks. 35

Figure 16: Aftershock location seismicity data from OGS across the Prague, OK fault site from February 3, 2024, to February 24, 2025 36

Figure 17: Excel plot showing that the aftershocks from the Prague 2024 event do not reach a breakoff point since our dataset only has a small number of aftershocks and time after this event occurred. The x axis shows the days since the 2024 mainshock while the y axis shows the amount of cumulative earthquakes. day 0 indicates that those events occurred on the day of the mainshock rupture on February 3, 2024. 37

Figure 18: Fault segment locations for the Pawnee Triple Junction correspond to the values seen in Table 1. Purple star represents the hypocenter of September 3, 2016, M_w 5.8 rupture along the SLF in Pawnee, OK. 39

Figure 19: Zoom in view of the seismicity clustering in white from Park et al., 2022 data and purple from OGS data. Both data catalogs were plotted on top of NEFZ 2 and 3 to show how this aligning was conducted based on seismic clustering. 40

Figure 20: Fault segment locations for the Prague, OK site. Showcasing the segments of the Wilzetta Fault System (WFS) and Meeker-Prague Fault (MPF) as well as locations for the segments of the other three faults in the site (F3, F4, and F5) 43

Figure 21: Deploying nodes to collect aftershocks of the 2024 M_w 5.1 earthquake in Prague, OK with OGS. a) Buried node b) Node used to collect aftershock data. 45

Figure 22: Depths of surrounding seismicity from the M_w 5.8 SLF earthquake in 2016. The deepest recorded depth was 13.36 km. Data from the USGS Pawnee County earthquake database. 49

Figure 23: Young's Modulus and Poisson's Ratio values from a series of lab testing and borehole testing. WZZ log data was utilized from these graphs since this well is relatively close to the three locations studied in this thesis (Kibikas, 2021) 50

Figure 24: Comparison of previous mapping results for the Sooner Lake Fault and the mapping done for this fault in this thesis. a) the 2017 mapping of this fault (Pennington, 2017; Chen et al., 2017), b) the 2025 mapping of this fault with higher resolution data from years of aftershock data. These two photos show the extension of the SLF to the east as done in this thesis. 53

Figure 25: Mohr Circle for the Pawnee County Triple Junction Faults. Created in Fault Slip Potential 2.0 (FSP2.0). Indicating some faults are extremely close to failure in the current stress state of Oklahoma while others are not close at all. Two of these close to failure faults are the two segments of the SLF and are indicated with labels and arrows. The NEFZ6 is also labeled for reference. 57

Figure 26: Mohr Circle for the Pawnee County Triple Junction Faults SLF1 and SLF2. a) SLF1 segment results showing this fault is on the Mohr-Coulomb failure envelope and is sitting at critical in the current stress state of Oklahoma b) SLF2 segment results showing this fault is just under the Mohr-Coulomb failure envelope and is close to critical in the current stress state of Oklahoma. Created in Fault Slip Potential 2.0 (FSP2.0). 58

Figure 27: Model set up parameters for the Coulomb Modeling Software 3.4 Coulomb stress mapping in the recreation of the M_w 5.8 earthquake. a) Pawnee Triple Junction with the added slip in the model along the Sooner Lake Fault. The section highlighted in light purple represents an added slip of -1.25m (negative for left lateral slip in Coulomb modeling software 3.4). This value was programed into experiment 1 within Coulomb modeling software 3.4. b) The published slip model used for the September 3, 2016, M_w 5.8 rupture event along the Sooner Lake Fault. The earthquake hypocenter is represented by the purple star (Moschetti et al. 2019). c) Slip diagram at depth showing how slip was distributed into the subsurface across the length of the purple highlighted section of the Pawnee Triple Junction in part a of this figure. 61

Figure 28: Reconstruction of the September 3, 2016, M_w 5.8 earthquake along the Sooner Lake Fault in the Pawnee County Triple Junction. Image shows a Coulomb stress change in map view with the purple star representing the hypocenter for the main rupture event. 62

Figure 29: Seismicity migration over time across the SLF and surrounding faults from the M_w 5.8 rupture to June 5, 2023. This shows how aftershocks propagated from the 2016 M_w 5.8 earthquake along the SLF to the other faults surrounding it. Lighter colors indicate earthquakes occurring first and darker ones indicate the more recent earthquakes. 64

Figure 30: Pawnee Triple Junction with slip added to the NEFZ segment 6. The section highlighted in light purple represents an added slip of 0.007-0.50 meters. This value was programed within Coulomb modeling software 3.4 to get the results for the Chen et al. (2017) hypothesis. Overlain is the slip diagram at depth shows how slip was distributed into the subsurface across the length of the purple highlighted section of the NEFZ. 66

Figure 31: Coulomb stress change plots in MPa showing how differences in slip magnitude along the NEFZ6 fault segment impacted coulomb stress changes along the hypocenter of the 2016 SLF earthquake. a) 0.007 meters of slip along NEFZ6, b) 0.015 meters of slip along NEFZ6, c) 0.031 meters of slip along the NEFZ6, d) 0.063 meters of slip along NEFZ6, e) 0.125 meters of slip along NEFZ6, f) 0.25 meters of slip along NEFZ6, g) 0.5 meters of slip along NEFZ6. 67

Figure 32: Pawnee Triple Junction with slip added to the Sooner Lake Fault segment 1 (SLF1). The section highlighted in light purple represents an added slip of 0.007-0.50 meters. This value was programmed within Coulomb modeling software 3.4 to get the results for the Walter (2017) hypothesis. Overlain is the slip diagram at depth shows how slip was distributed into the subsurface across the length of the purple highlighted section of the SLF. 70

Figure 33: Coulomb stress change plots in MPa showing how differences in slip magnitude along the SLF impacted coulomb stress changes along the hypocenter of the 2016 SLF earthquake. a) -0.007 meters of slip along SLF1 b) -0.015 meters of slip along SLF1, c) -0.031 meters of slip along SLF1, c) -0.063 meters of slip along SLF1, d) -0.125 meters of along SLF1, e) -0.25 meters of slip along SLF1, f) -0.5 meters of slip along SLF1. 71

Figure 34: a) 0.031 meters of slip along the SLF1 and NEFZ6, b) 0.25 meters of slip along the SLF1 and NEFZ6, c) 0.50 meters of slip along the SLF1 and NEFZ6. 73

Figure 35: Mohr Circle for Prague, OK faults. Created in Fault Slip Potential 2.0 (FSP2.0). Indicating some faults are extremely close to failure in the current stress state of Oklahoma, while others are not close at all. MPF4 is the fault segment for the 2011 Prague earthquake, and WFS2 is the fault segment for the 2024 Prague earthquake. 77

Figure 36: Mohr Circle for the Prague, OK faults 1.3 and 2.5. a) 1.3 segment results showing this fault is just under the Mohr-Coulomb failure envelope and is sitting just below critical in the current stress state of Oklahoma b) 2.5 segment results showing this fault is just under the Mohr-Coulomb failure envelope and is sitting just below critical (slightly closer to critical than 1.3) in the current stress state of Oklahoma. Created in Fault Slip Potential 2.0 (FSP2.0). 78

Figure 37: a) Prague, OK faults with light purple highlighted portion representing an added slip of 0.6m on the Meeker-Prague Fault. This value was programmed within Coulomb modeling software 3.4 to get the results for the reconstruction of the Prague 2011 mainshock, measuring M_w. 5.7. b) The slip model for the November 6, 2011, M_w 5.7 rupture event in Prague, OK. The purple star represents the earthquake hypocenter (McMahon et. al. 2017). c) Slip diagram at depth showing how slip was distributed into the subsurface across the length of the purple highlighted section of the Meeker-Prague Fault. 80

Figure 38: Reconstruction of the November 6, 2011, M_w 5.7 earthquake in Prague, OK. Image shows a Coulomb stress change in map view with the star representing the hypocenter for the main rupture event. 81

Figure 39: Prague, OK faults with light purple highlighted portion representing an added slip of 0.54m on the Wilzetta Fault System. This value was programed within Coulomb modeling software 3.4 to get the results for the reconstruction of the Prague 2024 mainshock measuring M_w 5.1. Overlain is the slip diagram at depth showing how slip was distributed into the subsurface across the length of the purple highlighted section of the Wilzetta Fault System. 84

Figure 40: Coulomb stress change plot from the reconstruction of the M_w 5.1 earthquake in Prague, OK on February 3, 2024. Purple star represents the hypocenter for the main rupture event. 85

Figure 41: Comparison of the Coulomb stress change plot from the 2016 M_w 5.8 reconstruction in Coulomb Modeling Software 3.4 with the aftershock data from OGS. Seismicity dates range from September 3, 2016, to May 15, 2023. 88

Figure 42: Seismicity with time showing how aftershocks propagated from the 2016 M_w 5.8 earthquake along the NEFZ. Lighter colors indicate earthquakes occurring first and darker ones indicate the more recent earthquakes. Dates of seismicity here range from September 3, 2016, to May 15, 2023. Inset is the Coulomb stress analysis results from Coulomb Modeling Software 3.4 to show how the Coulomb stress changes align with the aftershock migration patterns. 89

Figure 43: Seismicity with time showing how aftershocks propagated from the 2016 M_w 5.8 earthquake along the SLF. Lighter colors indicate earthquakes occurring first and darker ones indicate the more recent earthquakes. These are labeled as 1 (being the M_w 5.8 event itself) and 1,337 being the most recent earthquake in this catalog. The purple arrows indicate the tapering of seismicity migration. Light purple represents the earliest seismicity, medium purple represents the middle of the data set, and dark purple represents the latest seismicity recorded. Dates of seismicity here range from September 3, 2016, to May 15, 2023. Inset is the Coulomb stress analysis results from Coulomb Modeling Software 3.4 to show how the Coulomb stress changes align with the aftershock migration patterns. 91

Figure 44: Seismicity with time prior to the M_w 5.8 earthquake along the SLF in 2016. This shows what seismicity prior to the main rupture looked like. Additionally, indicates which areas had the most seismicity close to the main rupture. Top photo: foreshocks of the SLF M_w 5.8 rupture on September 3, 2016, dates range from November 8, 2013, to September 1, 2016. Bottom photo: aftershocks of the SLF M_w 5.8 rupture on September 3, 2016, dates range from September 3, 2016, to May 15, 2023. 93

Figure 45: Comparison of the Coulomb stress change plot from the 2011 M_w 5.7 reconstruction in Coulomb Modeling Software 3.4 with the aftershock data from OGS. Seismicity dates range from November 6, 2011, to April 20, 2013.....97

Figure 46: Seismicity by time after the M_w 5.7 earthquake along the MPF in 2011. This shows what seismicity after the main rupture looked like. Additionally, indicates which areas had the most seismicity close to the main rupture. Seismicity dates range from November 6, 2011, to April 20, 2013. 99

Figure 47: Comparison of the Coulomb stress change plot from the 2024 M_w 5.1 reconstruction in Coulomb Modeling Software 3.4 with aftershock data from OGS. Seismicity dates range from February 3, 2024, to February 24, 2025. 102

Figure 48: Seismicity with time after the M_w 5.1 earthquake along the WF in 2024. This shows what seismicity prior to the main rupture looked like. Additionally, indicates which areas had the most seismicity close to the main rupture. Seismicity dates range from February 3, 2024, to February 24, 2025 103

LIST OF TABLES

Table 1: Data catalog specifics for date range, magnitudes, number of events, relocation process, and depth range for each of the 5 data catalogs used in this thesis. 32

Table 2: Table includes the values of average dip calculations for each fault/fault segment in the Pawnee Triple Junction. Additional information in this table includes the latitude start and end, longitude start and end, strike, total fault length, easting start, and northing start values for each fault segment in the SLF area. 42

Table 3: Table includes the values of average dip calculations for each fault/fault segment in the Prague, OK site. Additional information in this table includes the latitude start and end, longitude start and end, strike, total fault length, easting start, and northing start values for each fault segment in Prague, OK. 44

Table 4: Inputs needed for stress modeling in Coulomb Modeling Software 3.4. 47

Table 5: Delta PP to slip values for each fault segment near the SLF showing how much coulomb stress increase in needed (in MPa) to cause each fault segment to rupture. 56

Table 6: Table includes the values of slip amount added to NEFZ6 and SLF1 and the coulomb stress change for the exact location of the hypocenter for the 2016 M_w 5.8 earthquake along the SLF at 96.929W, 36.425N, and 5.6km depth (hypocenter location from USGS) 68

Table 7: Table includes the values of slip amount added to NEFZ6 and SLF1 (at the same time) and the Coulomb stress change for the exact location of the hypocenter for the 2016 M_w 5.8 earthquake along the SLF at 96.929W, 36.425N, and 5.6km depth (hypocenter location from USGS). 74

Table 8: Delta PP to slip values for each fault segment in the Prague, OK site showing how much coulomb stress increase is needed (in MPa) to cause each fault segment to rupture. 76

Table 9: Coulomb stress changes at a point from the 2011 Prague event at the 2024 Prague event hypocenter. 82

Table 10: Coulomb stress change value for Experiment 1 from Prague, OK showing the Coulomb stress change calculated at the hypocenter of the 2024 mainshock because of the 2011 mainshock. 83

LIST OF EQUATIONS

Equation 1: Coulomb stress change equation (King et al. 1994; Stein, 1999). 8

Equation 2: Equation used for calculating the average dip value across each fault segment in the SLF area and Prague, OK. 41

Equation 3: Moment magnitude (M_0) equation from the USGS. 83

Equation 4: Equation used to calculate slip for Prague 2024. 83

ABSTRACT

Induced seismicity has been identified as a major concern in areas of hydrocarbon production, subsurface carbon sequestration, and enhanced geothermal systems, among others. Induced earthquakes are now commonly seen in many places around the world, including Oklahoma. In Oklahoma, the frequency of earthquakes with a M_w 3.0+ surged from just 2 per year in 2009 to 579 in 2014, peaking at 903 in 2015 before decreasing to 194 by 2018 and 16 in 2023. Wastewater injection was widely regarded as a significant contributor to this dramatic rise in seismic activity across the state. Most of the seismic activity has been located in the north-central portion of the state. The two sites of interest in this study are in Pawnee County, OK, and near Prague, OK. In both cases, a Coulomb stress analysis is being conducted. Coulomb modeling is used to determine how slip on faults can impact stress changes on surrounding faults, which can help determine where aftershocks patterns should be, how one earthquake impacts another, and the overall stress transfer patterns in these locations.

The first area of interest is the region termed the Pawnee Triple Junction (PTJ) in north-central Oklahoma, which consists of the Sooner Lake Fault (SLF), the Stillwater Fault (SWF), and a newly identified fault zone informally named the Northeast Trending Fault Zone (NEFZ). This region was the site of Oklahoma's largest recorded earthquake—a M_w 5.8 tremor in 2016—along the SLF and there are two main hypotheses for the production of this event that are of interest here. The first hypothesis is that aseismic slip along the NEFZ, resulting from wastewater injection, triggered the rupture along the SLF. The second hypothesis is that slip along the SLF itself triggered the M_w 5.8 rupture along the SLF. These will both be tested and compared to see if either, both, or neither are probable hypotheses.

A second site of interest in this study is a series of faults just north of Prague, OK, the Wilzetta Fault System (WFS) and the Meeker-Prague Fault (MPF). These two faults run parallel to one another for a portion of their lengths and have ruptured two mainshocks in the past 14 years. The first occurred on the MPF on November 6, 2011, and was a M_w 5.7 event. The second occurred on the WFS on February 3, 2024, and was a M_w 5.1 event. The 2011 event, similarly to the SLF mainshock, is attributed to wastewater injection as a byproduct of hydrocarbon collection. The 2024 event has had little research done on it, so this thesis is aiming to increase the understanding of this event.

To investigate stress interactions in the vicinity of the SLF and Prague, OK sites, a Coulomb stress analysis was conducted with the goal of assessing the stress transfer related to the two hypotheses discussed above as well as for the three mainshocks in these sites. Additionally, for Prague, OK this same analysis was done to assess how much how much stress the 2011 event transferred to 2024 event's epicentral region and how these two ruptures differentiate from one another with a focus on aftershock pattern differences. We utilized previously collected seismic data from the Oklahoma Geological Survey to better identify fault geometries and complexity. Software such as ArcGIS Pro, Coulomb Modeling Software 3.4 in MATLAB, and Fault Slip Potential 2.0 were used in the study to better understand the interplay of stress and seismicity in the region.

The results of the area around the SLF showed the likelihood of the two foreshock hypotheses that are discussed in this thesis. It helped to quantify that slip on the NEFZ and/or SLF could have contributed to the SLF M_w 5.8 rupture in 2016. This was concluded based on Fault Slip Potential 2.0 results showing how much Coulomb stress change was calculated for the SLF to slip and Coulomb Modeling Software 3.4 results showing how much Coulomb stress was added to the hypocenter of the M_w 5.8 rupture along the SLF from each of these foreshocks. Both of these

outputs were shown in the form of MPa of stress and by comparing them it was possible to see if these hypotheses were able to cause the mainshock to occur. If the hypothesized foreshock did not produce the same or more added Coulomb stress then it was determined that it was invalid since it would not have caused enough of a stress increase for the fault to slip. If the hypothesized foreshock produced the same or more added Coulomb stress increase then it was determined the hypothesis was valid since the foreshock generated enough Coulomb stress increase for the fault to slip. Comparing the Coulomb stress values for both foreshock hypothesis allowed for the identification of the more probable hypothesis as well. Whichever one added a higher amount of Coulomb stress during the Coulomb modeling portion would be interpreted as the higher probability foreshock since it caused more stress to accumulate at the hypocenter of the mainshock. Additionally, these results helped to assess the time-dependent aftershock distribution along the SLF based on ArcGIS Pro mapping and Coulomb stress change plots from Coulomb Modeling Software 3.4. For Prague, OK these results helped to determine the interplay between the 2011 and 2024 events and how they produced different aftershocks patterns. These findings offer insights into the stress patterns that caused these aftershocks in the locations they did since the areas of increased Coulomb stress are the areas we expect to see aftershocks. In addition to this, these results also helped to better explain the observed aftershock pattern differences in the two sites and how these two events interplayed to some extent.

The results from the modelling experiments of the two study sites provided insight into the questions proposed in this thesis. It was able to test the two SLF foreshock hypotheses, construct Coulomb stress change plots to compare to aftershock data for Pawnee and Prague, OK, as well as compare the M_w 5.7 Prague 2011 earthquake with the M_w 5.1 Prague 2024 earthquake. Each of these aspects of this research helped to contribute to the bigger picture of the propagation of these

earthquakes in Oklahoma and the role co-seismic Coulomb stress change plays a role in that propagation.

Keywords: Induced Seismicity, Coulomb Stress Analysis, Earthquake Triggering and Induction, Oklahoma, Prague Oklahoma, Pawnee Triple Junction

INTRODUCTION

1.1: Seismicity

Seismicity is used in this thesis to construct a study of stress in two areas of Oklahoma. Specifically, this study focuses on stress transfer between faults, which is manifested by the presence of seismicity. The relationship between induced seismicity and the stress changes they produce, as well as how stress changes produce seismicity, will provide insights into how stress is transferred in the subsurface between faults. Additionally, it will allow for more insight into the production of aftershocks and mainshocks based on the modeling conducted in this thesis. The study of seismicity is crucial information for areas that experience high volumes of earthquakes, so the people who live there are informed about what risk they are at. This information can be used to inform the odds of major earthquakes occurring per time periods; however, there are no exact scientific procedures to effectively predict earthquakes at this time. These "predictions" more so give an idea of when these events may occur to keep people aware of the potential risk coming their way (Schulte, 2024).

The impact of earthquakes (or seismicity) varies depending on earthquake magnitudes. Typically, the higher the magnitude, the higher the damage. Most induced seismicity causes small-scale earthquakes with some larger magnitude earthquakes. Most are lower than a M_w 4.0, but some can reach M_w 7.0 and higher, which can be very destructive (e.g. Witze, 2017). Earthquakes, both tectonically triggered and induced, were ranked the third top common disaster worldwide from 2000-2019, behind floods and storms (Mavrouli et al., 2023). These events tend to be unpredictable and can be destructive. In those 20 years, earthquakes were the cause of human casualties and injuries, loss of homes, and destruction of property. Many of the injuries obtained were due to the

collapsing of buildings, landslides that were generated from the main rupture event, fires that broke out after the earthquake, tsunamis, and hazardous chemicals that were leaked due to damage. All these injuries are a risk of seismicity and living in areas with increased earthquake activity (Mavrouli et al., 2023). In 2008, there was an approximately M_w 8.0 earthquake in Wenchuan, China. This is the largest earthquake to be claimed as being induced due to the impoundment of the reservoir behind the Zipingpu dam (Foulger et al., 2018). This earthquake occurred within 20 km of the dam within months of the impoundment being finalized and caused ~90,000 deaths as well as damage to roads, towns, and bridges (Zhang et al., 2008; Foulger et al., 2018). Another dam built in China in 1959 faced issues with induced seismicity as well. This dam had minor cracking after impoundment of the Xinfengjian Reservoir in China produced seismic activity within a month of being finished. A M_w 6.1 earthquake occurred in 1962 causing cracking along the dam (Foulger et al., 2018). These two examples show the vast differences in damage that can come from induced earthquakes. Some are extensive and cause massive loss of life and infrastructure, while others cause minor damage to infrastructure. Either way, it is known that these induced earthquakes can cause damage to life and property. Besides damage from dam impoundment-induced earthquakes, induced earthquakes from groundwater extraction, mining, and geothermal production, and waste-water disposal have also caused damage. One example of wastewater injection causing damage is the 2011 M_w 5.7 earthquake in Prague, OK (Keranen et al., 2013). This earthquake destroyed 14 houses and injured two people (Foulger et al., 2018). Most people who had property damage from this earthquake did not receive compensation for it due to not meeting their deductible or not being able to determine which earthquake damaged their property, due to several earthquakes occurring around the same time (Halkia & Ludwig, 2022). Years later, in 2016, another M_w 5.0+ earthquake occurred in Oklahoma. This was in Pawnee

County and measured at M_w 5.8. The owners of a historic building in Pawnee County, OK were the only people to get a one-time compensation for the M_w 5.8 earthquake in Pawnee (Halkia & Ludwig, 2022). Other noted damages included failed facades and chimneys in houses and buildings in Pawnee, County (Clayton et al., 2016; Fielding et al., 2017).

Induced seismicity has been identified as a major concern in areas of hydrocarbon production, subsurface carbon sequestration, and enhanced geothermal systems, among others (e.g. Suckale, 2009). Induced seismicity can be the product of many factors within these industries, such as fluid injection and CO^2 injection (White et. al. 2016). In the hydrocarbon industry, there are two main influences of induced seismicity, wastewater disposal/injection and hydraulic fracturing (fracking). Wastewater injection is a byproduct of hydrocarbon production. This occurs where water is produced as a part of the hydrocarbon collection process. The oil and gas are kept and sent off to be used in society while wastewater must be treated, recycled, or disposed of through injection wells. This disposal process pumps the wastewater into the subsurface, which can increase pore pressure along faults. Increased pore pressure results in an increase in Coulomb stress, which causes a decrease in normal stress; decreasing this normal stress can cause faults to reactivate. These Coulomb stress increases, as well as decreases, are discussed in section 1.3 of this thesis in greater detail. This reactivation can cause induced seismic earthquakes to occur (e.g., van der Baan and Calixto, 2017). This wastewater injection is likely a main cause of induced seismicity and has different spatial properties than induced seismicity related to fracking (Buchanan et al., 2014). Sometimes, fracking can induce earthquakes during the stimulation of reservoir rock. These earthquakes are typically “microearthquakes,” and earthquakes of this small scale (most of which are M_w 1.0 or less) are common from fracking. Wastewater disposal likely presents a larger risk for induced seismicity than the oil collection portion itself (Ellsworth, 2013).

States such as Oklahoma, Kansas, and Texas experience many of these induced seismic events. All three of these states have significant oil and gas development activities within them that may be resulting in the increase in induced seismicity seen (Skoumal et al. 2021; Walter et al., 2020; Buchanan, 2015). The Delaware Basin in Texas experienced 37 earthquakes with a magnitude of M_w 3.0+ from 2015-2018 alone (Skoumal et. al. 2019). This basin is one of the most seismically active and geologically complex basins in the United States. Additionally, this basin is one of the highest in hydrocarbon production in the United States, with more than 20,000 wells being drilled in it and ~3,000 wells being drilled per year in its peak years (2018, 2019, and 2022). More than 5 billion barrels of oil have been produced from this basin alone (Smye et al., 2024). However, with these barrels of oil comes more than twice as many barrels of water and since 2019 around 20 Bbbl of wastewater has been injected back into this basin. During the rise in wastewater injection, a rise in seismicity was seen. These M_w 3.0+ earthquakes rose from 10 per year in 2017 to 185 per year in 2022 (Smye et al., 2024) showing another increase in seismicity rates after that 2015-2018 time period. The Permian Basin, another high seismicity area of Texas, has experienced a drastic increase in seismicity over the last 20 years (Skoumal et. al. 2021). From 2000 to 2008, there was a low earthquake rate for M_w 3.0+ earthquakes (Hennings et al., 2024). In 2008, there were 2 earthquakes with M_w 3.0+ (Frohlich et al., 2016), throughout the 2010s there was an increase in seismicity (Hennings et al., 2024), and in 2016 the M_w 3.0+ earthquakes increased to 12 per year (Frohlich et. al. 2016). This increase in the mid-2010s raised concerns about seismicity in West Texas (Litherland, 2023), and during this time, there have been earthquakes as high as M_w 5.4+ (Hennings et. al., 2024). In 2013, Kansas had several small earthquakes in the South-central portion of the state. These were all recorded near wastewater disposal wells. Kansas did have some historical earthquakes before the introduction of oil and gas activity in the state, which does leave

the possibility that some of these earthquakes could be due to other factors. However, this big increase in seismicity and proximity to wastewater injection wells does indicate a strong likelihood that these 2013 events were induced seismic events (Buchanan et al., 2014). Kansas experienced a M_w 4.9 earthquake in November 2014, as well as hundreds of other events of varying sizes (Buchanan, 2015). From July 2021 to June 2022, there were 456 M_w 2.0+ earthquakes in Kansas. 200+ of these were within Saline County alone, according to the Kansas Geological Survey (KGS). This was the first time since 2016 that the number of earthquakes increased from the previous year. July 2020 to June 2021 had 289 M_w 2.0+ earthquakes in the state of Kansas showing how the number was smaller that year than the year after. The majority of these 456 earthquakes occurred where seismicity has historically been located and along those same prominent basement structures (KGS, 2023). Both Kansas and Texas have had high increases in induced seismicity over the past few decades. This is likely due to the increase in wastewater injection in these states which was a result of the increased hydrocarbon industry presence. The more wastewater injection that occurs, the more induced seismic activity these areas could have.

In Oklahoma, the frequency of earthquakes sized at M_w 3.0+ surged from just 2 per year in 2009 to 579 in 2014 (Walter et al., 2020), peaking at 903 in 2015 before decreasing to 16 in 2023 (USGS). Wastewater injection was widely regarded as a significant contributor to the dramatic rise in seismic activity across the state (e.g. Walter et al., 2020). A massive portion of this seismic activity has been in the north-central portion of the state which is where the sites in this study are both located. Wastewater injection was on the rise in Oklahoma during this period due to the drilling of the Mississippian limestone play. This limestone would produce significant amounts of wastewater since it was a high-water cut limestone and this water would be pumped into wastewater injection disposal wells. Hydrocarbon operators in Oklahoma then switched to the

lower-cut water units STACK and SCOOP (Pickett, 2018) due to increased cost of wastewater disposal, public relation concerns, and new exploration opportunities. These changes made companies shift to using these lower water-cut areas for their hydrocarbon collection (Machado et al., 2019).

1.2: Inducing and Triggering Earthquake Activity

Earthquakes are triggered or induced in many ways. Earthquake triggering is produced by a nearby event or stress change of natural causes (Stein & Wysession, 2003), while earthquake induction directly relates to events and stress changes from humans (Ellsworth, 2013). Triggering typically occurs when stress is redistributed after a nearby earthquake (Freed, 2005). Earthquakes can be triggered due to other earthquakes (Freed, 2005). Foreshocks can come before mainshocks and aftershocks can occur after these mainshocks based on the Omori law (Omori, 1894; Nandan et al., 2022). The Omori law describes the evolution of aftershocks which are triggered from some form of mainshock event (Omori, 1984; Zavyalov et al., 2022; Lippiello et al., 2007; Utsu et al., 1995). The process of earthquake triggering can take anywhere from seconds to years to complete. Delayed triggering is when the triggering process takes longer than the transient itself (Van der Elst and Savage, 2015). Rapid triggering, however, is when this transient occurs soon after the triggering event (Gahalaut et al., 2016). Delayed triggering can be explained though many mechanisms of time-dependent stress transfer. These mechanisms include viscous relaxation, poroelastic rebound, and reductions in fault friction (Freed, 2005). However, rapid triggering can be explained by the passage of dynamic seismic waves. This can induce Coulomb failure instantly or initiate another mechanism that will induce delayed triggering instead (Freed, 2005).

Induced earthquakes, or induced seismicity, can be caused by many different human activities. This is where activities such as wastewater injection, carbon sequestration, and geothermal stimulation procedures can influence earthquake occurrence and location. This study focuses on induced seismicity in Oklahoma. As previously mentioned, the prevailing hypothesis for this induced seismicity is that wastewater disposal is the driving factor in its occurrence. By pumping this water into the ground, increased pore pressure at depth occurs. As wastewater is disposed of in deep underground reservoirs, an increase in pore pressure can cause preexisting faults to slip. One study found that permeable faults at depth (3-7km) are close to the Coulomb failure line and faults that are viewed to be less permeable are further from that Coulomb failure line. From this study it was found that critically-stressed faults at depth are the ones that are more permeable (Ito and Zoback, 2000). Another study found that fluid pressures at depths of several kilometers for certain locations showed results of hydrostatic qualities. Each of these sites also showed the faults experiencing this hydrostatic fluid pressure in alignment with the Coulomb frictional failure theory. Additionally, several of these same sites had seismicity that was induced by fluid injection (Townend and Zoback, 2000).

1.3: Coulomb Stress Changes

Fault slip of any style will result in stress changes within the earth. Changes in stress due to seismic and aseismic slip are important to investigate to understand potential future seismic events. It is currently hard to detect when aseismic changes occur whereas we do know when seismic changes occur in the Earth. Seismic slip occurs when the earth suddenly moves and two blocks of lithosphere slip past one another such as these induced earthquakes discussed above. However, aseismic slip can also occur. This kind of slip occurs without measured radiated energy. Both aseismic and seismic slip can be induced on faults (Ye and Ghassemi, 2020). Seismic and aseismic

slip can also cause earthquakes to occur and these earthquakes can change the stress state of nearby faults in the range of the source fault – receiver faults – which can lead to many aftershocks on these receiver faults. Mapping Coulomb stress changes helps to gain insight into how a specific earthquake event can play a role in future earthquake generation, even years afterwards (Peikert et al., 2023; King et al. 1994). Coulomb stress change is calculated by *Equation 1* shown below. In this equation, $\Delta\tau$ is change in shear stress, μ is the friction coefficient, $\Delta\sigma_n$ is change in normal stress, and P is pore pressure (King et al. 1994; Stein, 1999).

$$\Delta CFS = \Delta\tau - \mu(\Delta\sigma_n - P)$$

Equation 1: Coulomb stress change equation (King et al. 1994; Stein, 1999).

As previously discussed, earthquakes can trigger other earthquakes (e.g. Kilb et al., 2002). Coulomb stress change can be utilized to determine where aftershocks are expected to be seen. These aftershocks are high in number from the three events studied in this thesis. These events consist of the 2016 Sooner Lake Earthquake along the Sooner Lake Fault (SLF) in a region known as the Pawnee Triple Junction (PTJ), the 2011 Prague earthquake on the Meeker-Prague Fault (MPF), and the 2024 Prague earthquake on the Wilzetta Fault System (WFS). These three events are discussed in greater detail in sections 1.4 and 1.5. In determining Coulomb stress change, Coulomb stress can increase, decrease, or remain unaffected. An increase in Coulomb stress indicates that any receiver faults are going to be closer to failure, which are the areas that aftershocks would be more expected to occur. If a decrease in Coulomb stress change is seen that means that the receiver fault is going to be further from failure, which are the areas where a lack of aftershocks would be expected to be seen (Stein, 1999). Coulomb stress change can influence the rupturing of faults in more than one way. The first occurs due to the raising or lowering of an applied load being accumulated over time. This occurs from forces such as plate tectonic loading.

The second is by modifying the fault and/or the fault's surroundings (Kilb et al., 2002). One way to change the immediate surroundings of a fault is by injecting wastewater into disposal wells around it (Buchanan et al., 2014), which is one topic looked at in this thesis.

An aftershock that is within the positive Coulomb stress change areas would be consistent with static stress triggering (Zhu and Miao, 2015). Static stress changes are directly related to the mainshock while dynamic stress changes are related to seismic waves moving in the Earth (Hardebeck, 2014). This relationship between static stress and spatial distribution of aftershocks is complex but important to understand (Zhu and Miao, 2015). Coulomb stress changes assist in this understanding by showing where these aftershocks are most likely to occur spatially based on that stress change. Additionally, these Coulomb stress change calculations can further explain these relationships by providing insight into earthquake sequence data in addition to the most probable aftershock distribution patterns (Freed, 2005).

A study done on the Kontinentales Tiefbohrprogramm der Bundesrpublik Deutschland (KTB) drill site showed that as depth increased so did stress. This added stress causes faults to be closer to critically stressed which means that this study showed a correlation with depth and how critically stressed a fault was (Zoback et al., 1993). Many of the preexisting faults that are likely to slip from an increase in pore pressure are already stressed at depth. When this increased pore pressure impacts a fault, it decreases the effective normal stress along it. This effective normal stress helps the fault resist slip since it acts perpendicularly to the fault. Therefore, by decreasing this effective normal stress the likelihood of slip along the fault goes up (Rudnicki and Rice, 2006; Walsh and Zoback, 2015).

1.4: Pawnee Triple Junction

One focus of this thesis is to gain a deeper understanding of the Coulomb stress transfer among the faults that comprise the Pawnee Triple Junction (PTJ) (Chen et al., 2017) and its possible role in reactivating the Sooner Lake Fault (SLF) (Pennington, 2017). Additionally, the investigation will extend to the faults in Prague, OK as discussed in section 1.5. Locations for both sites are highlighted in *Figure 1.*

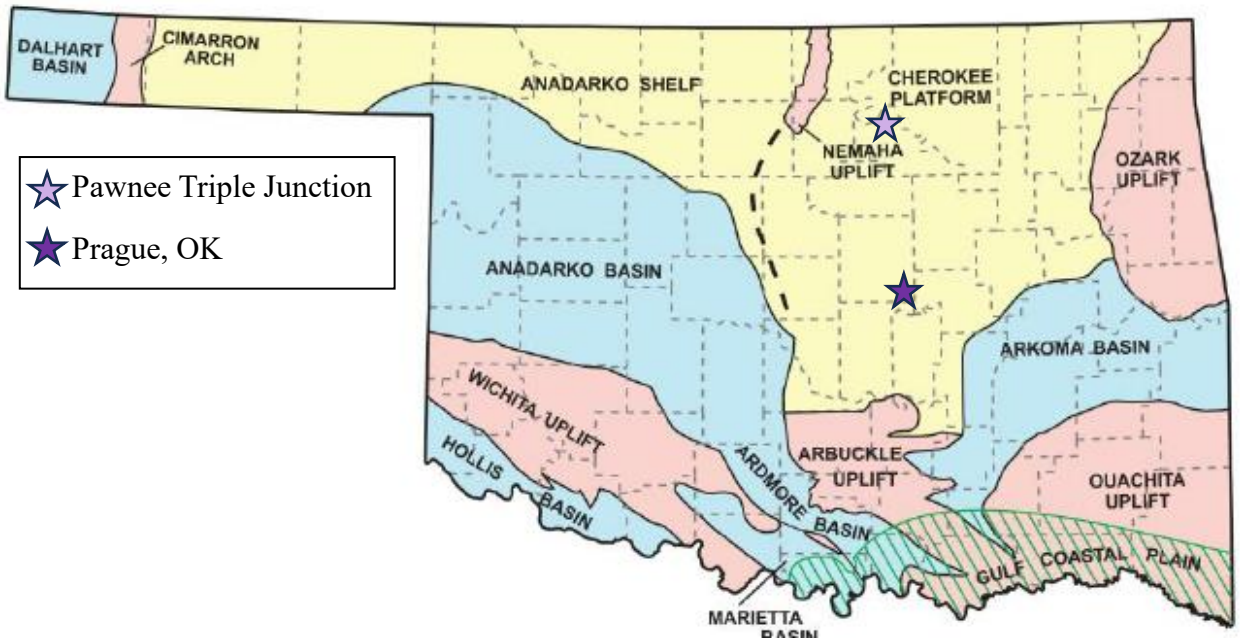

Figure 1: Map of Oklahoma with starred locations for the Pawnee and Prague, OK earthquake sites (modified from Johnson, 2008).

Our first area of attention is directed towards the influence of aseismic slip and subsurface stress transfer on the reactivation of the SLF. Understanding these factors is crucial for gaining a better understanding of the largest earthquake in Oklahoma history, which occurred on September 3, 2016, and measured M_w 5.8 along the SLF. The rupture location is indicated by the purple star in *Figure 2*. This earthquake occurred at 5.6 km depth according to the USGS and was felt widely

across the state. There are two foreshock hypotheses being tested in this thesis that are talked about more in depth in section 2.3 of this thesis. The first is from Chen et al. 2017 and the second is from Walter et al. 2017. The testing of these hypotheses will show if either foreshock scenario was the probable driving factor in the production of the M_w 5.8 event, if one is more likely than the other, and/or if these foreshocks could have worked together to produce this event.

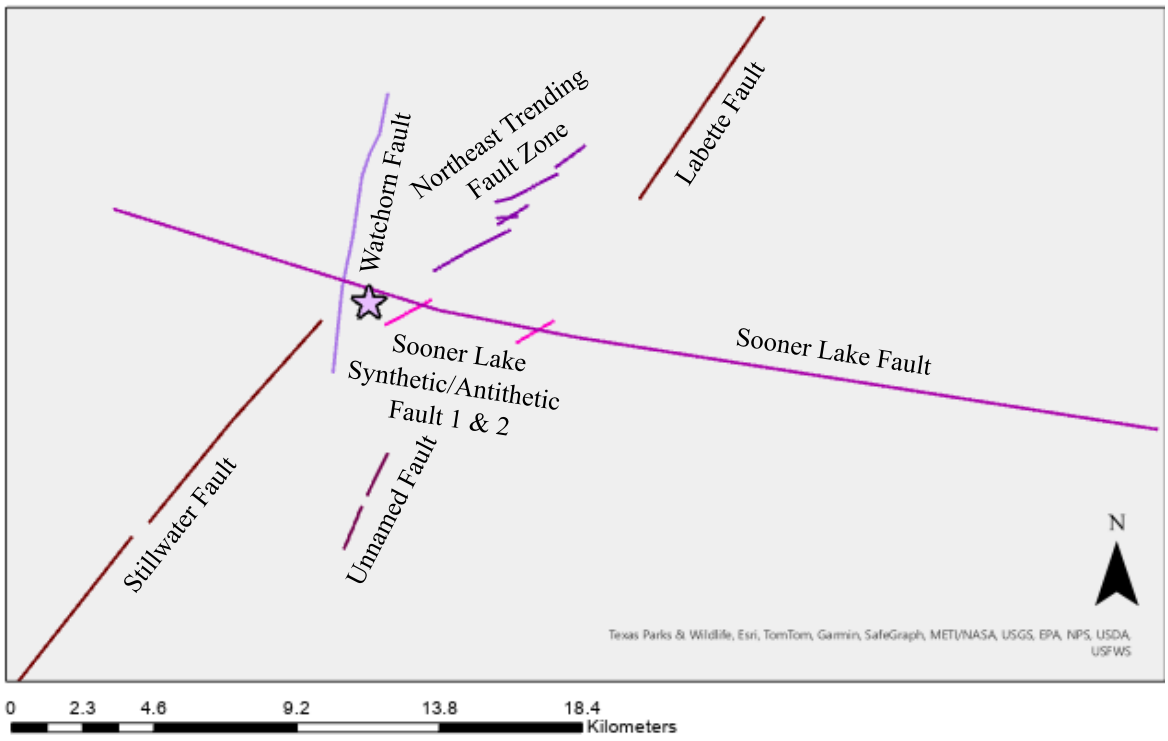

Figure 2: ArcGIS Pro map of the PTJ showing the locations of the SWF, SLF, WF, and NEFZ. SWF and WF were identified using the Oklahoma Geological Survey fault map, while the SLF and NEFZ were mapped by Emily Hencey based on Park et al. 2022 seismicity data in ArcGIS Pro. Purple star is the hypocenter of the 2016 M_w 5.8 rupture along the SLF.

Coulomb stress changes from the SLF mainshock produced a widespread area of aftershock production. These aftershocks can be seen in the data catalogs used in this thesis. As stated before, aftershocks occur as a direct result of the mainshock (e.g. Zavyalov et al., 2022), in part, due to a

change in Coulomb stress from the mainshock. A deeper look into the Coulomb stress change from the M_w 5.8 event in 2016 is sought in this thesis.

1.5: Prague, OK

Prague, OK is the site of two major earthquakes in Oklahoma history. The first occurred on November 6, 2011, and measured at M_w 5.7. Over 10 years later, on February 3, 2024, another earthquake occurred just northeast of this event. This event measured at M_w 5.1. This site is indicated by the purple star in *Figure 1* and the individual event hypocenters are shown by the stars in *Figure 3.* In this figure the light purple star is the 2011 epicenter and the dark purple star is the 2024 epicenter. These events are extremely close together but hosted different aftershock locations and patterns. Additionally, the hypocenters of each event were along different faults and activated different fault systems, potentially driving the difference in aftershock patterns. The 2011 event ruptured along the Meeker-Prague Fault (MPF) and the 2024 event ruptured along the Wilzetta Fault System (WFS). A better insight into the difference in aftershock patterns is sought in this thesis. Coulomb modeling software was used to look at how the stress patterns of these two events differentiate from one another and how the interplay of faults where these ruptures occurred may also have contributed to the vast differences seen in the aftermath of each event. Additionally, insight into whether the 2011 earthquake could have attributed to the cause of the 2024 earthquake is sought. This will increase the understanding of the stress propagation in this area and how these two earthquakes may be interconnected.

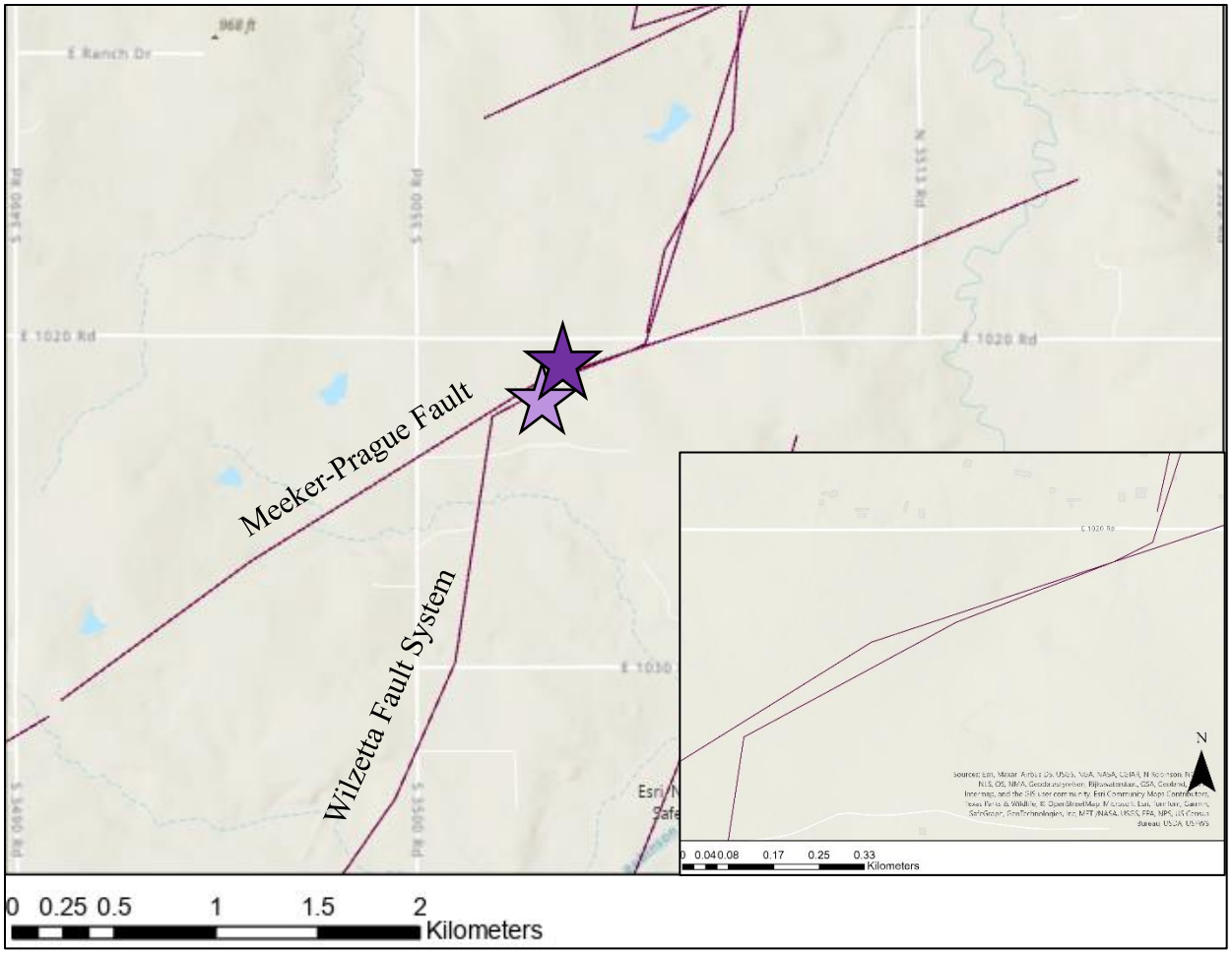

Figure 3: Fault map of Prague, OK with the hypocenters of the 2011 and 2024 ruptures shown in the light and dark purple stars. The top star is the 2024 event and the bottom star is the 2011 event. Faults are from the Oklahoma Geological Survey.

GEOLOGICAL BACKGROUND AND HISTORY OF RECENT SEISMICITY

2.1: Geological Background

The SLF event occurred in north-central Oklahoma in Pawnee County while the other two earthquakes occurred in more Central Oklahoma just north of Prague, OK. However, the geology is very similar in these locations since they are both in the Cherokee Platform as seen in *Figure 1.* The two sites in this study are underlain by Oklahoma basement rocks, which begin at approximately 1 km depth and consist of Precambrian and Cambrian igneous and metamorphic formations. These rock formations are granites and rhyolites that are 1.4 billion years old. After these rocks formed other layers of igneous rocks including granites and rhyolites formed in and on top of them. The cross section shown in *Figure 4* illustrates an area just west of the SLF area, revealing how the SLF and Prague, OK, overlie this Precambrian basement rock (Johnson, 2008). A good portion of the seismicity in the dataset catalogs of this study occurs below 1 km depth and within the Precambrian rock units of Oklahoma.

Above basement rock there are thinner layers of rock units from the Mississippian, Devonian, Silurian, Pennsylvanian, and Permian shown in the cross section in *Figure 4.* Many of these layers are where the oil and gas in Oklahoma are found. Hydrocarbon collection in Oklahoma focuses on layers within the Pennsylvanian, Mississippian, Devonian, Silurian, and Ordovician. Included in these layers are sedimentary rocks showing how the geology of this area consists of mostly igneous rocks with some sedimentary and metamorphic rocks throughout it (Johnson, 2008). Most of the wastewater disposal discussed in this thesis was injected into the Arbuckle Group since it is a very porous layer. This layer is late Cambrian-Ordovician in age (Machado et al., 2019; Gogri, 2018).

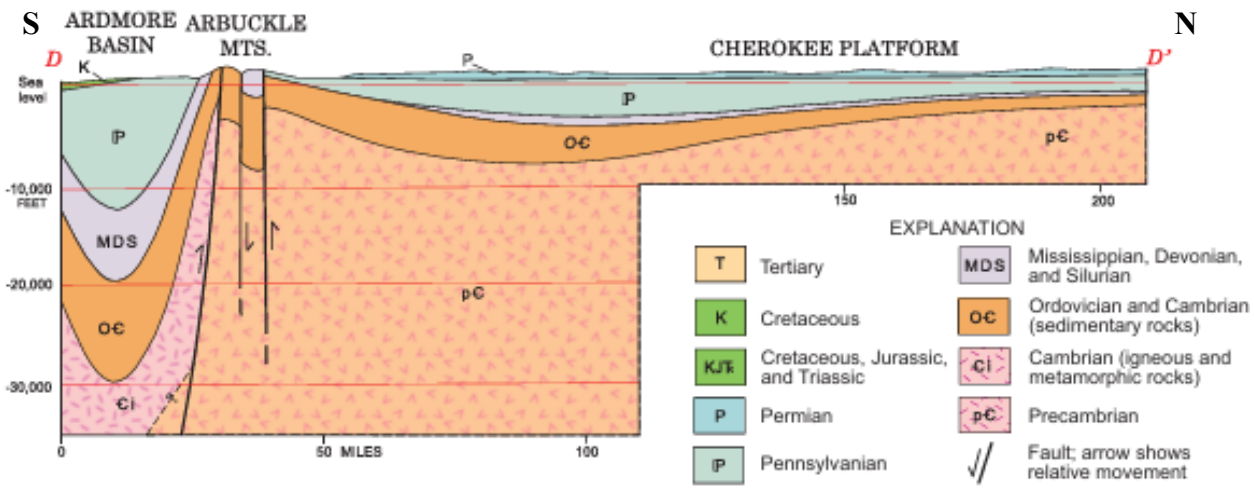

Figure 4: Cross-sectional view of the area just west of the SLF showing the basement rock composition (Johnson, 2008). This cross section is a good representation for all three sites since they are all located in similar areas of Oklahoma and all have the same geological rock composition within them.

2.2: Seismic History in Oklahoma

Seismicity records in Oklahoma date back to the early 1900s in many studies (Hough and Page, 2015). *Figure 5* shows seismicity over time starting with the first M_w 4.0+ event just before 1900. The amount of M_w 3.5+ events ramped up starting in 2009 when there was a massive increase in this seismicity. The presence of wastewater injection increases also occurred starting in 2009 (Hough and Page, 2015) which shows both seismicity and wastewater injection rates increasing simultaneously.

The rate of M_w 4.0+ earthquakes in Oklahoma went from 1 per decade before 2009 to 24 in 2014 alone. This rate of one per decade dates back to 1882, highlighting the significant increase in induced seismicity during the 2008 to 2019 period (Walsh and Zoback, 2015). This increase in earthquakes per year can be seen in *Figure 5.* From 2014 to today these rates have changed. In

2014 there were 579 M_w 3.0+ earthquakes, but by 2015 there were 903 of these (Walter et al., 2020). However, by 2023 there were only 16 of these M_w 3.0+ earthquakes in a year according to the USGS earthquake catalog; the rate significantly decreasing from 2015 to 2023.

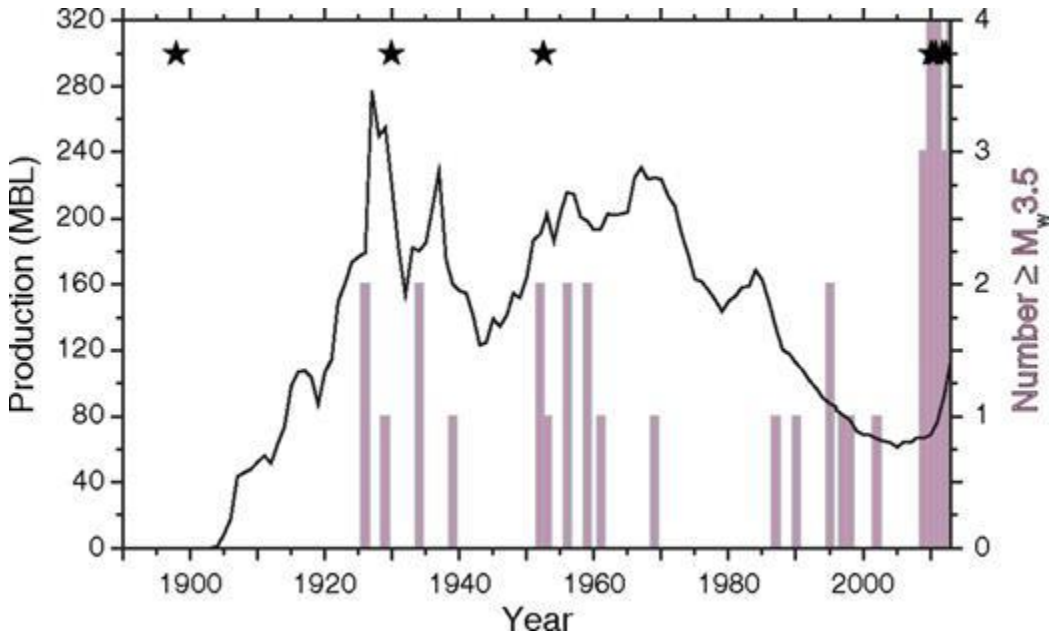

Figure 5: Seismicity data in Oklahoma from the early late 1800s/early 1900s to 2014. The black stars represent events M_w 4.0 and greater (Hough and Page, 2015).

From 2009 to 2019, seismicity in Oklahoma increased significantly and is strongly believed to be associated with wastewater injection. During this period (2009–2019), the two largest earthquakes in Oklahoma's recorded history occurred. In 2024, another significant earthquake took place, ranking third in the state's history (USGS). The Mw 5.1 rupture in Prague, OK is tied for third with a Mw 5.1 event that occurred in Waynoka, OK on February 2, 2016. The first earthquake discussed in this study is the Mw 5.8 event that occurred on the Sooner Lake Fault (SLF) in Pawnee County, OK. Aftershocks are still interpreted to be occurring on faults in this region. The second event is the 2011 Mw 5.7 earthquake on the Meeker-Prague Fault, just north of Prague, OK. The third event, while lower in magnitude, is of particular interest due to its proximity to the 2011

Prague earthquake. This is the Mw 5.1 earthquake that occurred on the Wilzetta Fault System (WFS) north of Prague, OK. Numerous aftershocks from this event are still being recorded in the area. In 2014, Oklahoma experienced a higher rate of Mw 3.0+ earthquakes than California. The dramatic rise in seismicity from 2008 to 2014 reached levels comparable to California's rates for Mw 3.0+ earthquakes (Keranen et al., 2014). A comparison between wastewater injection well sites and areas of increased seismicity across Oklahoma suggests that wastewater injection likely contributed to the rise in earthquakes between 2009 and 2015 (Walter et al., 2020). Seismic activity has since declined, likely due to reduced injection depths and the implementation of other mitigation measures. By redirecting wastewater into shallower formations, a notable decrease in induced seismic events has been observed (Skoumal et al., 2024). Based on prior studies and the data collected, it is likely that the earthquakes examined in this study were induced by wastewater injection across Oklahoma.

2.3: Seismic History of the PTJ

In 2016, the Sooner Lake Fault (SLF), which comprises one arm of the PTJ, generated the largest recorded earthquake in Oklahoma history, measuring M_w 5.8. This significant event produced a wealth of data that has enabled more robust and complex mapping of faults near the SLF. The focal mechanism for this 2016 event is seen in *Figure 6* and shows that it was a left-lateral strike slip event with a strike and dip of 289°/72°.

The mainshock occurred on September 3, 2016, with a M_w 5.8. Prior to this mainshock there is very little seismic activity in the recorded database, at least in comparison to after the 2016 mainshock occurred. The seismicity from August 11, 2013, to September 1, 2016, is seen in *Figure 6.* In total the recorded seismic events from the OGS database used in this study is 1337. The total

seismic events prior to the mainshock were 69 and from the mainshock until May 15, 2023, is 1268. The second portion of this data is a much larger database of events and spans from September 3, 2016, to May 15, 2023, and can be seen in *Figure 6.* This is the remainder of the seismicity database provided from OGS for this thesis.

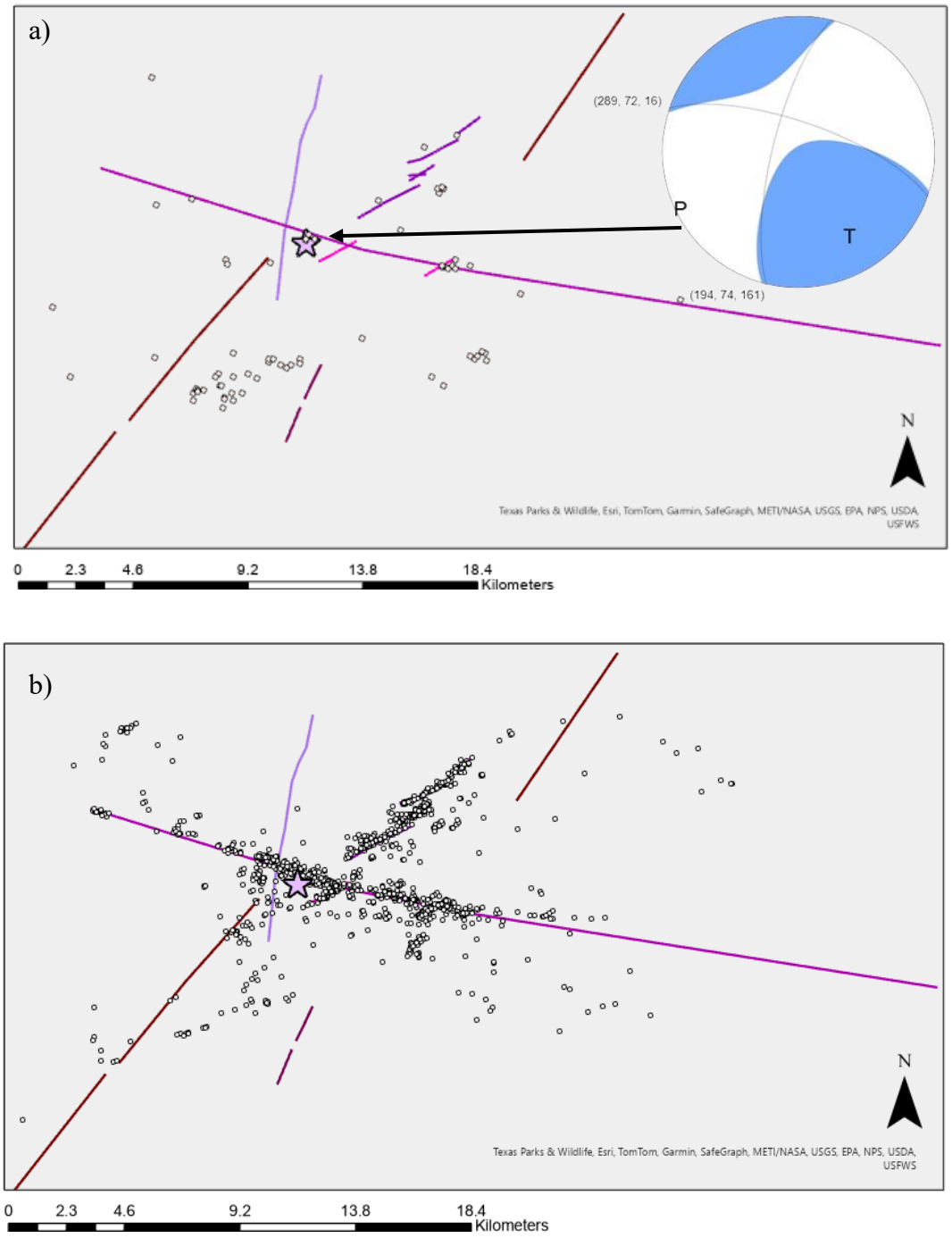

Figure 6: USGS focal mechanism beachball of the 2016 M_w 5.8 rupture on the Sooner Lake Fault with seismicity maps of a) seismicity prior to the mainshock (August 11, 2013, to September 1, 2016) and b) seismicity after the mainshock (September 3, 2016, to May 15, 2023). Purple star = hypocenter of the M_w 5.8 earthquake along the Sooner Lake Fault in 2016.

This big increase in seismicity is attributed to aftershock production from the 2016 M_w 5.8 earthquake along the SLF. There are two proposed foreshock hypotheses that are discussed in this thesis. The first is by Chen et al. (2017), and the second comes from Walter et al. (2017). Both are discussed and tested in Coulomb Modeling Software 3.4 in this thesis.

The hypothesis from Chen et al. (2017) for the production of this M_w 5.8 earthquake states that it was likely attributed to slip along an extension of the Labette fault called the Optimally Oriented Fault (OOF) (Chen et al., 2017). The OOF has now been replaced with the Northeast Trending Fault Zone (NEFZ) to better reflect the geometry of structures illuminated, and then mapped, by subsequent aftershock seismicity. This remapping is discussed later in the Methods and Results sections, but is relevant to understand the basis of the testing of this hypothesis in this thesis. With a newly updated fault map of the area, this study seeks to gain insight into how adding different amount of slip values to NEFZ6, a strand of the Northeast Trending Fault Zone, causes Coulomb stress change at the hypocenter of the M_w 5.8 SLF rupture in 2016. The location of the proposed foreshock in this hypothesis is shown in *Figure 7* as the white star and occurred on June 8, 2016 (Pennington, 2017). The newly updated NEFZ location in comparison to the OOF is shown in *Figure 8.* Additionally, if the amount of slip along this fault zone is unreasonable then other factors will be considered in conjunction with aseismic slip along the NEFZ.

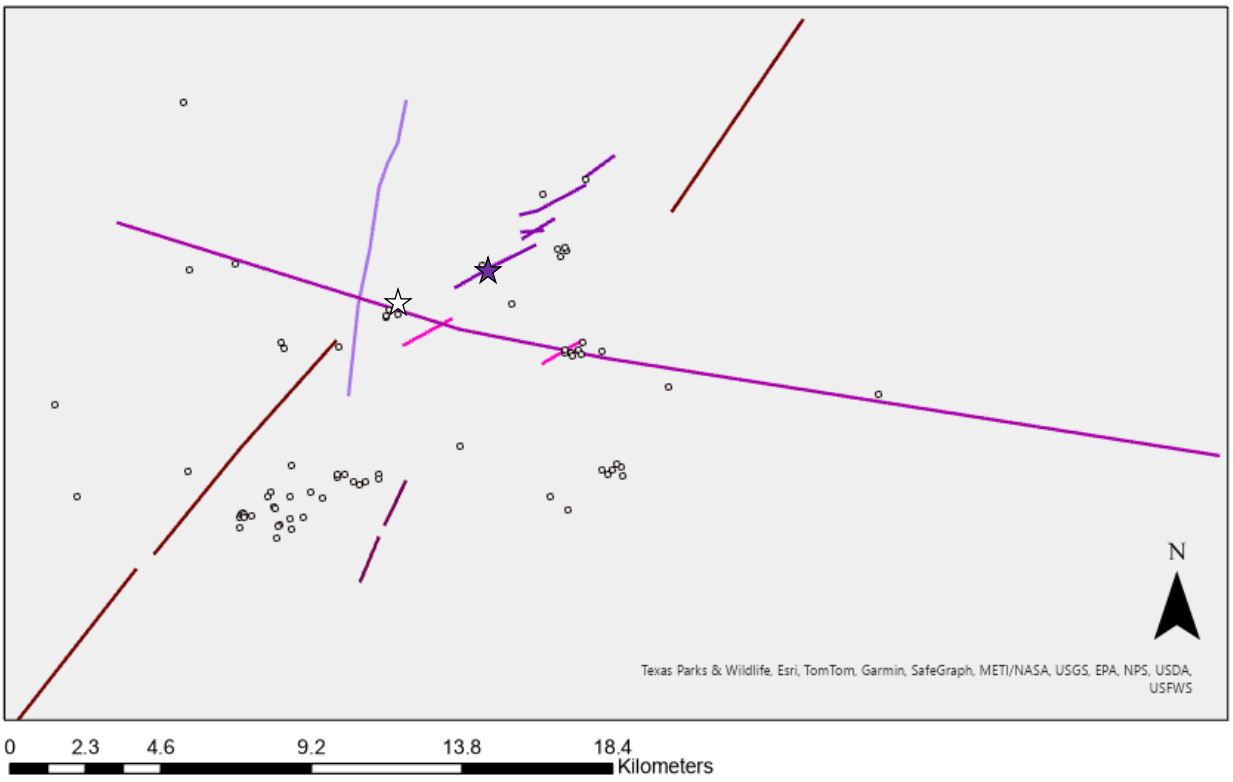

Figure 7: Locations of the two hypothesized foreshocks on top of the seismicity data leading up to the main rupture in 2016. that caused the 2016 M_w 5.8 rupture along the SLF. Dark purple star = Chen 2017 hypothesis, white star = Walter 2017 hypothesis. Seismicity dates range from August 11, 2013, to September 1, 2016.

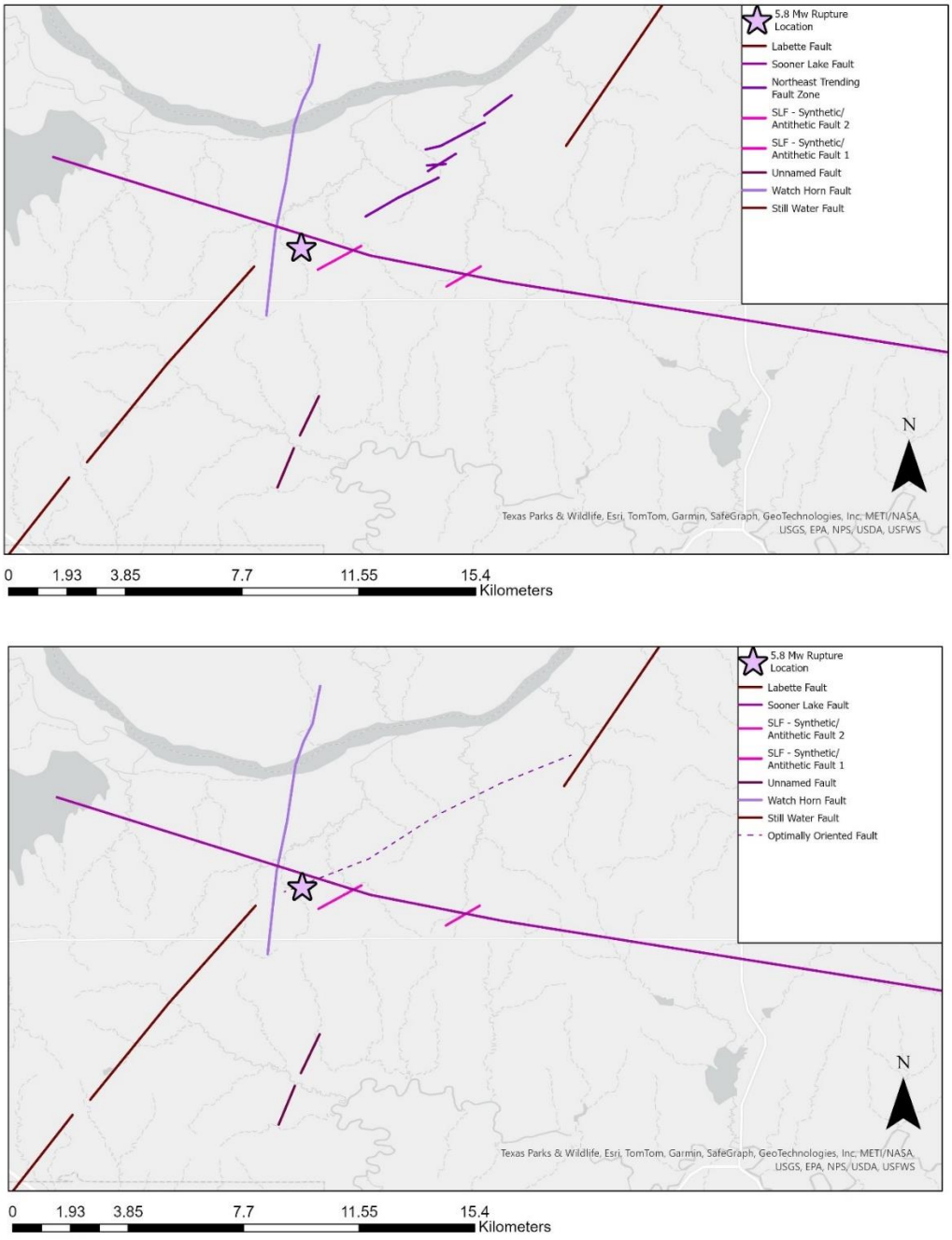

Figure 8: ArcGIS Pro map of the PTJ showing the locations of the SWF, SLF, WF, and NEFZ. SWF and WF were identified using the Oklahoma Geological Survey fault map, while the SLF and NEFZ were mapped by Emily Hencey based on Park et al. 2022 seismicity data in ArcGIS Pro. Top photo shows the OGS fault map with the dashed line being the OOF (Chen et al., 2017) (extension of the Labette fault). Bottom photo shows Hencey fault map with the NEFZ.

The secondary hypothesis, from Walter et al. (2017), states that slip along the SLF triggered the M_w 5.8 main rupture to occur (Walter et al., 2017). This proposed foreshock occurred on June 6, 2016, according to Pennington (2017), two days before the Chen et al. (2017) foreshock. The hypothesis is tested very similarly to the Chen 2017 hypothesis in this thesis, but has some differences. Instead of the slip occurring along the NEFZ segment 6 it is hypothesized by Walter (2017) that this slip occurred along the SLF itself very close to the actual hypocenter of the mainshock. The Walter (2017) hypothesis places slip along the western portion of the SLF, just east of that M_w 5.8 hypocenter. Testing slip on this portion of the SLF caused by a foreshock months before the mainshock will give insight into the Coulomb stress changes caused from this slip. This will be tested to see if a reasonable amount of slip along the SLF would produce this 2016 M_w 5.8 rupture or if other factors would be needed in addition to it. The location of the proposed foreshock in this hypothesis is shown in *Figure 7* as the dark purple star.

The testing of these two hypotheses will provide an increase in understanding of what Coulomb stress changes they both apply to the SLF and the hypocenter of the M_w 5.8 event along it. Additionally, the testing of these two hypotheses will allow for determination of it they are both probable or improbable and if one was more likely the root cause of the M_w 5.8 or not. This will allow for a deeper understanding of the seismic history of the PTJ and the earthquakes produced around it.

Before this M_w 5.8 earthquake there was not enough seismicity data to map out the SLF and NEFZ. These two structures are incredibly important for understanding the interplay of the faults near the SLF and have been critical in understanding the seismicity of this area. Prior to the M_w 5.8 earthquake there were some faults mapped out in the OGS database which were used in this study.

2.4: Seismic History of Prague

As previously mentioned, Prague, OK has had seismicity within and around it for years. The first main shock of interest occurred on November 6, 2011, with a M_w 5.7 along the MPF seen in *Figure 9* and ranks second largest in Oklahoma recorded history. 13 years after this event, another M_w 5.0+ rupture occurred. This was the M_w 5.1 earthquake on February 3, 2024. This earthquake occurred on the WFS as shown in *Figure 9.*

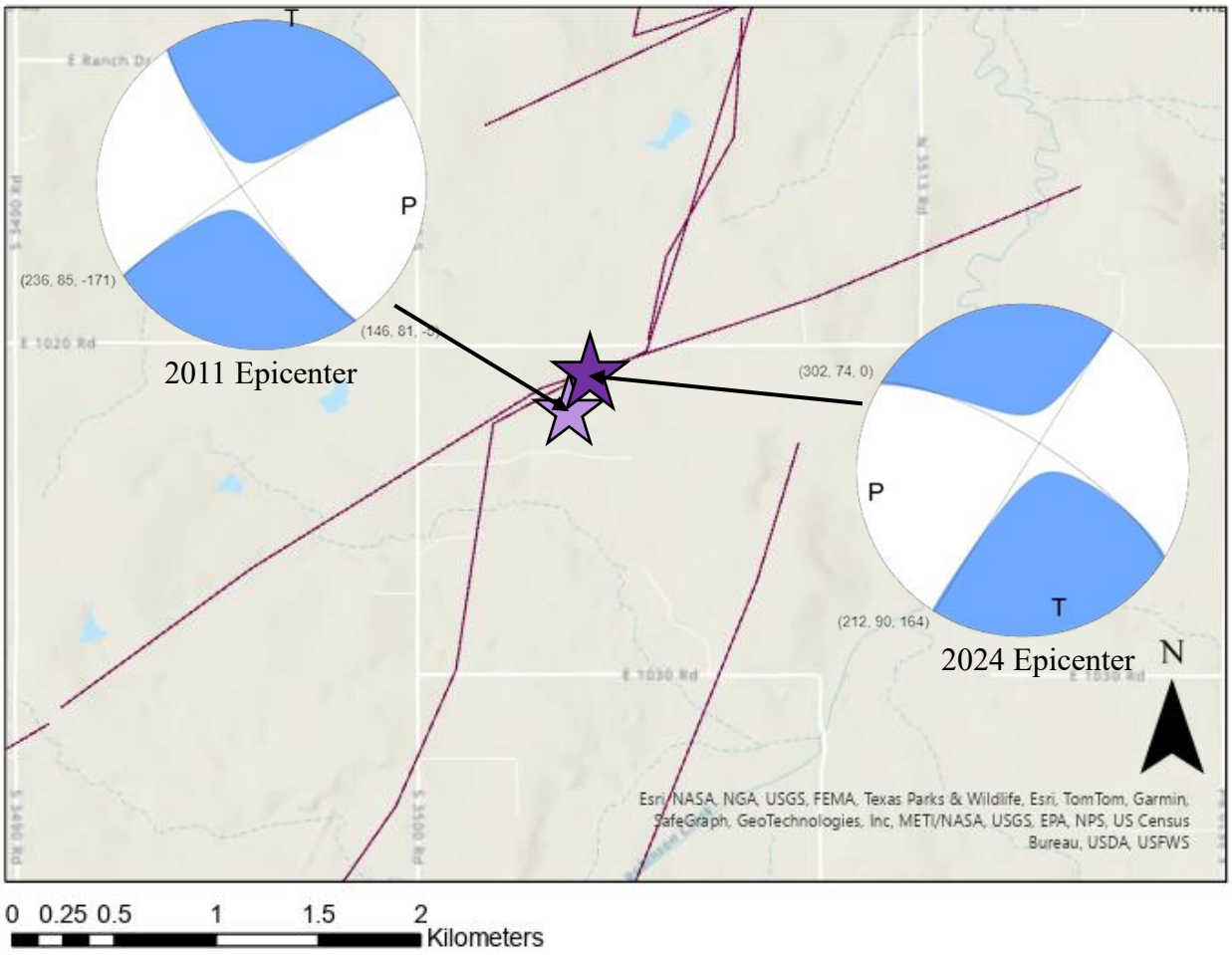

Figure 9: ArcGIS Pro map of the Prague, OK site showing the locations of the 2011 Prague, OK Mainshock along the Meeker-Prague Fault on November 6, 2011, and the 2024 Prague, OK mainshock along the Wilzetta Fault System on February 3, 2024. Overlain this map is the focal mechanism beach balls for each main shock with the year labelled below each one.

Prior to this earthquake on November 6, 2011, the OGS catalog has 66 earthquakes from June 29, 2010, to November 4, 2011. Each of these 66 events were smaller in nature and occur across several of the faults in the Prague area. Additionally, 42 of the earthquakes in this catalog occurred on the day of and day before this mainshock and of the 494 days recorded in the OGS catalog prior to the mainshock, 49 of these events occurred in the 121 days prior which shows almost half of these

events prior to the mainshock occurred closer to the mainshock then the start of the catalog. This shows a ramp up in seismicity in the time approaching the mainshock. Seismicity data prior to this mainshock was limited due to both a lack of instruments at the field site and a lower number of recorded earthquakes. From the 2011 M_w 5.7 earthquake until May 26, 2024, there are 2421 recorded earthquakes. These aftershocks are critical in understanding how this M_w 5.7 earthquake impacted the faults around it. There are 4806 aftershocks recorded after the M_w 5.1 earthquake on February 3, 2024. This aftershock dataset is not as robust in time length due to timing constraints since this earthquake was very recent and aftershock data is still accumulating. Both of these OGS data catalogs provide great insights into the production of these two M_w 5.0+ earthquakes and their aftershocks.

The focal mechanism for the 2011 and 2024 Prague, OK events can be seen in *Figure 9.* The 2011 event had a strike and dip of 146°/81° while the 2024 event had 302°/74°. This difference in strike and dip is likely a contributing factor to the differences in aftershock patterns across the same areas. According to the USGS, the 2011 earthquake was a right-lateral strike slip event and the 2024 earthquake was a left-lateral strike slip event.

These two events ruptured along two different fault systems. The 2011 event occurred on the Meeker-Prague fault (MPF) while the 2024 event ruptured along the Wilzetta Fault System (WFS). The difference in seismicity produced from these separate earthquakes can be seen in *Figure 10*. The aftershock patterns are drastically different, which is likely attributed to the parameters just discussed.

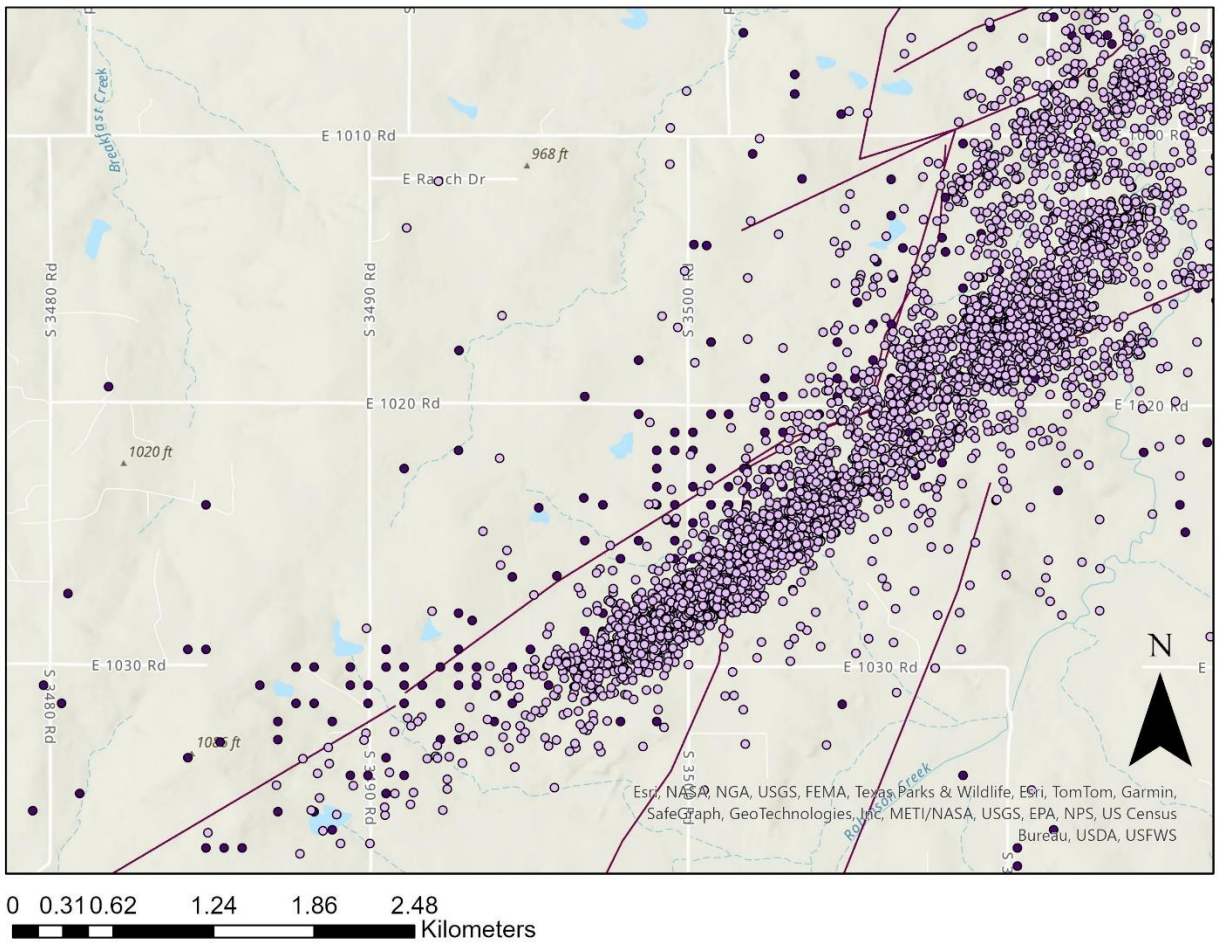

Figure 10: Map of locations for the aftershocks from the 2011 and 2024 Prague, OK earthquakes. Dark purple = 2011 aftershock data, light purple = 2024 aftershock data. Seismicity dates range from November 6, 2011, to April 20, 2013, and February 3, 2024, to February 24, 2025.

METHODOLOGY

3.1 Data Collection

The Coulomb modeling portion of this thesis requires seismicity catalogs, Poisson's Ratio, Young's Modulus, fault location data, and focal mechanism data. These are used as follows: seismicity catalogs for fault mapping and seismic clustering; Poisson's ratio and Young's modulus to calculate Coulomb stress changes; fault location data to construct the Coulomb model; and focal mechanism data to determine the average dip along each fault segment. The Fault Slip Potential 2.0 portion of this thesis requires fault location data, Oklahoma's stress state, and fault segment dips.

Data for the SLF and surrounding faults was provided by the Oklahoma Geological Survey (OGS) and taken from Park et al. (2022). OGS supplied seismicity point data, focal mechanism data, and the latest version of the Oklahoma fault map (Hollowway et al., 2016). The seismicity data and focal mechanism data were sent directly from the state seismologist Dr. Jacob I. Walter. The details for each of these catalogs are provided in *Table 1*. The Oklahoma Fault Map was taken from the publicly available OGS website. The dataset from Park et al. (2022) utilized machine learning to detect smaller seismic events than done in the OGS dataset as well as seismicity at deeper depths. This dataset contains more events than the OGS and is depicted in *Figure 11* and *Table 1*. This data catalog was instrumental in determining more precise fault segments and geometries. *Figure 12* shows the OGS seismicity data, which is still very useful but much less robust. For Prague, OK, another seismicity catalog and focal mechanism catalog from OGS was utilized. This catalog is

shown in *Table 1* and *Figure 13*. The public OGS fault map of Oklahoma was used for this area as well.

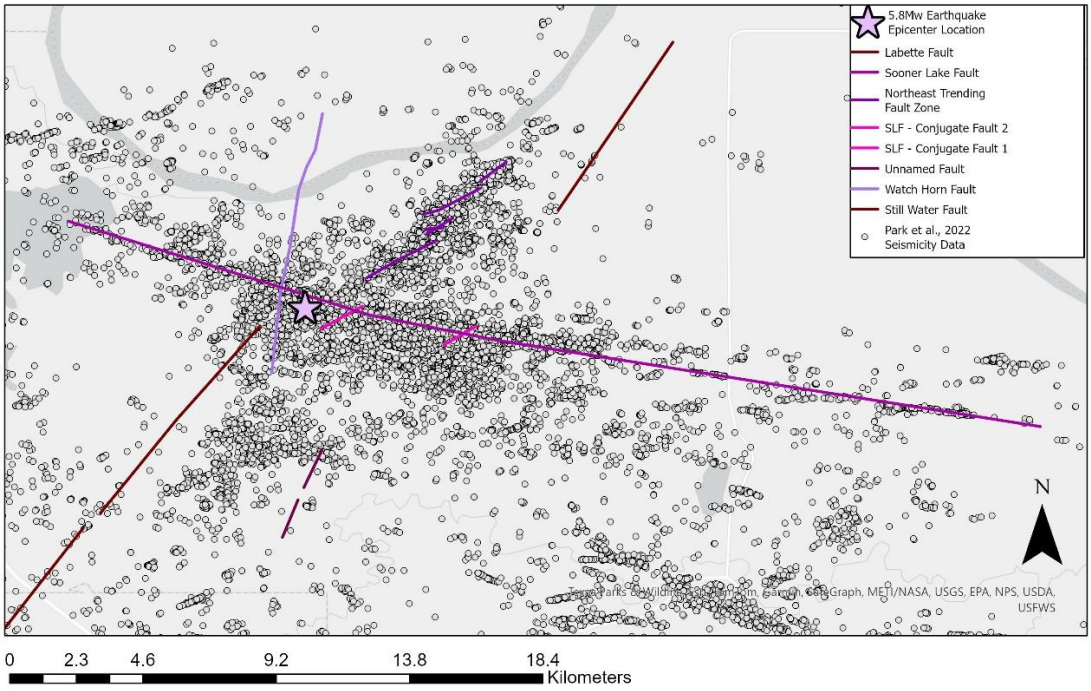

Figure 11: ArcGIS Pro map of the PTJ showing locations of the SWF, SLF, WF, and NEFZ. SWF and WF were identified from the Oklahoma Geological Survey fault map, while the SLF and NEFZ were mapped by Emily Hencey using the Park et al. (2022) seismicity data (white dots) in ArcGIS Pro. Seismicity Dates range from January 1, 2013, to December 31, 2019.

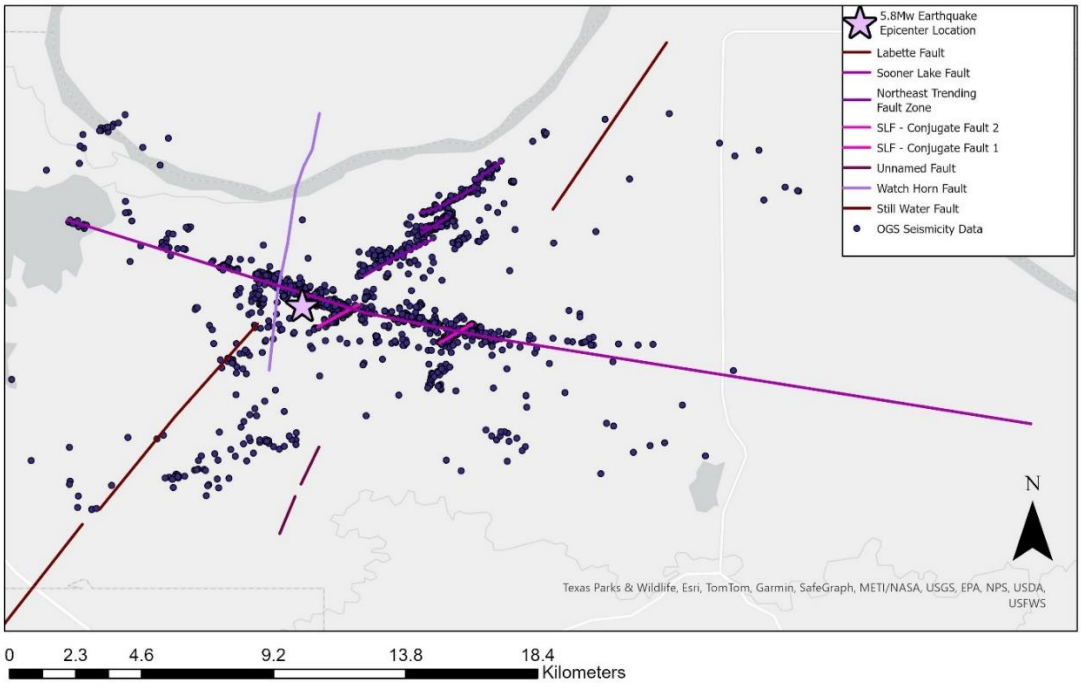

Figure 12: ArcGIS Pro map of the PTJ showing locations of the SWF, SLF, WF, and NEFZ. SWF and WF were identified from the Oklahoma Geological Survey fault map, while the SLF and NEFZ were mapped by Emily Hencey using the OGS seismicity data (purple dots) in ArcGIS Pro. Seismicity dates range from November 8, 2013, to May 15, 2023.

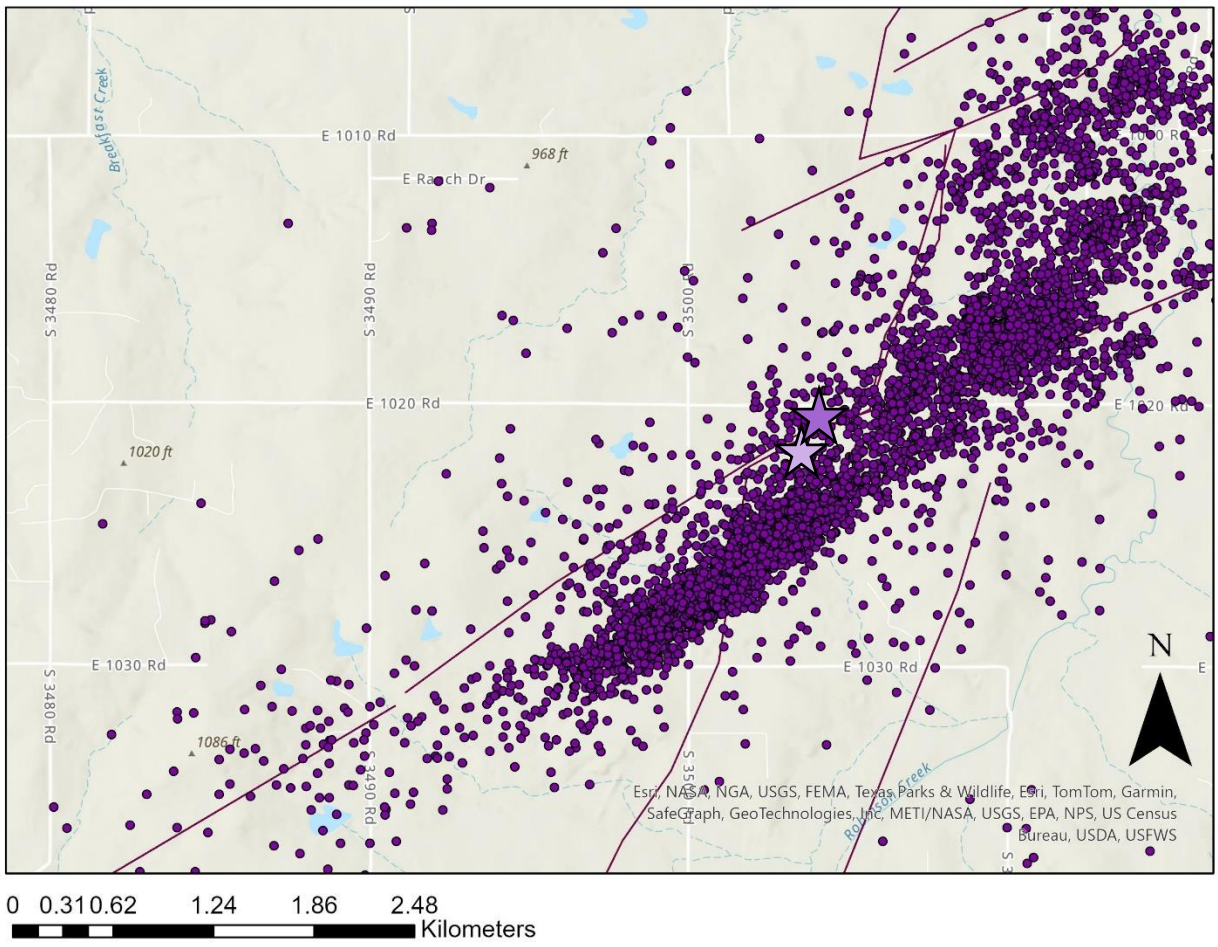

Figure 13: Seismicity data over the OGS fault map in Prague, OK. Purple stars represent the two major ruptures in this location including the 2011 M_w 5.7 event (light purple star) and 2024 M_w 5.1 event (dark purple star). Seismicity dates range from June 29, 2010, to February 24, 2025.

Data Catalog	Date Range	Magnitude of Minimum Earthquake	Number of Events	Seismicity Depth Range
Pawnee Seismicity (OGS)	8/11/2013 to 05/15/2023	M_w -0.39	1337	1.47 km to 13.77 km
Pawnee Seismicity (Park et al., 2022)	1/1/2010 to 12/31/2019	M_w -0.62	310043	0 km to 64.37 km
Prague, OK Seismicity (OGS)	5/29/2010 to 5/29/2024	M_w -2.07	5440	0.085 km to 9.875 km
Pawnee Focal Mechanisms (OGS)	4/7/2014 to 2/25/2024	M_w -0.31	807	N/A
Prague, OK Focal Mechanisms (OGS)	3/22/2010 to 5/26/2024	M_w 0.3	545	N/A

Table 1: Data catalog specifics for date range, magnitudes, number of events, relocation process, and depth range for each of the 5 data catalogs used in this thesis.

Aftershock populations for the 2011 and 2024 Prague events were determined by plotting the cumulative number of earthquakes vs the days since the mainshock to show when these aftershocks should be separated into separate groupings. The assumptions from this allowed us to have one population of aftershocks for the 2011 earthquake and one for the 2024 earthquake instead of having one shared population for both. For the 2011 earthquake, this occurs around April 20, 2013, which was 532 days after the mainshock. The aftershocks for this earthquake can be seen in *Figure 14*. This aftershock break is seen in the plotted data line in *Figure 15*. The section where it levels out shows that less aftershocks were being produced from that time onwards since the cumulative number of earthquakes stopped going up as rapidly. The same process was done for the 2024

mainshock and can be seen in *Figures 16* and *17*. The difference here is that the data stopped before leveling off showing that all the data after this event are aftershocks for it. This event was so recent that the aftershocks are still likely occurring and still likely to occur in the near future. This will level off at some point but has not yet. This data will be useful when comparing the plots built in Coulomb modeling software to the aftershock patterns from each of these events. We can determine these are the relative cut off for aftershocks by assuming that where there is a sudden decline in earthquakes is where aftershocks are essentially stopping. Omori's law states that the most aftershocks will occur directly after the mainshock and over time these will slowly come to a stop (Omori, 1894; Utsu et al., 1995). Based on this law we can assume that when we see these earthquakes slowly come to a sudden plateau on these excel plots is where we can assume the aftershocks stop.

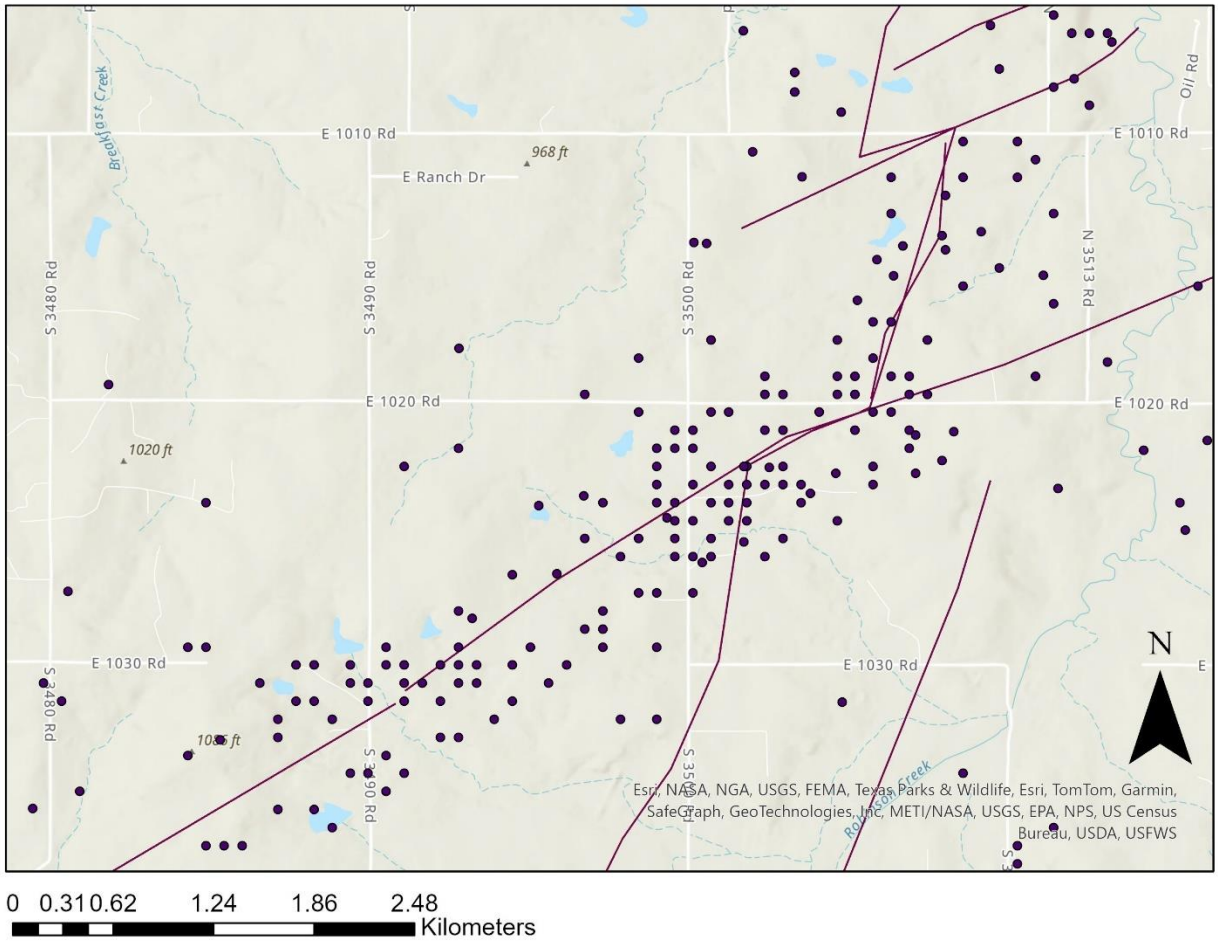

Figure 14: Aftershock location seismicity data from OGS across the Prague, OK fault site from November 6, 2011, to April 20, 2013.

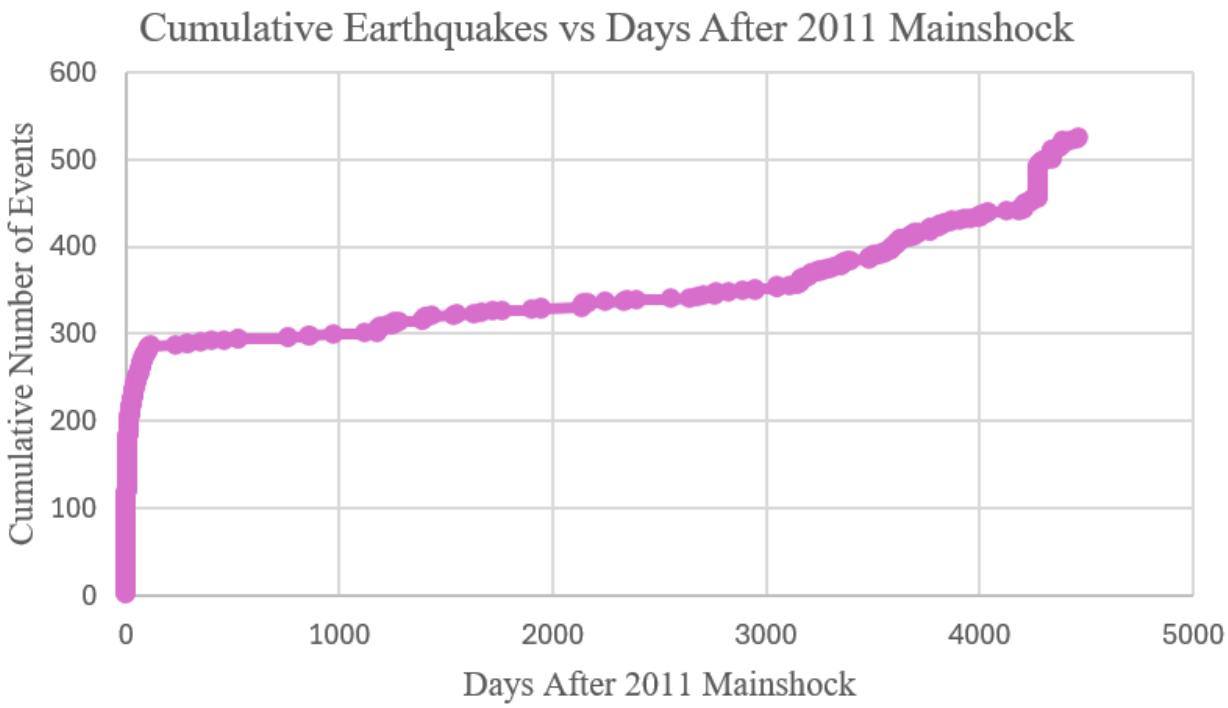

Figure 15: Excel plot showing where the aftershocks from the 2011 Prague earthquake break off. The x axis shows the days since the 2011 mainshock while the y axis shows the amount of cumulative earthquakes. day 0 indicates that those events occurred on the day of the mainshock rupture on November 6, 2011.The increase after 4,000 days is the 2024 earthquake and its aftershocks.

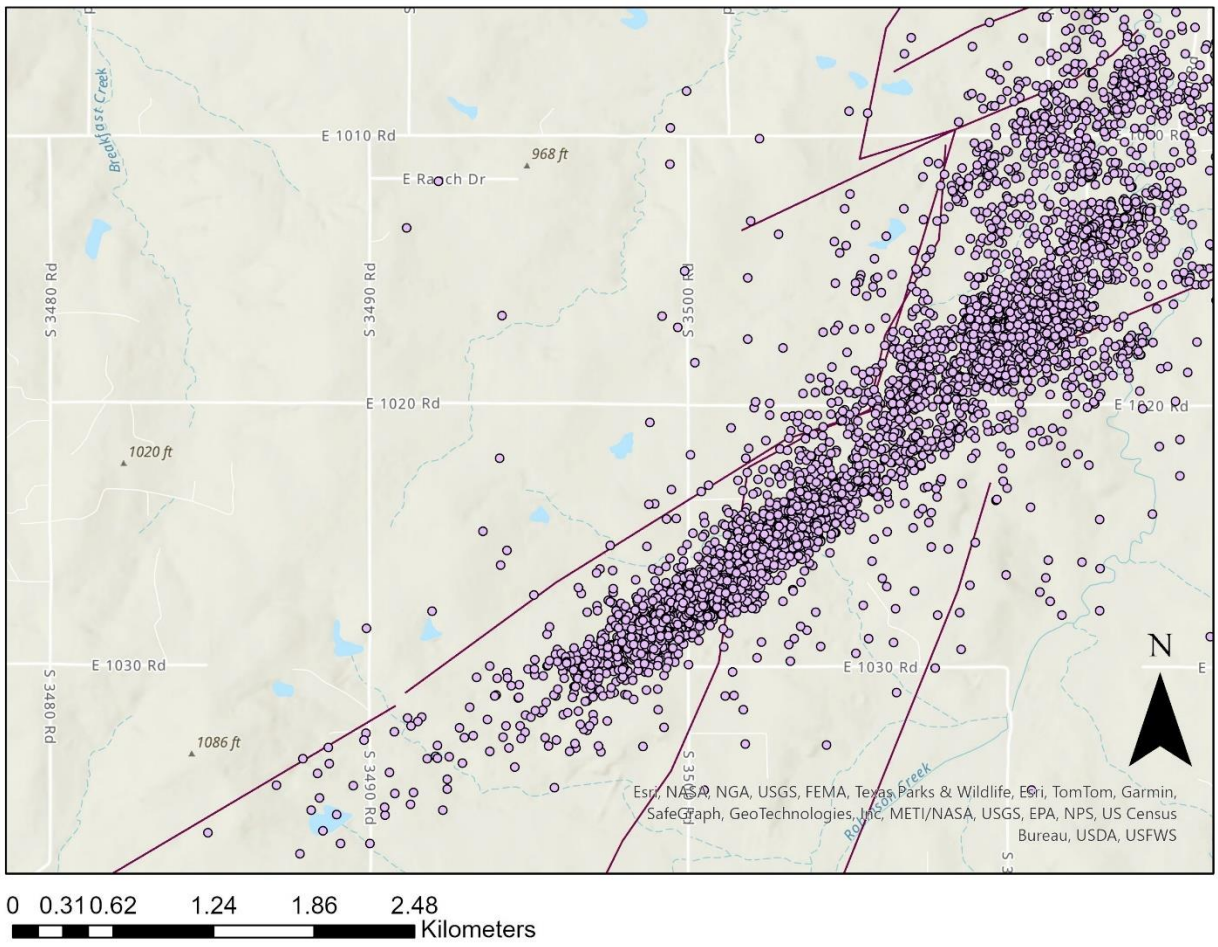

Figure 16: Aftershock location seismicity data from OGS across the Prague, OK fault site from February 3, 2024, to February 24, 2025

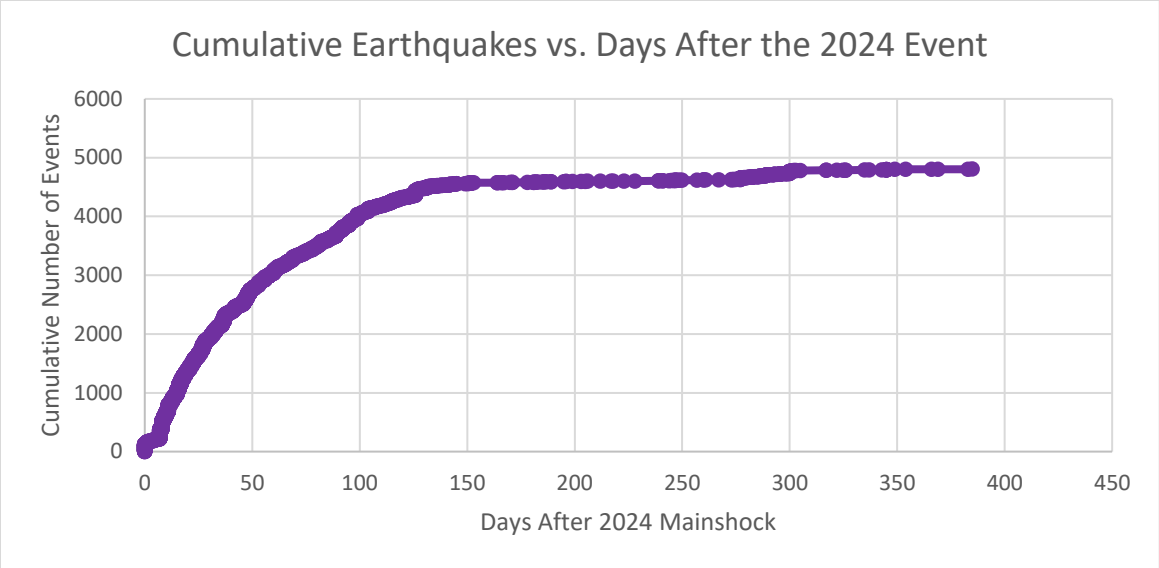

Figure 17: Excel plot showing that the aftershocks from the Prague 2024 event do not reach a breakoff point since our dataset only has a small number of aftershocks and time after this event occurred. The x axis shows the days since the 2024 mainshock while the y axis shows the amount of cumulative earthquakes. day 0 indicates that those events occurred on the day of the mainshock rupture on February 3, 2024.

The acceleration in seismicity prior to the 2024 event is interesting as it shows increased activity leading up to the 2024 Prague mainshock. Increased rate of foreshocks can be explained by the inverse power law which has been modified from Omori's law (Jones & Molnar, 1979; Peng et al., 2007). This law shows that foreshocks follow an upward pattern opposite of aftershocks and we expect them to increase leading up to a mainshock (Peng et al., 2007). Assumptions that these foreshocks change the stress distribution for the mainshock have been made before (Peng et al., 2007) and with the acceleration in seismicity prior to the mainshock for Prague 2024 we can assume these foreshocks are impacting the stress distribution for the mainshock.

3.2 Fault Mapping

Using the two seismicity catalogs for the SLF and surrounding areas, an in-depth analysis of seismicity along the associated faults was conducted in ArcGIS Pro. Fault lines were traced based on seismicity patterns, focusing on areas with increased data point density. Since this study primarily addresses the SLF, NEFZ, and surrounding pre-mapped faults, regions with minimal seismicity were excluded to maintain a manageable model complexity. The assumption that seismic clustering indicated the presence of a fault structure was used for this mapping. This mapping of the faults involved zooming in on seismic data points to identify clusters of high seismic activity. These clusters often had linear patterns to them which allowed for easy and straight fault line mapping. Bends in the clustering were interpreted as bends in these fault structures and were mapped as such. The location of each fault segment in the PTJ and faults surrounding the SLF are shown in *Figure 18* and an example of the zoomed in mapping of the NEFZ is shown in *Figure 19*. The minimum amount of points for this study to consider data points a cluster was in the 10s for the OGS data and the 100s for the Park et al., 2022 data. Some clusters had 10-30 data points for OGS while others had closer to 40-60. For the Park et al., data some were much higher with some reaching up to several hundreds. Additionally, the assumption of these structures to be straight lines was due to earthquakes in this area indicated the presence of vertical/subvertical strike slip faults. Placing a straight line through these clusters allowed for fault strands/lineaments to be estimated. Utilizing the Park et al. (2022) dataset, these fault locations were able to be located more precisely due to the increase in data resolution. This process helped complete a more complex and robust fault map, encompassing the NEFZ, SLF extension to the east, and the SLF synthetic/antithetic faults. End points for each of the faults were taken from the fault map in ArcGIS Pro by copying the coordinates at each end point seen in *Tables 3* and *4*

Additionally, focal mechanisms helped determine where the end of one segment ended and another began. This helped to determine the segments of each fault by looking at abrupt changes in dip to guide this placement of bends of a fault and new segments within a fault. This method aided in constraining these segmented points for areas of heightened seismicity.

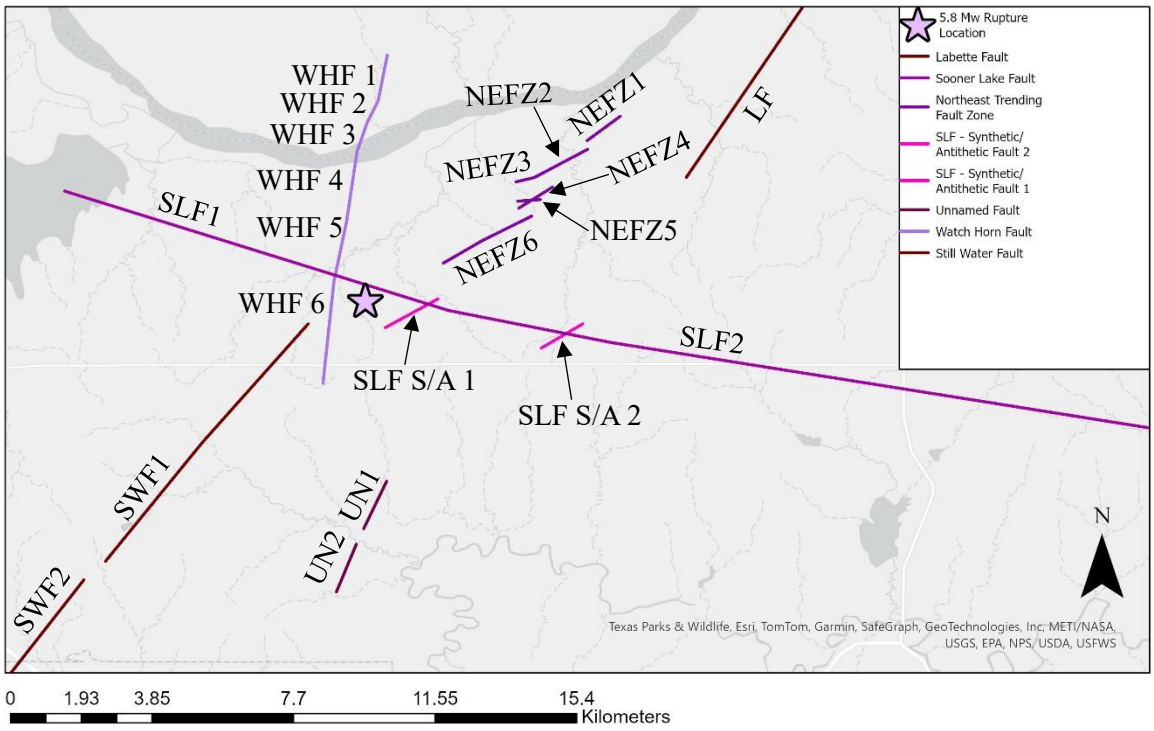

Figure 18: Fault segment locations for the Pawnee Triple Junction correspond to the values seen in Table 1. Purple star represents the hypocenter of September 3, 2016, M_w 5.8 rupture along the SLF in Pawnee, OK.

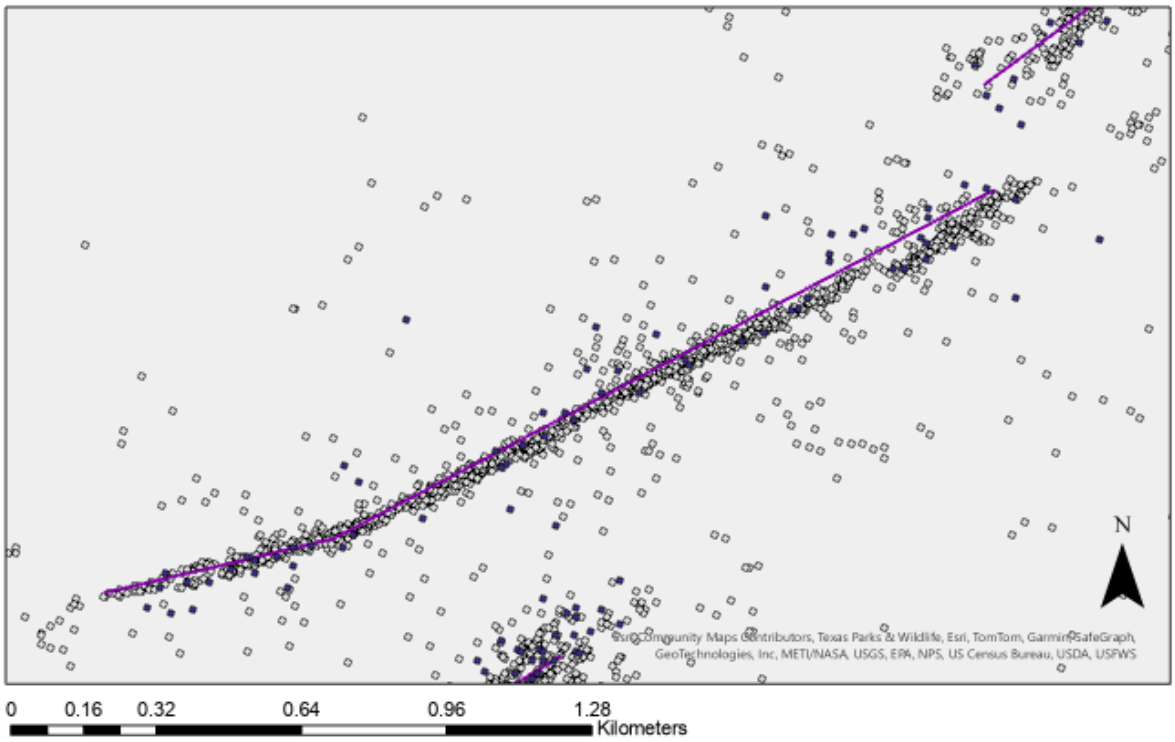

Figure 19: Zoom in view of the seismicity clustering in white from Park et al., 2022 data and purple from OGS data. Both data catalogs were plotted on top of NEFZ 2 and 3 to show how this aligning was conducted based on seismic clustering.

Focal mechanisms were also used to ascertain strike and dip values, which are further discussed and presented in *Table 5* in Section 3.3 of this thesis. These values were critical for utilizing Fault Slip Potential 2.0 and Coulomb Modeling Software 3.4, both of which will be discussed later in this methods section. For Prague, OK, the seismicity and focal mechanism data was provided from OGS and a similar approach to the SLF and surrounding area was taken. However, no faults were remapped for this site since the seismicity data aligned with the current OGS fault map and seismicity data of the aftershocks or did not indicate any mappable new structure locations. However, there could be some new structures based on the 2024 Prague data, just none we can map out yet. The focal mechanisms from OGS were utilized to determine the average dips of each

fault segment as well as the strike of each fault segment. These strikes and dips were needed as data inputs for FSP 2.0 and Coulomb Modeling Software 3.4.

Focal mechanism data provided by OGS was used to calculate the average dip for each fault segment in Pawnee and Prague, OK and is shown in *Tables 2* and *3*. This was done in ArcGIS Pro by determining dip amounts along each fault segment based on focal mechanism points plotted across each fault segment. This was done using the OGS focal mechanism catalogs for Pawnee and Prague, OK. Once dips were found along each fault segment, average dip measurements for each fault in these sites were calculated. This was done by taking the values of as many focal mechanism locations along each fault segment as possible (some had 3-4 and others had 10-15 or more). The sum of these dips was then divided by the number of focal mechanisms used to get the average value (*Equation 2*). These values are the ones seen in *Tables 2* and *3* and were used to make the Coulomb Modeling Software 3.4 model more realistic. This inclusion of dip data and fault complexity contributed to a more detailed and robust stress map, providing better insight into how factors such as slip and subsurface stress transfer may be contributing to rupture events. Faults lacking focal mechanisms were put as "-" in *Tables 3* and *4* to show no data was provided for them. Each of these fault segments were assumed to be 90° and vertical within Coulomb Modeling Software 3.4.

$$Average = \frac{(a_1 + a_2 + a_3 + \cdots + a_n)}{n}$$

Equation 2: Equation used for calculating the average dip value across each fault segment in the SLF area and Prague, OK.

Fault Segment	Lat Start (N)	Long Start (W)	Lat End (N)	Long End (W)	E Start	N Start	Average Dip	Length (km)	Strike
NEFZ1	36.46	96.88	36.47	96.87	690191.65	4037147.07	84	1	227°
NEFZ2	36.45	96.89	36.46	96.88	689071.01	4036117.37	81	1.28	237°
NEFZ3	36.45	96.89	36.45	96.89	688658.49	4035987.03	88	0.32	253°
NEFZ4	36.44	96.89	36.45	96.89	688734.69	4035278.19	79	0.92	232°
NEFZ5	36.44	96.89	36.45	96.89	688707.09	4035474.06	83	0.34	265°
NEFZ6	36.44	96.89	36.43	96.91	689275.51	4035091.45	85	2.07	232°
SW1	36.39	96.97	36.42	96.95	681944.61	4028786.13	87	4.49	215°
SW2	36.36	97.00	36.39	96.97	684177.94	4032054.16	86	4.46	213°
SLF1	36.45	97.00	36.42	96.91	678782.92	4035523.83	81	7.07	291°
SLF2	36.41	96.91	36.38	96.70	687269.67	4032467.3	86	13.47	282°
SLF S/A 1	36.41	96.93	36.42	96.91	685887.25	4031975.95	87	1.28	236°
SLF S/A 2	36.41	96.89	36.42	96.88	689316.81	4031492.57	84	1.06	234°
LF	36.45	96.85	36.50	96.82	692374.17	4036276.44	-	7.78	209°
UNF1	36.37	96.93	36.38	96.93	685524.65	4026527	-	1.71	201°
UNF2	36.35	96.94	36.36	96.93	684973.15	4024788.04	-	1.73	199°
WHF1	36.47	96.93	36.48	96.93	685595.84	4038144.6	-	1.62	189°
WHF2	36.46	96.93	36.47	96.93	685353.14	4037489.73	-	0.87	204°
WHF3	36.46	96.93	36.46	96.93	684923.35	4036711.08	-	1.03	195°
WHF4	36.44	96.94	36.46	96.93	684963.27	4034841.45	-	2.45	189°
WHF5	36.43	96.94	36.44	96.94	684719.65	4033177.65	-	2.18	190°
WHF6	63.40	96.94	36.43	96.94	684554.46	4030451.33	-	3.57	195°

Table 2: Table includes the values of average dip calculations for each fault/fault segment in the Pawnee Triple Junction. Additional information in this table includes the latitude start and end, longitude start and end, strike, total fault length, easting start, and northing start values for each fault segment in the SLF area.

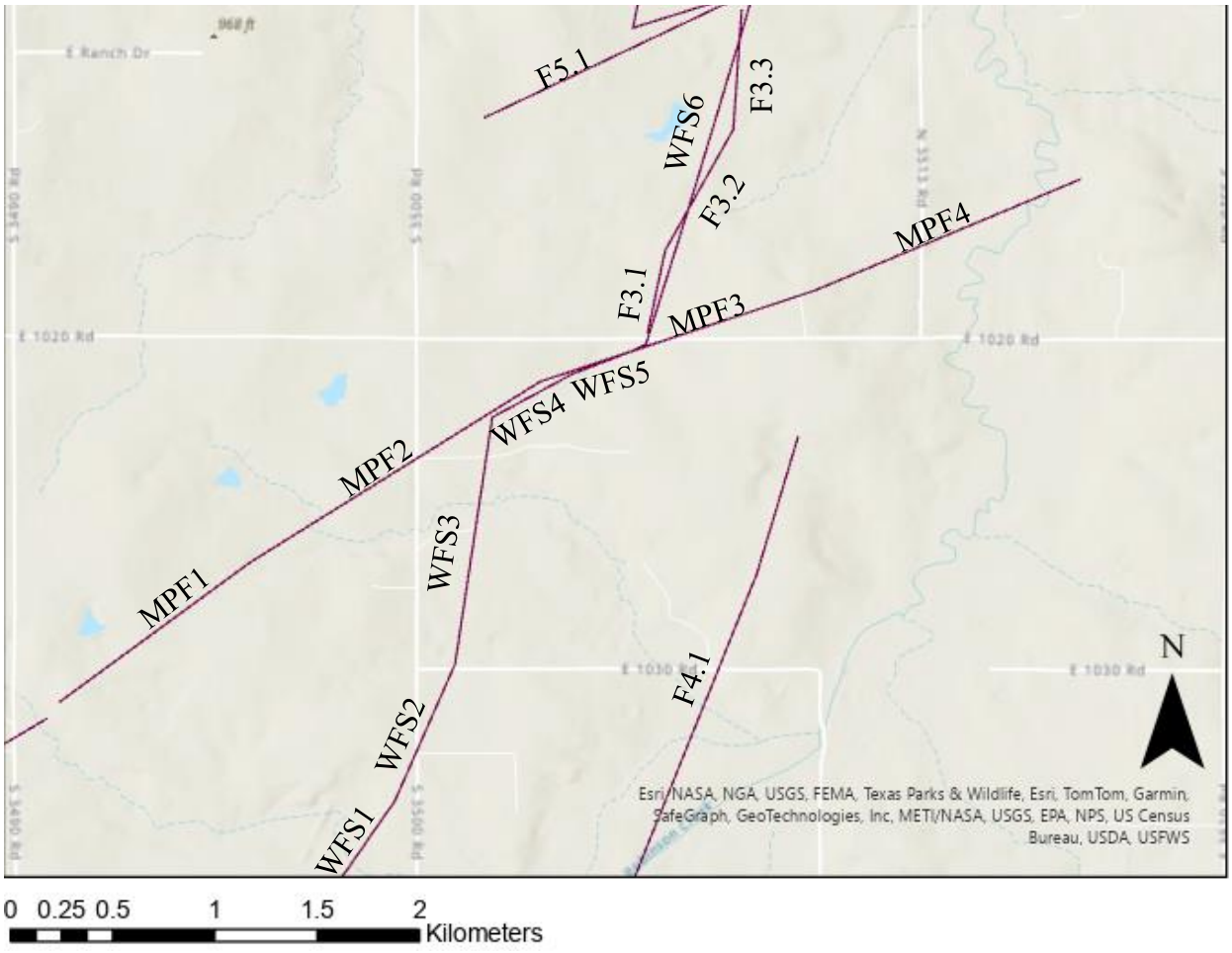

Figure 20: Fault segment locations for the Prague, OK site. Showcasing the segments of the Wilzetta Fault System (WFS) and Meeker-Prague Fault (MPF) as well as locations for the segments of the other three faults in the site (F3, F4, and F5)

Fault Segment	Lat Start (N)	Long Start (W)	Lat End (N)	Long End (W)	E Start	N Start	Average Dip	Length (km)	Strike
MPF1	35.52	96.78	35.52	96.79	700677.19	3932916.74	84	1.11	229°
MPF2	35.53	96.77	35.53	96.78	702551.54	3934544.74	87	1.76	232°
MPF3	35.54	96.75	35.53	96.77	703659.09	3935022.99	84	1.46	249°
MPF4	35.54	96.74	35.54	96.75	704676.63	3935544.61	81	1.37	243°
WFS1	35.51	96.77	35.51	96.77	702013.84	3932448.51	86	0.24	210°
WFS2	35.52	96.77	35.52	96.77	702246.75	3933151.52	75	0.78	198°
WFS3	35.53	96.77	35.52	96.77	702363.63	3934341.14	83	1.23	187°
WFS4	35.53	96.76	35.53	96.77	702720.80	3934593.86	79	0.51	241°
WFS5	35.54	96.76	35.53	96.76	702979.22	3934695.96	84	0.34	247°
WFS6	35.55	96.76	35.53	96.76	703361.81	3936436.69	84	1.86	194°
F3.1	35.54	96.76	35.54	96.76	703025.79	3935189.82	77	0.44	189°
F3.2	35.54	96.76	35.54	96.76	703301.7	3935757.82	68	0.68	207°
F3.3	35.55	96.76	35.54	96.76	703305.14	3936256.25	62	0.51	181°
F4.1	35.53	96.75	35.51	96.76	703581.01	3934269.11	-	2.15	195°
F5.1	35.55	96.76	35.55	96.77	703045.83	3936259.45	63	1.05	239°

Table 3: Table includes the values of average dip calculations for each fault/fault segment in the Prague, OK site. Additional information in this table includes the latitude start and end, longitude start and end, strike, total fault length, easting start, and northing start values for each fault segment in Prague, OK.

The strikes seen in *Tables 3* and *4* were measured during the fault-mapping portion of this thesis. The strike directions were determined based on the focal mechanisms along each fault segment. This allowed for the general strike direction to be known (N, S, E, or W). Then this strike was measured for all the faults in Pawnee and Prague, OK.

3.3 Field Work

Field work was conducted in collaboration with the Oklahoma Geological Survey (OGS) to collect aftershock data from the February 3, 2024, Mw 5.1 earthquake just north of Prague, OK. This effort involved deploying nodes with three geophone orientations (x, y, and z) to gather seismic

data to conduct the Coulomb stress analysis of the 2024 Prague earthquake in this thesis (*Figure 20*). The nodes remained buried for approximately one month before being retrieved by OGS for data extraction. This data was then compiled by the seismologists at OGS and exported as earthquakes (with location, depth, time, and size data) for this thesis. This catalog is the Prague 2011-2024 catalog provided by OGS, as previously mentioned. The data starting on Feb 3, 2024, came from the 2024 event and its aftershocks. The data prior to that date in this catalog came from prior fieldwork and instrument usage.



Figure 21: Deploying nodes to collect aftershocks of the 2024 M_w 5.1 earthquake in Prague, OK with OGS. a) Buried node b) Node used to collect aftershock data.

3.4 Fault Slip Potential

FSP 2.0 – a fault slip potential software – (Walsh III et al., 2017) calculates show much delta PP is required for slip to occur on a fault in its current stress state. It estimates the amount of stress

required for a fault to rupture based on the surrounding influences from both natural and human activities. The assumptions made to achieve these calculations include stress state, fault parameter, aquifer parameter, and well data sets. Fault parameters were taken from the previously made fault maps, either from this study directly or the OGS fault map. Aquifer data was taken from the USGS. The aquifer in the SLF and Prague, OK sites is the ADA-Vamosa aquifer (USGS). Aquifer thickness, porosity, and permeability were taken from the USGS for this portion of data inputs. Well data was taken from an online database by the Oklahoma Corporation Commission.

These assumptions allowed the program to determine how close to failure all the faults used in this study are in the current stress state of Oklahoma and it outputs this data in many forms including a Mohr circle showing how close to failure each fault is. The Coulomb stress change output was simplified into a change in shear stress since if faults are close to failure a change in shear stress makes a big impact in failure. FSP 2.0 was used to make sure these faults were close to failure since any faults far from failure would not be greatly impacted by shear stress changes. FSP 2.0 also gives a change in pore pressure (PP) needed for failure and a positive change in PP would decrease normal stress. Increasing Coulomb stress would have the same effect in decreasing normal stress in terms of failure. The friction sets the failure criterion which allows us to determine the amount of normal stress decrease or shear stress increase needed for failure to occur on a fault. This shear stress increase is looked at as Coulomb stress increase for this study in Coulomb Modeling Software 3.4.

This software was used to determine how close to failure the SLF and surrounding faults are in the current stress state of Oklahoma. This was conducted for all of the faults in the SLF and Prague sites. This information was combined with the results from the Coulomb Modeling Software to help determine how much slip along the NEFZ was needed for the SLF to reach its failure stress.

3.5 Stress Change Mapping

Input Needed:	Value Used:	Source:
Coefficient of Friction	0.68	Kolawole et al., 2019
Fault Locations	Varies (Tables 3 and 4)	OGS Fault Map and Hencey 2025 Remapping
Fault Strikes	Varies (Tables 3 and 4)	OGS Fault Map and Hencey 2025 Remapping
Fault Dips	Varies (Tables 3 and 4)	OGS Focal Mechanism Catalogs
Young's Modulus	80 GPa	Kibikas, 2021
Poisson's Ratio	0.25(-)	Kibikas, 2021
Fault Depth	0-15 km	OGS Seismicity Catalogs

Table 4: Inputs needed for stress modeling in Coulomb Modeling Software 3.4.

To calculate Coulomb Stress change amounts and patterns, Coulomb Modeling Software 3.4 in MATLAB was employed. This program is an earthquake modeling package that is provided by the USGS. It utilizes knowledge of earthquake mechanics, crustal deformation, and scientific observations and theories to make predictions on stress changes after earthquakes. It is specifically designed in order to model the Coulomb stress changes from these events that can be caused by many sources, including slip, as used in this thesis. The program solves these stress changes using the Coulomb Failure Stress change formula (*Equation 1*) to determine the impact on stress on receiver faults from a specific source. The numerical approach involves using finite rectangular fault patches, elastic principles (such as Okada's solutions, 1992), and specific functions such as Green's Functions. Once the fault geometry is input is complete, slip can be added to the source fault(s). After this, the program will calculate displacement and stress changes based on the previously discussed numerical approach and will output this visually with color-coded maps.

The model incorporates assumptions about fault locations, strikes, and dips, as previously discussed (e.g. Toda et al., 2011). Additionally, assumptions about the depth of interest, Poisson's

Ratio, and Young's Modulus are required. The depth was selected based on the deepest seismicity detected, which is 13.77 km (*Figure 21*). Consequently, a depth of 15 km is used for the SLF site to ensure the stress map extends just beyond previously measured seismicity. This depth will also be utilized for Prague, OK.

The Young's Modulus and Poisson's Ratio for these areas of Oklahoma were provided by Will Kibikas' dissertation (Kibikas, 2021). These values were a critical data input needed for the Coulomb stress analysis to run in Coulomb Modeling Software 3.4, so the results could show as accurate calculations as possible. These values can be seen in *Figure 22*. Since the majority of the earhtquakes seen in this study occur at a depth greater than 3.5 km the values of 80 GPa and 0.25 (-) are used since they are the averaged values for the deepest data points we have for the WZZ borehole data. This borehole is located in Oklahoma in the vicinity of the SLF. Due to this wells's proximity to the SLF and Prague, OK faults, this data set from Will Kibikas proved very useful in determining the Young's Modulus and Poisson's Ratio for these two sites.

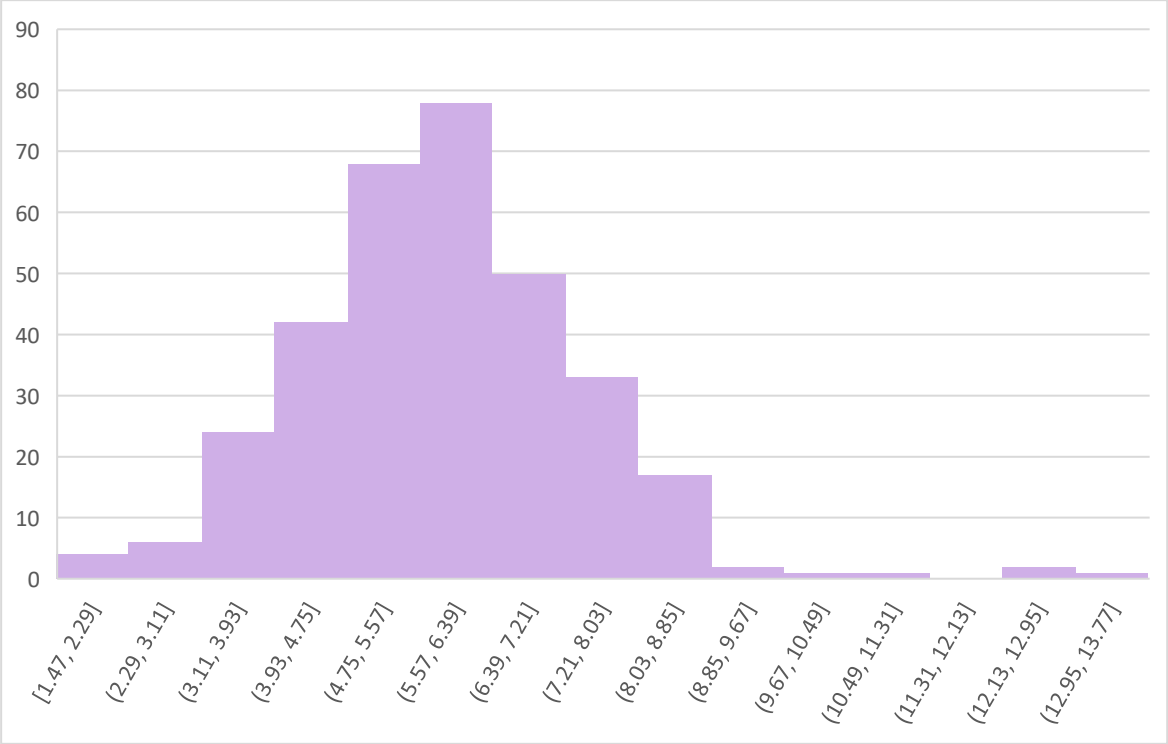

Figure 22: Depths of surrounding seismicity from the M_w 5.8 SLF earthquake in 2016. The deepest recorded depth was 13.36 km. Data from the USGS Pawnee County earthquake database.

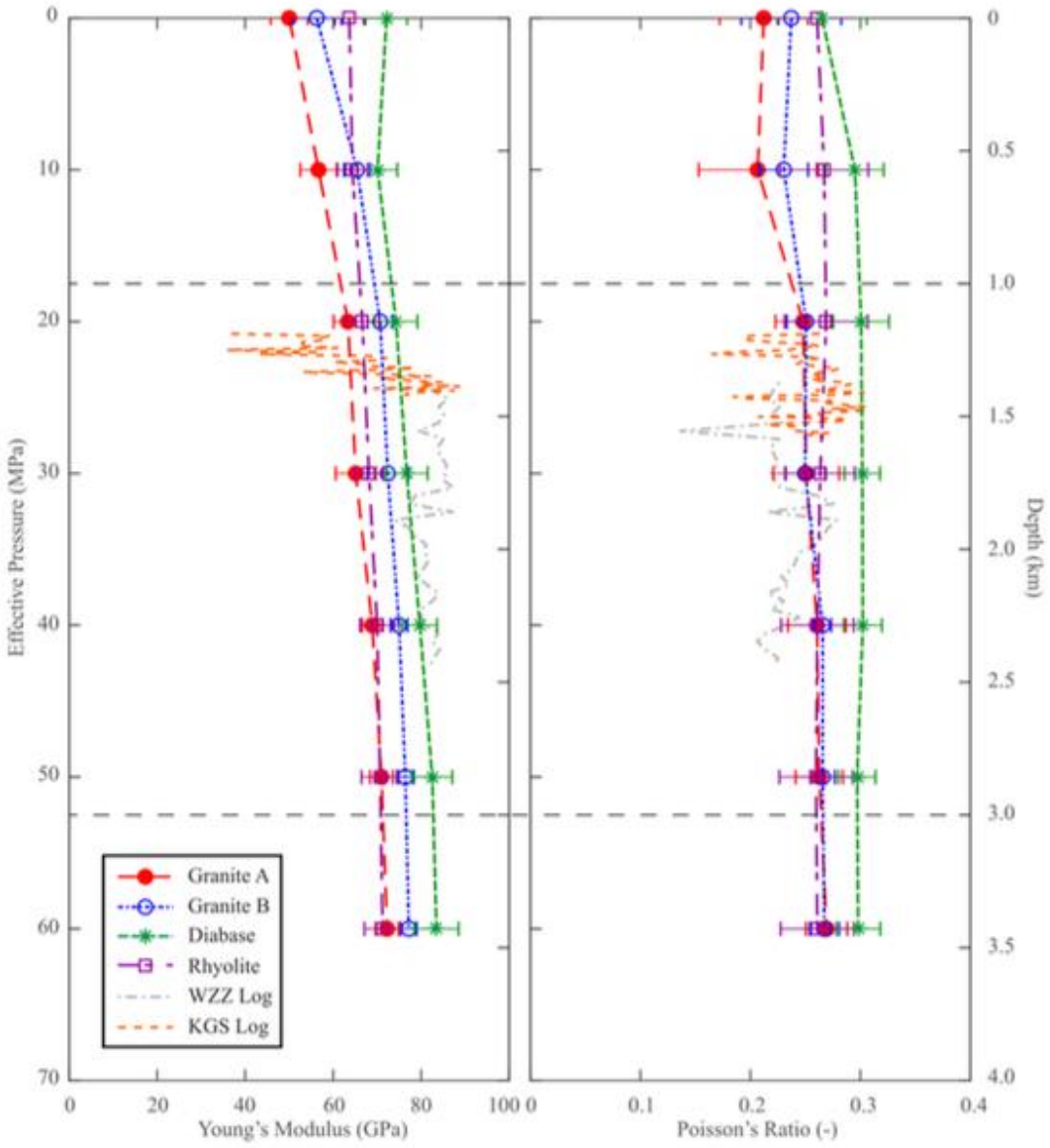

Figure 23: Young's Modulus and Poisson's Ratio values from a series of lab testing and borehole testing. WZZ log data was utilized from these graphs since this well is relatively close to the three locations studied in this thesis (Kibikas, 2021)

Within the Coulomb modeling software, the coefficient of friction was needed to run an accurate Coulomb stress change calculation. This coefficient of friction value was taken from Kolawole et al. (2019) as a value of 0.68 and was determined specifically for the basement granite faults in

Oklahoma. This was the final critical data assumption needed to complete the analysis and generate a successful Coulomb stress assessment for this thesis, and can be seen with the other inputs in *Table 5*.

RESULTS

4.1: Pawnee Triple Junction

4.1.1: Fault Mapping

Several faults were mapped with greater complexity in ArcGIS Pro as a result of the fault mapping portion of this thesis. The SLF is one of these and is a primary focus of this Coulomb stress analysis for Pawnee, OK. The fault's extent was revised to continue to the east beyond previous interpretations, based on seismicity and focal mechanism data compiled by OGS and Park et. al. 2022. Prior to the 2016 M_w 5.8 rupture there was not enough data to map out the location of this fault. Once this rupture occurred the aftershock data was used to increase the perceived fault extent (Pennington, 2017). An accumulation of aftershock data for years after this event made this seismicity data compilation more robust and even more useful for determining more precise locations for the SLF. An enhanced catalog that used machine learning from Park et al. (2022) also greatly increased the resolution of the aftershock data from the 2016 rupture to create a more robust seismicity data set once again. This machine learning was able to locate smaller seismic events than seismologists were able to which helped create more accurate fault mapping due to the increased seismicity resolution (Park et al., 2022). All of these advancements allowed for more in-depth mapping of the SLF as seen in *Figure 24*.

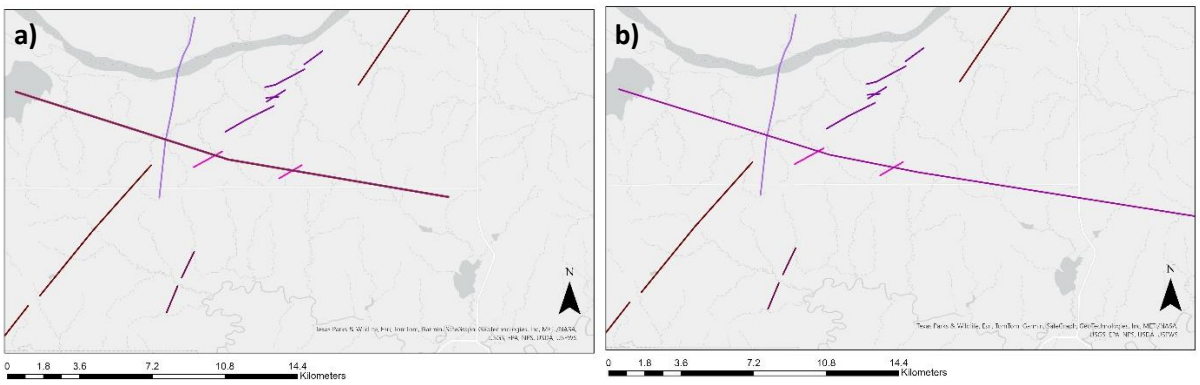

Figure 24: Comparison of previous mapping results for the Sooner Lake Fault and the mapping done for this fault in this thesis. a) the 2017 mapping of this fault (Pennington, 2017; Chen et al., 2017), b) the 2025 mapping of this fault with higher resolution data from years of aftershock data. These two photos show the extension of the SLF to the east as done in this thesis.

Additionally, the NEFZ was reinterpreted as a series of en echelon faults (fault zone) rather than a single fault line due to its high complexity and the segmented nature of associated seismicity. Previously, this structure was identified as a single fault, the Optimally Oriented Fault (OOF), which was considered an extension of the Labette Fault (Chen et al., 2017; Pennington, 2017). However, closer examination revealed that the NEFZ is a distinct fault zone that is slightly further north and segmented. The OOF is now only represented as a dashed line in the few figures that showcase it in this these for reference purposes. The OOF and laterally extensive Labette Fault that crosses most of Osage County were identified as an unconformity separating basement meta rhyolitic rocks to the northwest and rhyolitic rocks to the southeast (Denison, 1981); its classification as a fault is currently being evaluated by OGS staff. The updated seismicity dataset from the M_w 5.8 SLF rupture helped identify a more accurate location for the faults being activated in this location. Both the focal mechanisms from OGS and the seismicity data from Park et al.

2022 made the resolution of these faults clear enough to identify and map in a more robust way. This will aid in the increase of data resolution within this study and ones after it.

The last change to the fault map was the addition of the two synthetic/antithetic faults along the SLF called SLF Synthetic/Antithetic Faults 1 and 2 (SLF S/A F1 and SLF S/A F2). These two faults were only revealed very recently due to seismicity not occurring much along them until 2020. There was some seismicity along them before this, but it was a very small number of events. In 2020, this seismicity ramped up and created better clustering, which allowed for assumptions on structure locations to be made. These clusters showed seismicity clustering along the two locations of these small conjugate faults which made them mappable.

4.1.2: Fault Slip Potential 2.0

FSP 2.0 results showed how close to critical faults in the SLF site were. These values are shown in *Table 8* and plotted on *Figure 25* in a Mohr circle and show the calculated amount of increased pore pressure needed to make each fault segment slip. In this study, we are assuming stress increases would come from Coulomb stress instead of pore pressure so we are using the MPa stress values for increased pore pressure from FSP 2.0 as the amount of Coulomb stress increase needed for slip to occur. SLF1 and SLF2 are shown in *Figure 26*. Both faults need very little Coulomb stress added to them to produce slip along the fault. SLF1 (the segment where the M_w 5.8 rupture occurred) needed 0 MPa of Coulomb stress added for it to slip since it is critical in the current stress state of Oklahoma based on the assumptions we made about this fault and the stress parameters around it. SLF2 (the Eastern portion of the SLF) is close to critical and only needs 3.399 MPa of Coulomb stress added to slip. FSP 2.0 results for the Pawnee area show that many of the other faults near the SLF are critical or close to critical and several are not close to critical. These results are all good indicators of how much Coulomb stress change is needed for them to

rupture and gives good insight into where the Coulomb stress increases seen in the next few experiments would have the most impact on aftershocks.

Fault Segment	Δ PP to Slip (MPa)
NEFZ1	3.144
NEFZ2	0
NEFZ3	8.853
NEFZ4	1.200
NEFZ5	21.229
NEFZ6	0
SW1	18.326
SW2	21.912
SLF1	0
SLF2	3.399
SL S/A 1	0
SL S/A 2	0
LF	29.503
UNF1	47.071
UNF2	51.780
WHF1	76.077
WHF2	40.217
WHF3	61.384
WHF4	76.077
WHF5	73.636
WHF6	61.418

Table 5: Delta PP to slip values for each fault segment near the SLF showing how much coulomb stress increase in needed (in MPa) to cause each fault segment to rupture.

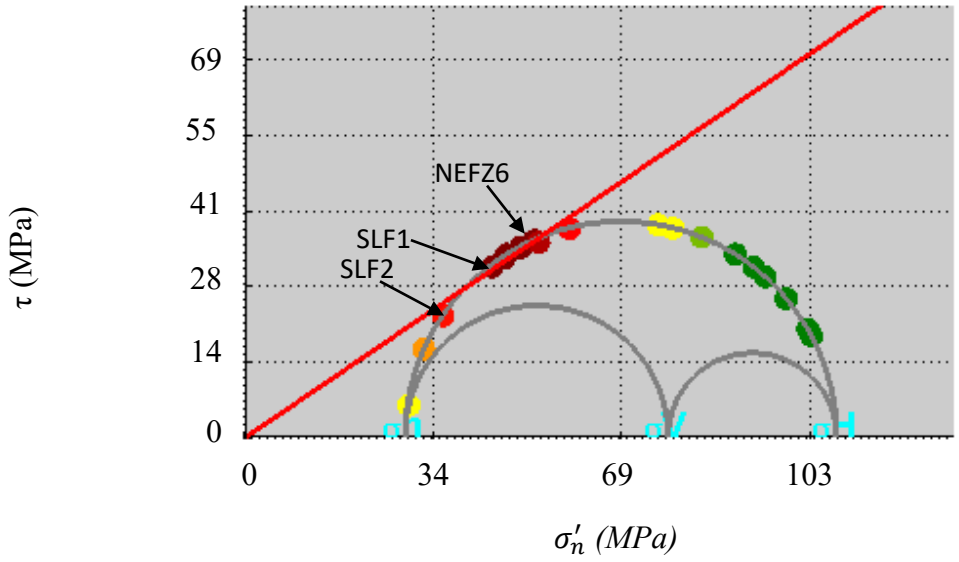

Figure 25: Mohr Circle for the Pawnee County Triple Junction Faults. Created in Fault Slip Potential 2.0 (FSP2.0). Indicating some faults are extremely close to failure in the current stress state of Oklahoma while others are not close at all. Two of these close to failure faults are the two segments of the SLF and are indicated with labels and arrows. The NEFZ6 is also labeled for reference.

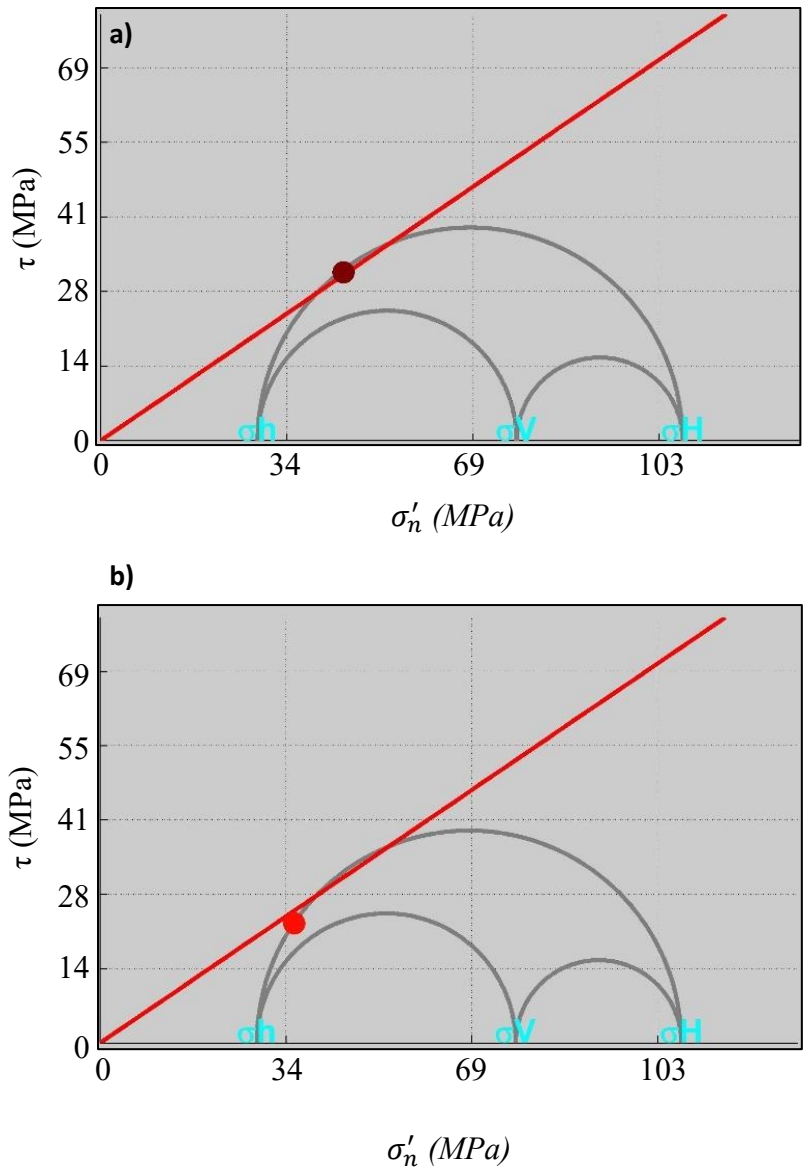

Figure 26: Mohr Circle for the Pawnee County Triple Junction Faults SLF1 and SLF2. a) SLF1 segment results showing this fault is on the Mohr-Coulomb failure envelope and is sitting at critical in the current stress state of Oklahoma b) SLF2 segment results showing this fault is just under the Mohr-Coulomb failure envelope and is close to critical in the current stress state of Oklahoma. Created in Fault Slip Potential 2.0 (FSP2.0).

4.1.3: Coulomb Modeling Results

Coulomb stress change experiment 1 is set up on a series of assumptions made for this area and the faults within it. This experiment was set up to do a reconstruction of the 2016 M_w 5.8 earthquake along the SLF segment 1. *Figure 27* shows the slip values on the SLF from the 2016 M_w 5.8 rupture event with the pink star representing the hypocenter (Moschetti et al., 2019). This slip model was used to determine the location, depth, and amount of slip to put on the SLF1 to reconstruct this rupture event in Coulomb Modeling Software 3.4. The depth chosen was 4-6 km deep based on the depth of greatest slip and a slip value of -1.25 meters was put over the purple highlighted portion of the SLF1 seen in *Figure 29*. -1.25 meters was used instead of 1.25 meters since Coulomb modeling software 3.4 uses negative slip values for left lateral slip and positive slip values for right lateral slip. These were the main assumptions made for the fault itself since depth and slip amount were the two factors that could have been done in many ways. The other assumptions included the friction coefficient, Poisson's Ratio, Young's Modulus, and the strike, dips, and locations of each fault segment. Once all of this was input into the Coulomb model the results were able to be output.

This Coulomb stress change calculation was done for the depth of 4-6 km with a friction coefficient of 0.68 since that is the friction coefficient of Oklahoma basement rocks (Kolawole et al., 2019). 4-6 km was chosen since it encapsulates the depth of the rupture and the depth of the maximum slip value. Additionally, other variations of depth were chosen but this depth segment hosted the cleanest Coulomb modeling results whereas wider depth segments caused errors and outliers in it. Therefore, we decided to assume that 4-6 km would host the best results since the 2 km segment outputs the cleanest data. The results show four lobes of negative Coulomb stress change and four lobes of positive Coulomb stress change. These positive lobes are shown in warm colors of red,

orange, and yellow, while these negative lobes are shown in cool colors of dark to light blues. The reds indicate the areas of greatest positive Coulomb stress change, and yellows show a lesser positive Coulomb stress change. The darkest reds indicate a Coulomb stress change of 0.5 MPa and goes to white at 0 MPa with the oranges and yellows falling between these values. The darker the blue color indicates areas of greater negative Coulomb stress change while the lighter blues indicate areas with smaller amounts of negative Coulomb stress change. The darkest blues indicate a Coulomb stress change of -0.5 MPa and goes to white at 0 MPa, with the lighter blues falling between these values. The different lobe patterns give a good indicator of where aftershocks are likely to occur since Coulomb stress increases the likelihood of aftershocks. The positive lobes strongly correlate with the aftershock patterns, and the negative lobes strongly correlate with the areas lacking aftershocks, which is what we would expect to see in a correctly constructed Coulomb stress model. Therefore, this shows that the model was very successful in creating an estimated Coulomb stress change plot since the reconstruction of the M_w 5.8 rupture in 2016 matched the aftershock patterns seen in real data. *Figure 28* shows this Coulomb stress construction for experiment 1

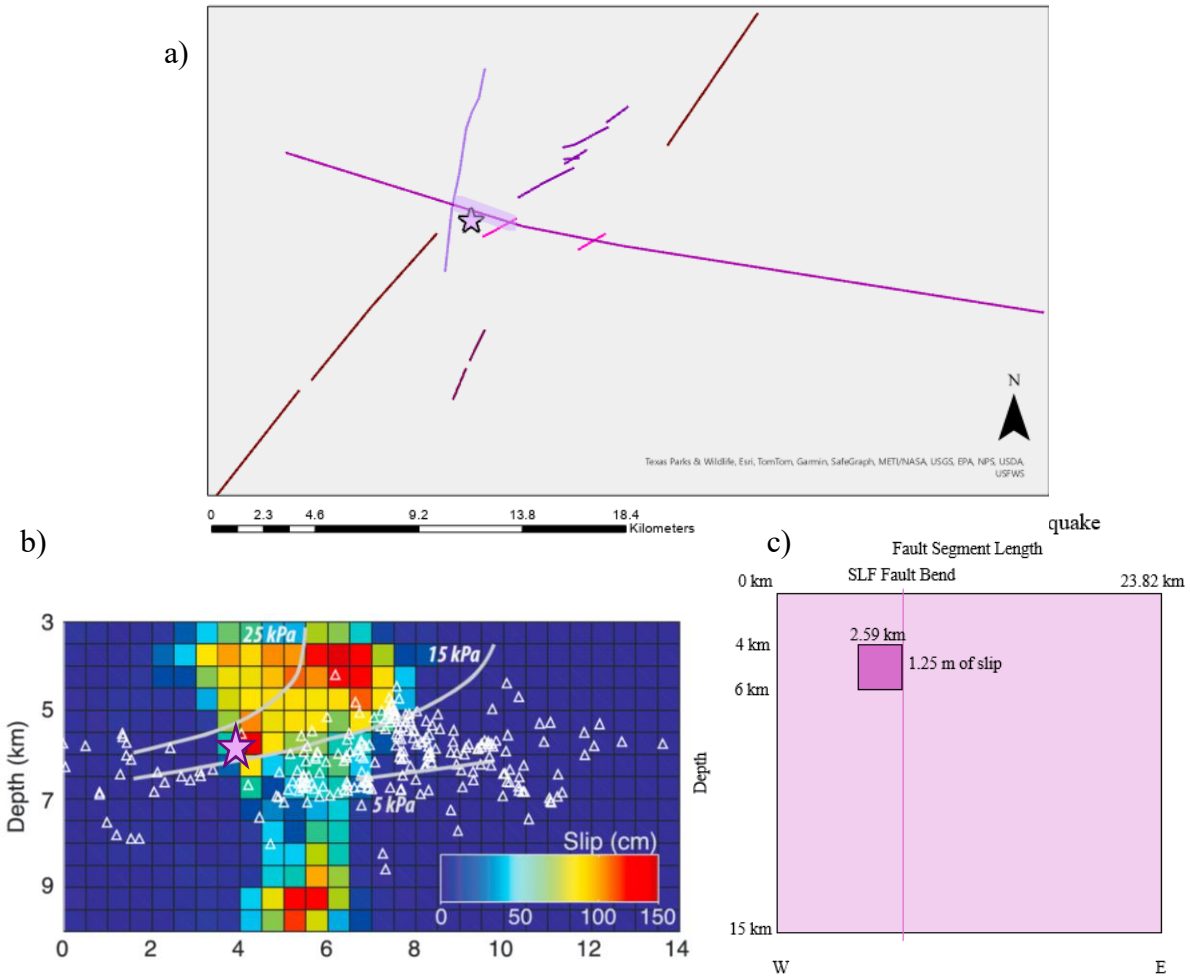

Figure 27: Model set up parameters for the Coulomb Modeling Software 3.4 Coulomb stress mapping in the recreation of the M_w 5.8 earthquake. a) Pawnee Triple Junction with the added slip in the model along the Sooner Lake Fault. The section highlighted in light purple represents an added slip of -1.25m (negative for left lateral slip in Coulomb modeling software 3.4). This value was programed into experiment 1 within Coulomb modeling software 3.4. b) The published slip model used for the September 3, 2016, M_w 5.8 rupture event along the Sooner Lake Fault. The earthquake hypocenter is represented by the purple star (Moschetti et al. 2019). c) Slip diagram at depth showing how slip was distributed into the subsurface across the length of the purple highlighted section of the Pawnee Triple Junction in part a of this figure.

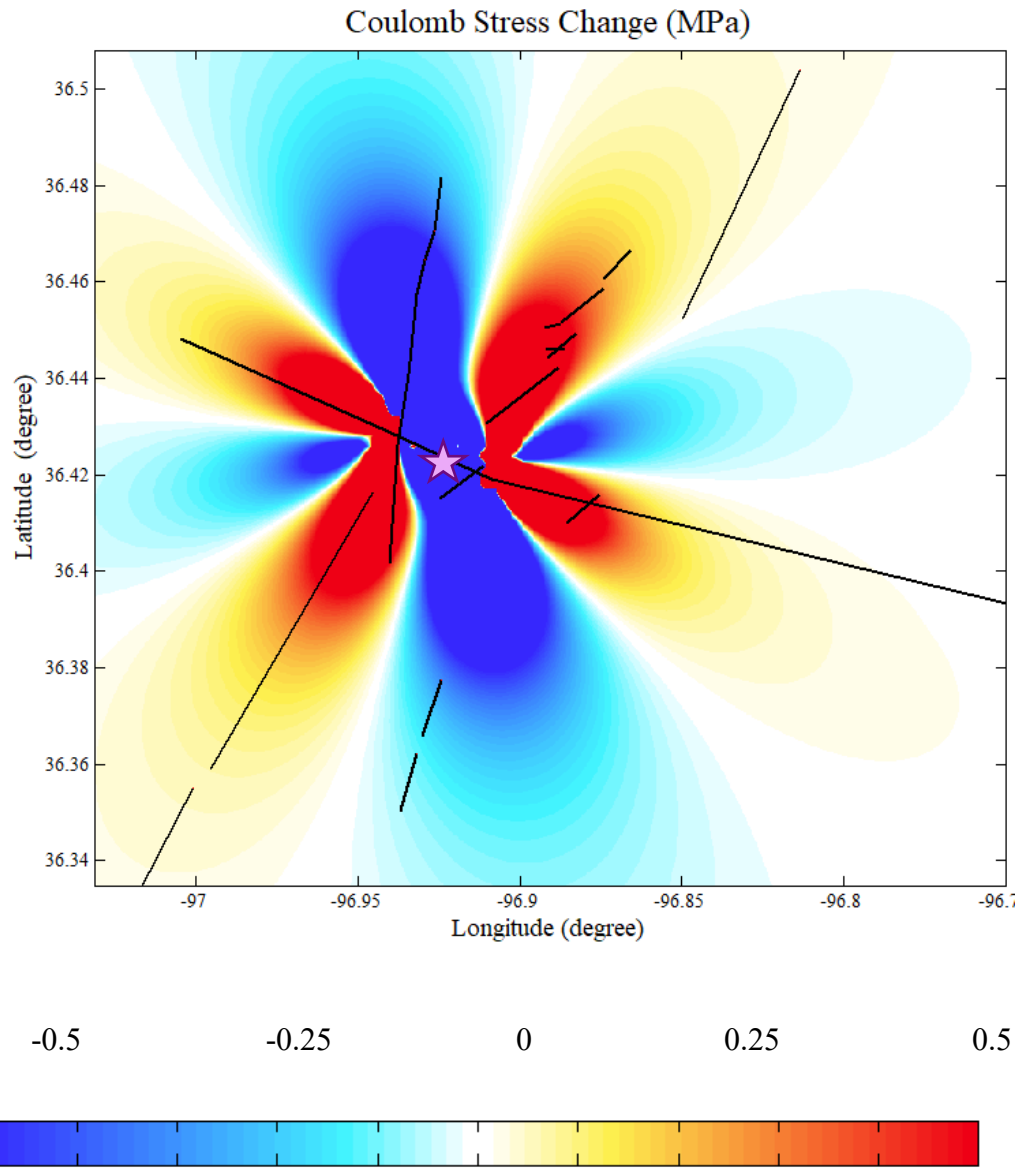

Figure 28: Reconstruction of the September 3, 2016, M_w 5.8 earthquake along the Sooner Lake Fault in the Pawnee County Triple Junction. Image shows a Coulomb stress change in map view with the purple star representing the hypocenter for the main rupture event.

The results of this Coulomb stress change plot show four negative Coulomb stress change lobes and four positive Coulomb stress change lobes. These four positive lobes align nicely over the SLF segments, the SWF, and the NEFZ segments, while the four negative lobes align well over the

WHF segments and UNF segments. The negative Coulomb stress change under and around the location of the mainshock is seen due to this location experiencing a stress drop when slipping during the rupture. Coulomb stress can increase in this area shortly after due to aftershocks nearby; however, Coulomb stress changes to this complexity were not mapped out for the sites of this study but is something to keep in mind when observing aftershock patterns. This is why aftershocks can still occur here but don't occur often in the other negative lobes. Aftershock patterns will be compared to these lobes in the discussion section of this thesis.

ArcGIS Pro was used to make a time map of seismicity on and near the SLF to see the migration patterns in seismicity from the M_w 5.8 rupture to June 5, 2023. This time plot is seen in *Figure 29* and shows some clear migration patterns to be discussed in the discussion portion of this thesis. These time plots are a new addition to the understanding of the SLF and its M_w 5.8 rupture in 2016. This allowed more insight into how the Coulomb stress change patterns impacted seismicity migration over time.

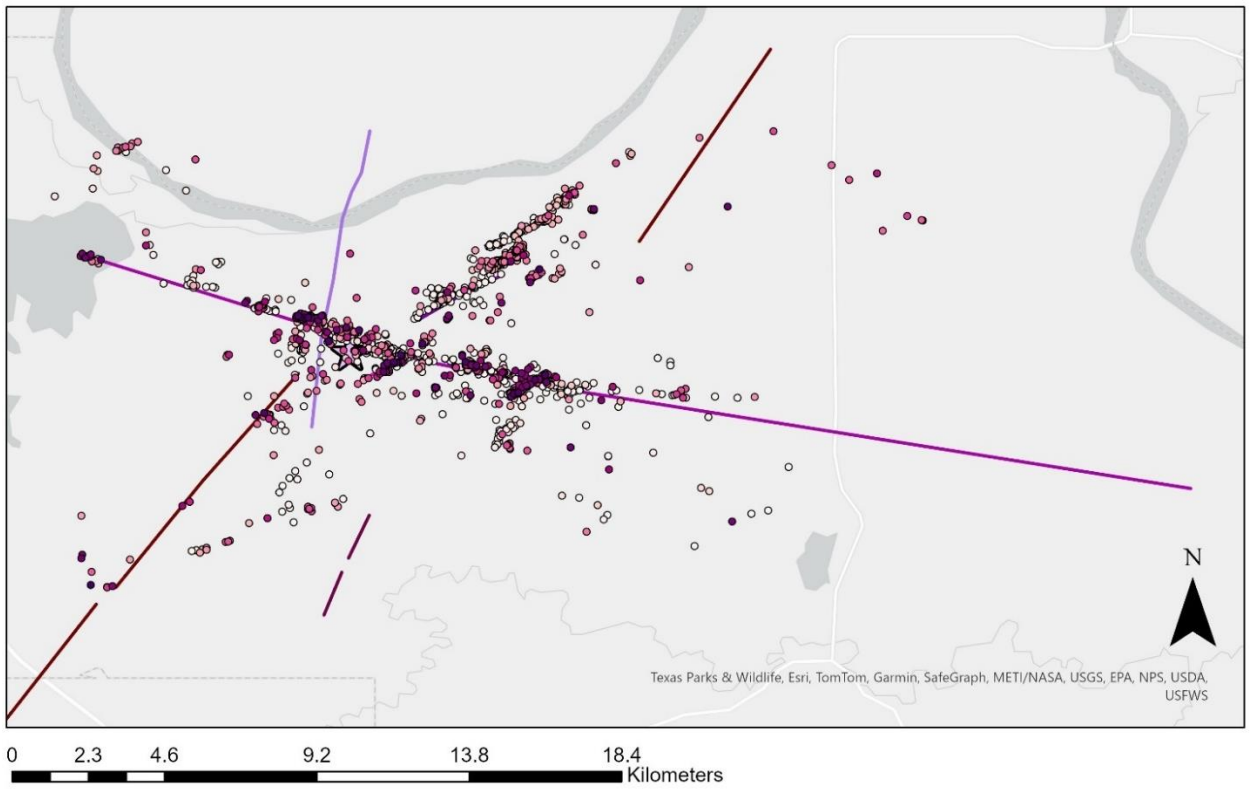

Figure 29: Seismicity migration over time across the SLF and surrounding faults from the M_w 5.8 rupture to June 5, 2023. This shows how aftershocks propagated from the 2016 M_w 5.8 earthquake along the SLF to the other faults surrounding it. Lighter colors indicate earthquakes occurring first and darker ones indicate the more recent earthquakes.

Experiment 2 for the SLF consisted of adding slip along NEFZ segment 6 to determine how different magnitudes of slip along this segment of the NEFZ would increase Coulomb stress values along the SLF. The goal of this was to see if this Coulomb stress increase would be high enough to cause a rupture or not. This scenario was constructed to try and determine how much slip was needed for the 2016 M_w 5.8 rupture to occur, since one hypothesis is that aseismic slip

along NEFZ6 (previously called the OOF) caused the SLF to rupture (Chen et al., 2017). This was tested by adding different amounts of slip along NEFZ6 to get a Coulomb stress change plot across the SLF and surrounding faults. This was done for slip values ranging from 0.007 meters to 0.5 meters. This section of the NEFZ is highlighted in purple in *Figure 30,* and the slip patch is also shown in *Figure 30*. After this, a second test was done to calculate the exact Coulomb stress change for the hypocenter of the 2016 M_w 5.8 rupture along the SLF to see the exact value of Coulomb stress change for this location. The slip values used for this portion of the testing were the same for the first portion of this hypothesis testing. The results of this experiment are shown in *Figure 31* and *Table 6*. The results of this Coulomb stress change plot show four negative Coulomb stress change lobes and four positive Coulomb stress change lobes.

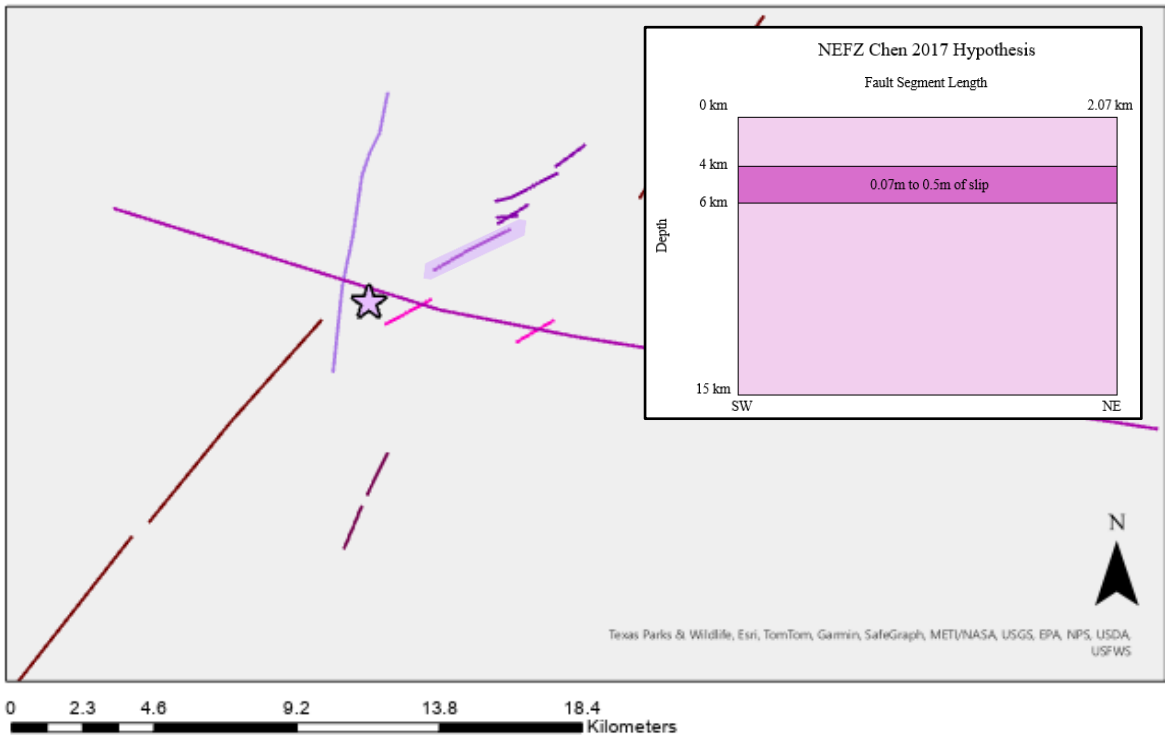

Figure 30: Pawnee Triple Junction with slip added to the NEFZ segment 6. The section highlighted in light purple represents an added slip of 0.007-0.50 meters. This value was programed within Coulomb modeling software 3.4 to get the results for the Chen et al. (2017) hypothesis. Overlain is the slip diagram at depth shows how slip was distributed into the subsurface across the length of the purple highlighted section of the NEFZ.

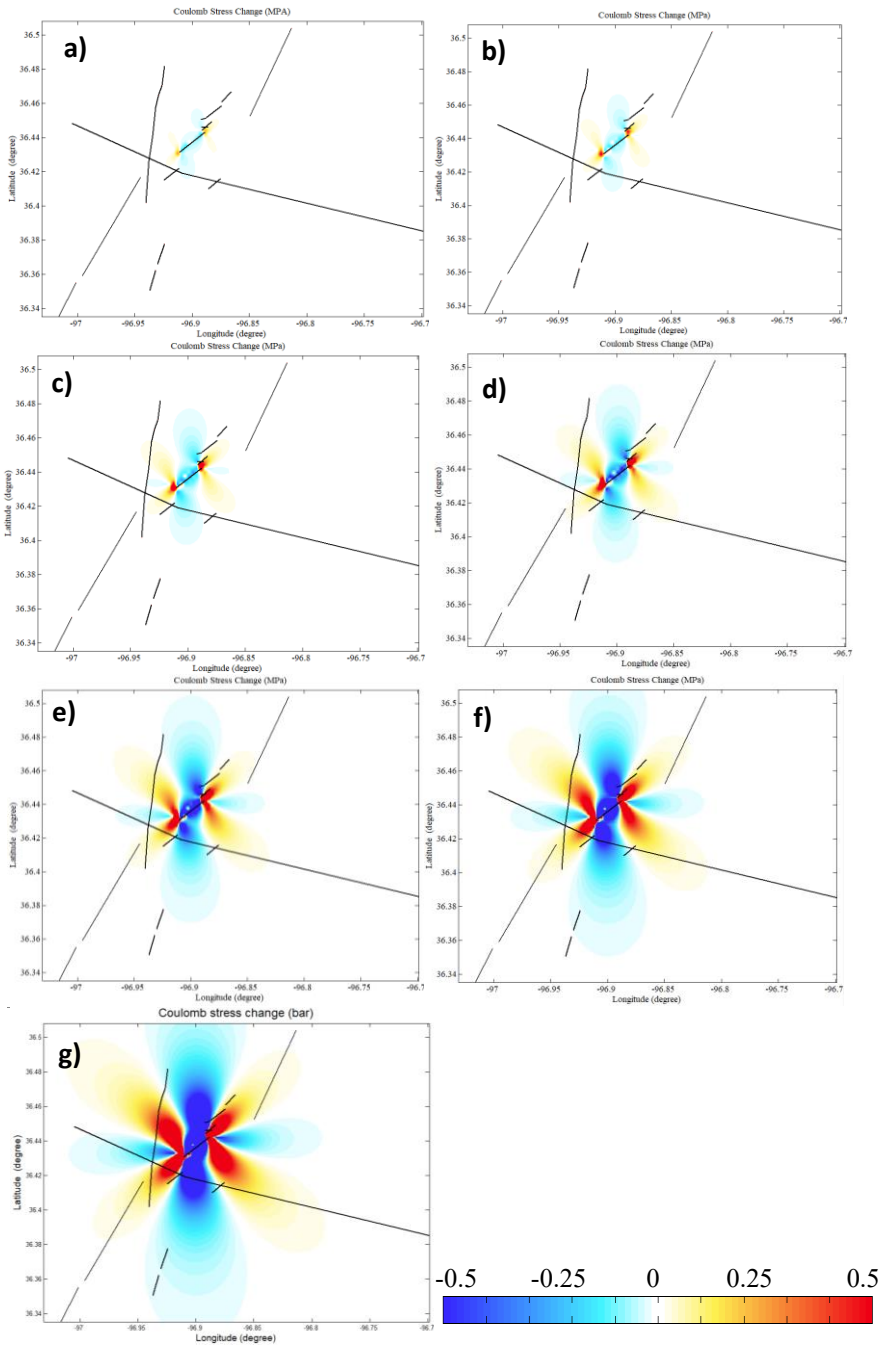

Figure 31: Coulomb stress change plots in MPa showing how differences in slip magnitude along the NEFZ6 fault segment impacted coulomb stress changes along the hypocenter of the 2016 SLF earthquake. a) 0.007 meters of slip along NEFZ6, b) 0.015 meters of slip along NEFZ6, c) 0.031 meters of slip along the NEFZ6, d) 0.063 meters of slip along NEFZ6, e) 0.125 meters of slip along NEFZ6, f) 0.25 meters of slip along NEFZ6, g) 0.5 meters of slip along NEFZ6.

Fault Segment with Added Slip	Slip Amount (m)	Coulomb Stress Change (MPa)
NEFZ6	0.007	0.0086
NEFZ6	0.015	0.0156
NEFZ6	0.031	0.0323
NEFZ6	0.063	0.0657
NEFZ6	0.125	0.1303
NEFZ6	0.25	0.2607
NEFZ6	0.5	0.5214
SLF1	-0.007	-0.0145
SLF1	-0.015	0.0116
SLF1	-0.031	0.0239
SLF1	-0.063	0.0485
SLF1	-0.125	0.0963
SLF1	-0.25	0.1926
SLF1	-0.5	0.3852

Table 6: Table includes the values of slip amount added to NEFZ6 and SLF1 and the coulomb stress change for the exact location of the hypocenter for the 2016 M_w 5.8 earthquake along the SLF at 96.929W, 36.425N, and 5.6km depth (hypocenter location from USGS)

Experiment 3 on the SLF tested a secondary hypothesis. This hypothesis comes from Walter et al. 2017 and states that slip along the Western portion of the SLF is what caused the 2016 M_w 5.8 rupture to occur along the SLF. This was tested in Coulomb Modeling Software 3.4 by putting differing amounts of slip magnitude along the portion of the SLF hypothesized by Walter et al. 2017. This test aimed to gain insight into what amount of slip would be required to create enough positive Coulomb stress at the hypocenter of the 2016 M_w 5.8 rupture to cause them to occur. The same slip values as used for experiment 2 were used in experiment 3 to keep them consistent, 0.007 meters to 0.5 meters. However, these values were put in as -0.007 meters to -0.5 meters since SLF1 is a left-lateral strike-slip fault, and Coulomb modeling software has left-lateral slip as negative values. The section of the SLF where this slip was added is highlighted in purple in Figure 31, and the slip patch is shown in *Figure 32.* This shows how the model was set up in the subsurface along

the SLF segment 1. The same depth values as the NEFZ hypothesis (4-6 km) were used to keep consistency. NEFZ6 had a right-lateral strike slip, so the values for that one were inputted in Coulomb Modeling Software 3.4 as positive values (since this is how the program recognizes right-lateral slip values). Additionally, the same model was used, but the fault receiving slip was changed. The results for this can be seen in *Figure 33* and *Table 6*. The results of this Coulomb stress change plot show four negative Coulomb stress change lobes and four positive Coulomb stress change lobes.

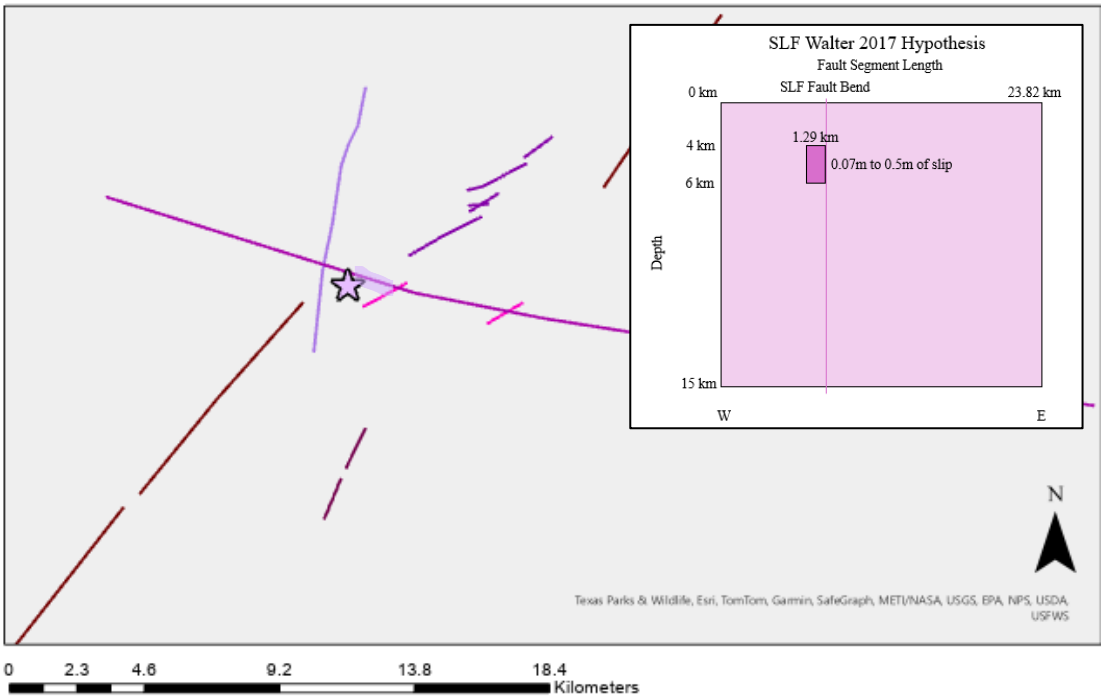

Figure 32: Pawnee Triple Junction with slip added to the Sooner Lake Fault segment 1 (SLF1). The section highlighted in light purple represents an added slip of 0.007-0.50 meters. This value was programmed within Coulomb modeling software 3.4 to get the results for the Walter (2017) hypothesis. Overlain is the slip diagram at depth shows how slip was distributed into the subsurface across the length of the purple highlighted section of the SLF.

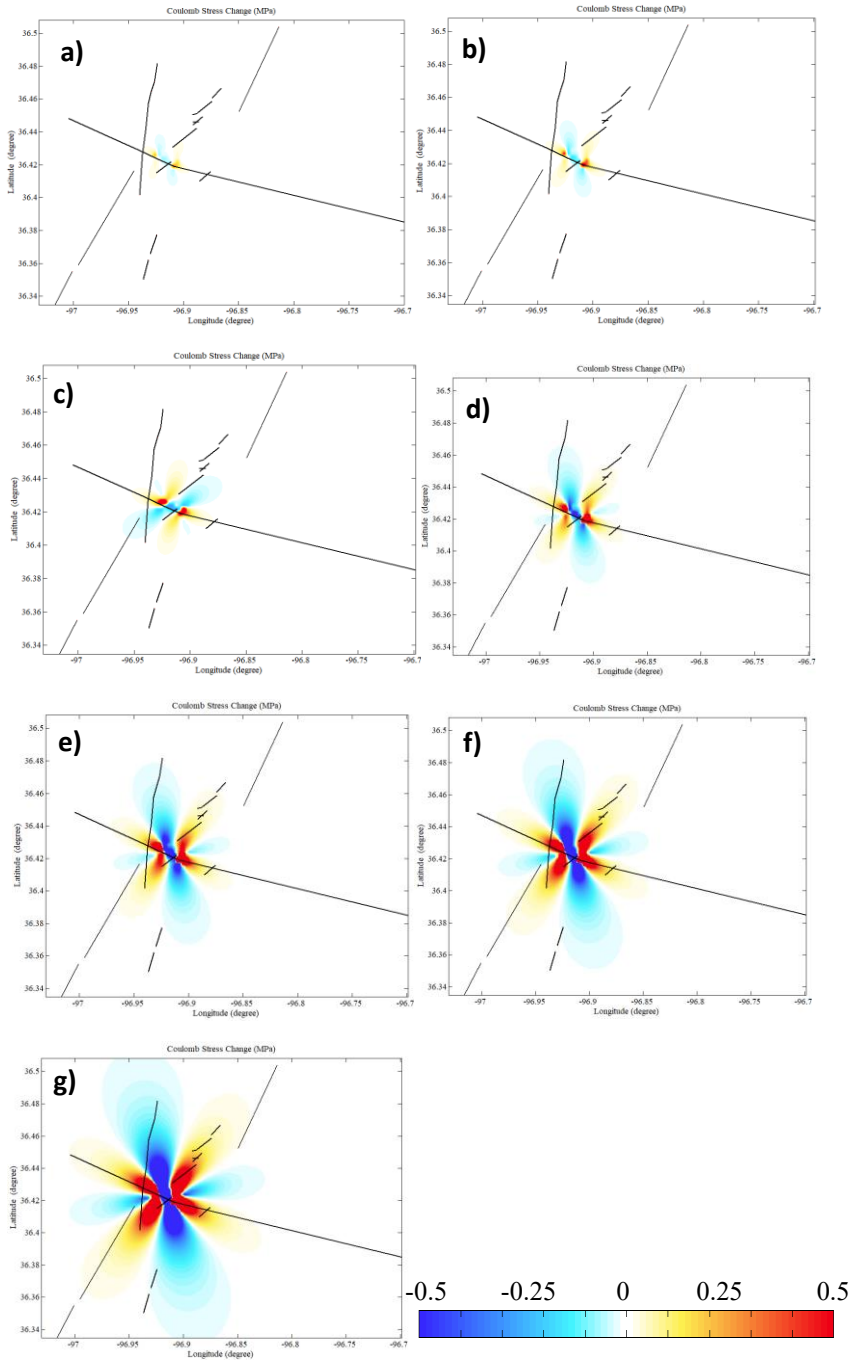

Figure 33: Coulomb stress change plots in MPa showing how differences in slip magnitude along the SLF impacted coulomb stress changes along the hypocenter of the 2016 SLF earthquake. a) -0.007 meters of slip along SLF1 b) -0.015 meters of slip along SLF1, c) -0.031 meters of slip along SLF1, c) -0.063 meters of slip along SLF1, d) -0.125 meters of along SLF1, e) -0.25 meters of slip along SLF1, f) -0.5 meters of slip along SLF1.

Figure 34 shows the Coulomb stress changes for slip along the SLF1 and NEFZ6 simultaneously to see how these two events interact on the hypocenter of the 2016 mainshock. The numerical results of this are shown in *Table 7*, and it shows that more positive Coulomb was added to the 2016 mainshock than when either foreshock was considered individually.

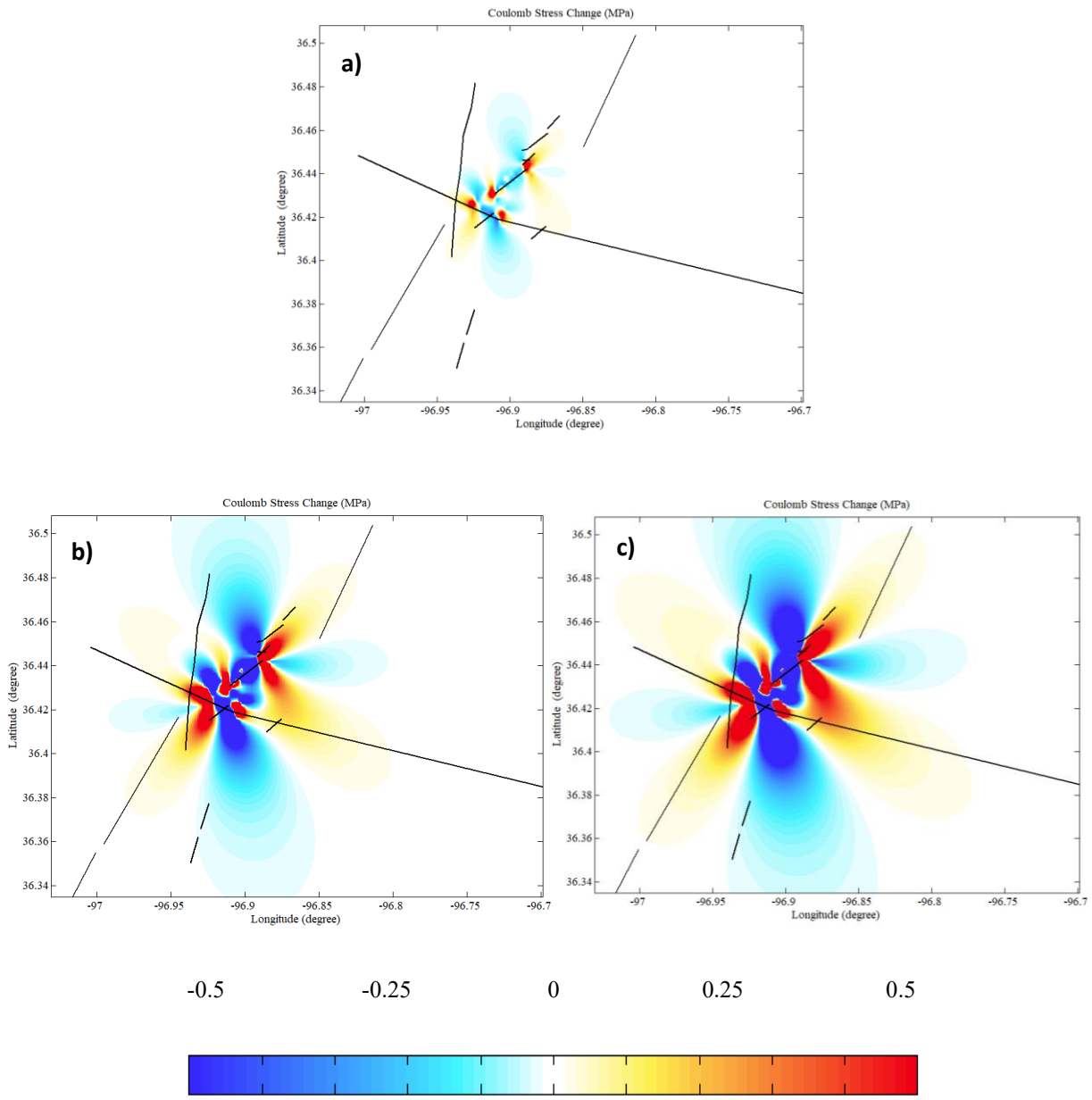

Figure 34: a) 0.031 meters of slip along the SLF1 and NEFZ6, b) 0.25 meters of slip along the SLF1 and NEFZ6, c) 0.50 meters of slip along the SLF1 and NEFZ6.

Slip Amount on SLF1 and NEFZ6 (m)	Coulomb Stress Change (MPa) on 2016 Mainshock Hypocenter
0.007	0.0241
0.015	0.0516
0.031	0.1066
0.063	0.2166
0.125	0.4298
0.25	0.8597
0.5	1.7194

Table 7: Table includes the values of slip amount added to NEFZ6 and SLF1 (at the same time) and the Coulomb stress change for the exact location of the hypocenter for the 2016 M_w 5.8 earthquake along the SLF at 96.929W, 36.425N, and 5.6km depth (hypocenter location from USGS).

4.2 Prague, OK

4.2.1: Dip Calculations

Equation 2 was used again with the ArcGIS Pro focal mechanism data provided by OGS. These results are displayed in *Table 4* and show the average dip values for each fault segment in the Prague, OK site. The addition of these dip values helped to generate a model that is both more realistic and more complex. This aided in providing better insight into the impact factors, such as slip and subsurface stress transfer may be contributing to rupture events along these faults and the aftershock patterns seen. This model was then built in Coulomb modeling software 3.4, where two experiments were conducted to test the questions proposed in this thesis.

4.2.2: Fault Slip Potential 2.0

FSP 2.0 results showed how close to critical faults in the Prague, OK site were. These values are shown in *Table 8* and plotted on *Figure 35* in a Mohr circle. This table shows the amount of positive Coulomb stress change needed for each fault segment to slip. *Figure 36* shows that MPF3 and

WF2 are or are extremely close to being critically stressed. These fault segments are the segments where the 2011 and 2024 main shocks occurred, respectively. A very minimal Coulomb stress increase is needed along each of these segments for a rupture to occur. The Meeker-Prague Fault segment, where the 2011 earthquake occurred, needs 0.01 MPa to slip, and the WFS segment, where the 2024 earthquake occurred, needs 0 MPa to slip. These results show that while these two segments were super close to critical, not all of the other fault segments are. Some of these segments need quite a bit of Coulomb stress increase to rupture. However, the two of interest in this study are very close to critically stressed.

Fault Segment	Delta PP to Slip (MPa)
WFS1	1.61
WFS2	0
WFS3	4.30
WFS4	0.39
MPF1	34.43
MPF2	53.75
MPF3	80.25
MPF4	0.01
MPF5	2.59
MPF6	63.65
3.1	74.02
3.2	36.05
3.3	79.34
4.1	61.42
5.1	5.84

Table 8: Delta PP to slip values for each fault segment in the Prague, OK site showing how much coulomb stress increase is needed (in MPa) to cause each fault segment to rupture.

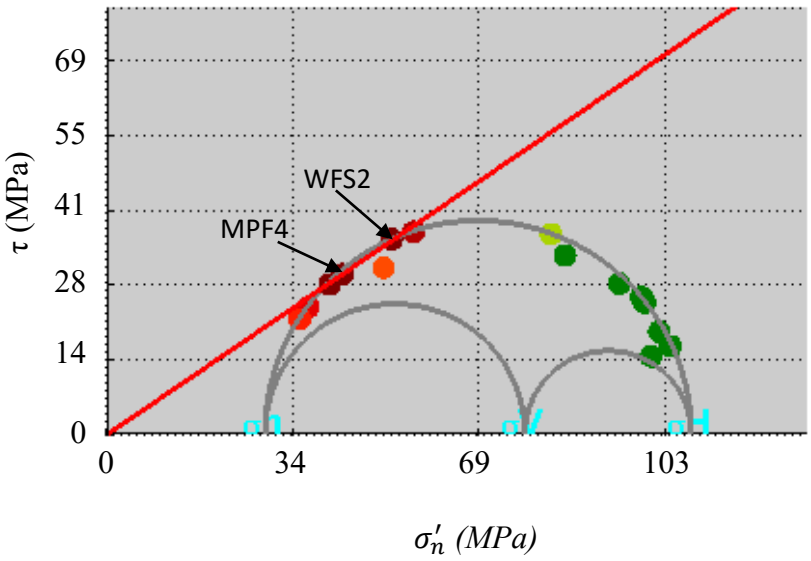

Figure 35: Mohr Circle for Prague, OK faults. Created in Fault Slip Potential 2.0 (FSP2.0). Indicating some faults are extremely close to failure in the current stress state of Oklahoma, while others are not close at all. MPF4 is the fault segment for the 2011 Prague earthquake, and WFS2 is the fault segment for the 2024 Prague earthquake.

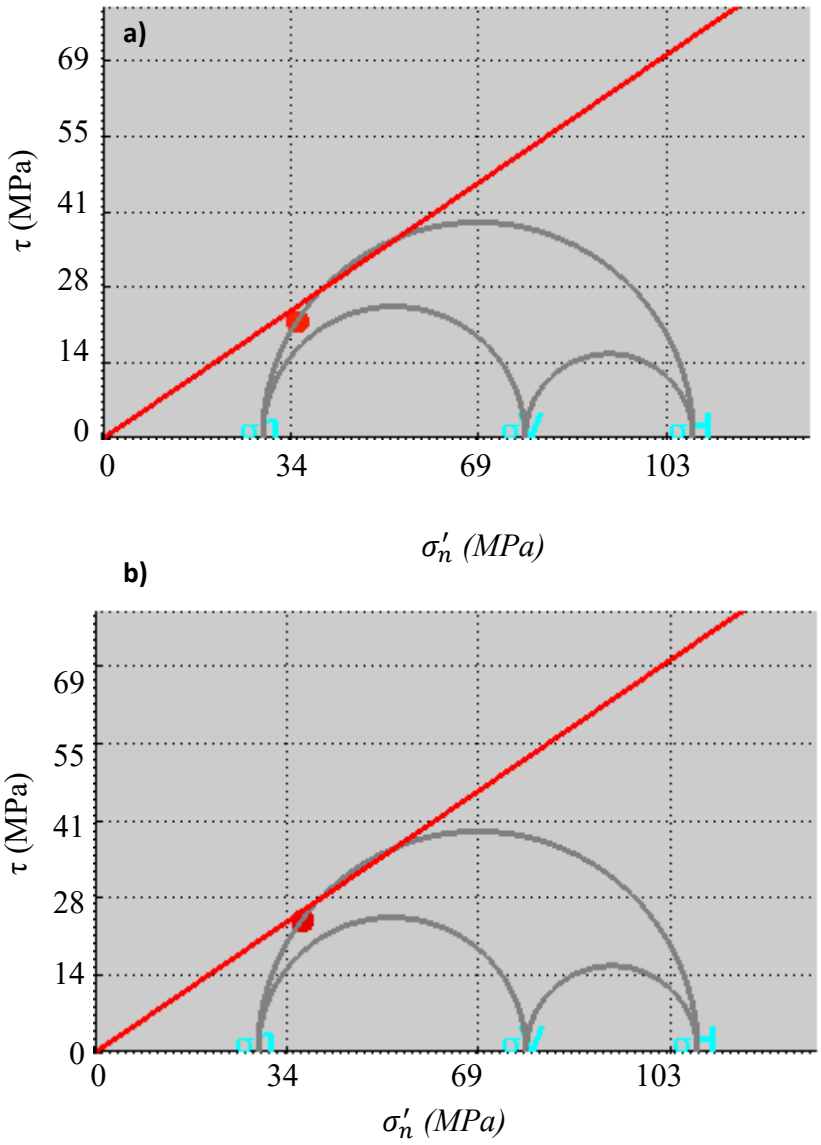

Figure 36: Mohr Circle for the Prague, OK faults 1.3 and 2.5. a) 1.3 segment results showing this fault is just under the Mohr-Coulomb failure envelope and is sitting just below critical in the current stress state of Oklahoma b) 2.5 segment results showing this fault is just under the Mohr-Coulomb failure envelope and is sitting just below critical (slightly closer to critical than 1.3) in the current stress state of Oklahoma. Created in Fault Slip Potential 2.0 (FSP2.0).

4.2.3: Coulomb Modeling Results

Experiment 1 for Prague, OK, consisted of reconstructing the November 6, 2011, earthquake that measured M_w 5.7. The results of this Coulomb stress change plot from reconstructing this earthquake were as follows. *Figure 37* shows the slip values in Prague, OK, along the hypocenter of the 2011 M_w 5.7 rupture event and its surroundings. The purple star represents the hypocenter of this event (McMahon et. al. 2017). This slip model was used to determine the location, depth, and amount of slip to put on the MPF to reconstruct this rupture event in Coulomb Modeling Software 3.4. The depth chosen was 3.5-4.5 km deep with a slip value of 0.6 meters over the purple highlighted portion of the MPF seen in *Figure 37,* and the slip patch is shown in *Figure 37*. *Figure 38* shows the Coulomb stress results from this experiment.

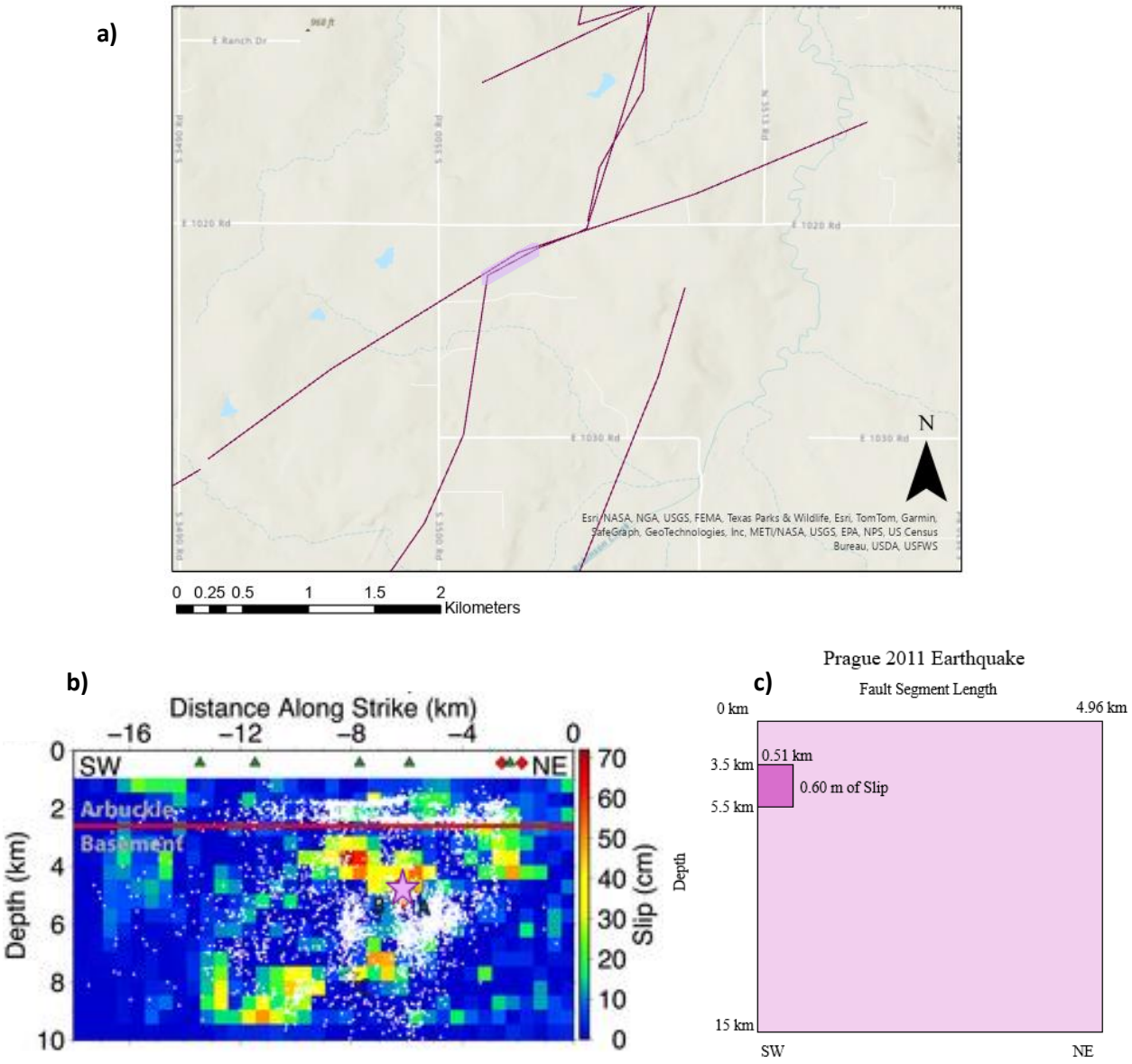

Figure 37: a) Prague, OK faults with light purple highlighted portion representing an added slip of 0.6m on the Meeker-Prague Fault. This value was programmed within Coulomb modeling software 3.4 to get the results for the reconstruction of the Prague 2011 mainshock, measuring M_w. 5.7. b) The slip model for the November 6, 2011, M_w 5.7 rupture event in Prague, OK. The purple star represents the earthquake hypocenter (McMahon et. al. 2017). c) Slip diagram at depth showing how slip was distributed into the subsurface across the length of the purple highlighted section of the Meeker-Prague Fault.

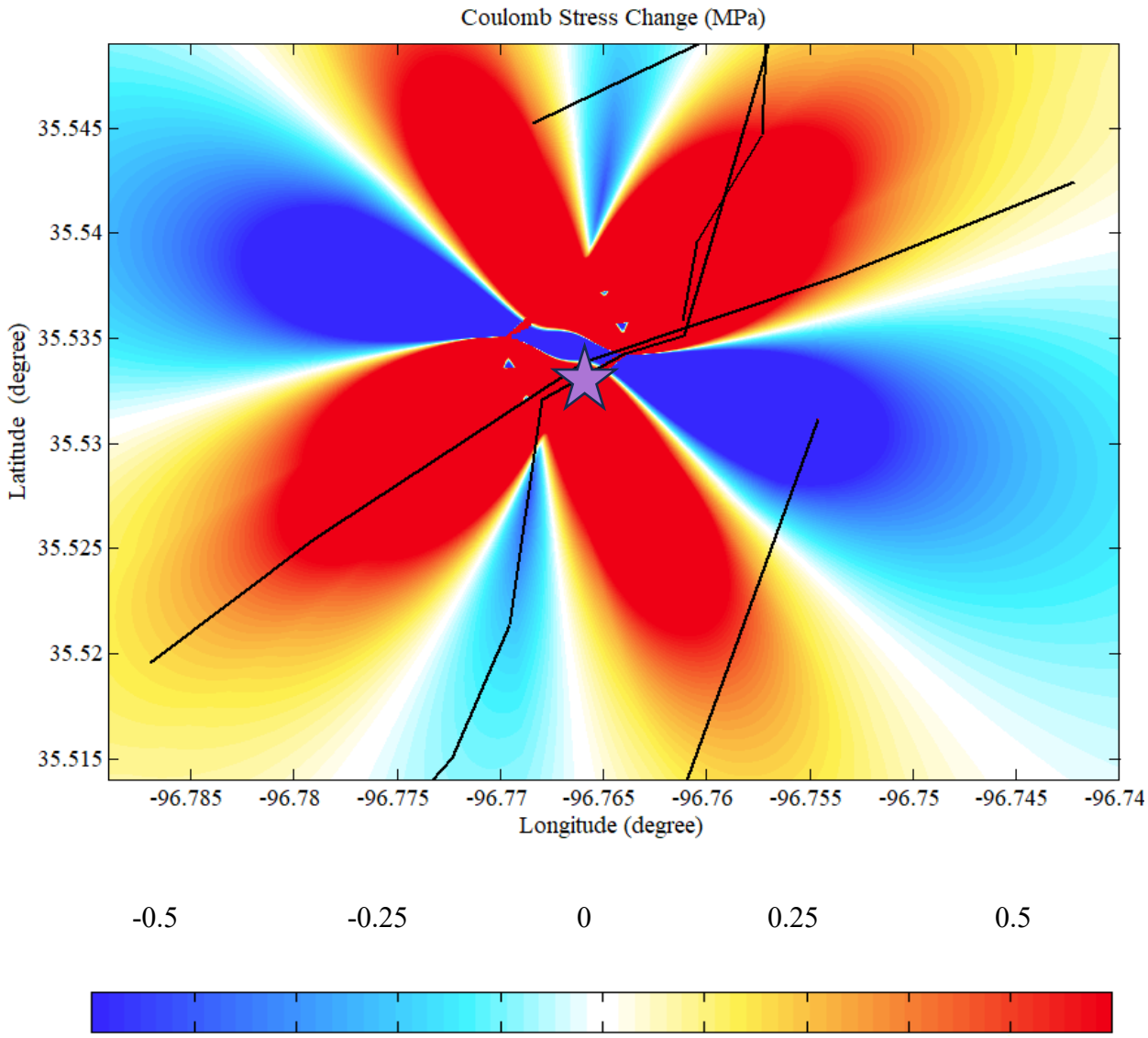

Figure 38: Reconstruction of the November 6, 2011, M_w 5.7 earthquake in Prague, OK. Image shows a Coulomb stress change in map view with the star representing the hypocenter for the main rupture event.

The results of this Coulomb stress change plot show four negative Coulomb stress change lobes and four positive Coulomb stress change lobes. The positive lobes align well with the aftershock patterns (discussed more in the discussion), and, likewise, the negative lobes strongly align with the areas lacking aftershocks, which is shown in the discussion section of this thesis. This shows

that the model was very likely to be accurate in making Coulomb stress change calculations since the reconstruction of the M_w 5.7 rupture in 2011 generally matched the aftershock patterns seen in real data.

Coulomb stress change at a specific point was done to see how much Coulomb stress change occurred on the hypocenter of the 2024 earthquake in Prague, OK, from the 2011 event specifically. The location and depth of this event's hypocenter were provided by publicly available USGS data and are 35.534, -96.764 at 3 km depth. The results of this Coulomb stress change at a specific point can be seen in *Table 9* below.

Event	Coulomb Stress Change at 2024 Hypocenter (MPa)
2011 M_w 5.7 earthquake	0.74

Table 9: Coulomb stress changes at a point from the 2011 Prague event at the 2024 Prague event hypocenter.

Experiment 2 of Prague consisted of reconstructing the 2024 M_w 5.1 earthquake along the WFS. This was done differently than the SLF M_w 5.8 and Prague 2011 events since there is no public dataset for the slip values calculated for the Prague 2024 earthquake. Due to this, a calculation had to be made for the slip value for the M_w 5.1 earthquake in 2024, which was explained in the Methods section of this thesis. This slip of 0.54 m was added from 2 km to 4 km depth since the USGS published that this earthquake occurred at 3km depth. The same friction coefficient of 0.68 was used since this earthquake also occurred in the basement rock of Oklahoma like the two previous reconstruction experiments. *Figure 39* shows the highlighted portion of the WFS which is where this slip was added and *Figure 39* shows the slip model to visually show how this slip was distributed in the subsurface. The results of this reconstruction are seen in *Figure 40* and show four positive Coulomb stress change lobes and four negative Coulomb stress change lobes

Additionally, before the Coulomb modeling portion could be completed, one last calculation was required for the amount of slip from the M_w 5.1 earthquake on February 3, 2024. There is no slip model published at the time of this thesis since this earthquake occurred relatively recently. Therefore, an estimation of slip from this event is needed in order to complete a Coulomb stress analysis of this earthquake. The equations used are seen below in *Equations 3 & 4* and *Table 10* shows the values used for each of the constants in this equation and the displacements calculated from them.

$$M_0 = rigidity * area * slip$$

Equation 3: Moment magnitude (M_0) equation from the USGS.

Since the M_0 for the Prague 2011 and 2024 events are known, the same area and rigidity are used for both events, and the slip for Prague 2024 is known due to a publicly available slip model from (McMahon et al., 2017), *Equation 4* can be used to find the slip for the 2024 event.

$$\frac{M_{0\ 2011}}{M_{0\ 2024}} = \frac{Slip_{2011}}{Slip_{2024}}$$

Equation 4: Equation used to calculate slip for Prague 2024.

Earthquake	M_0	Slip
2011	5.7	0.60 m
2024	5.1	0.54 m

Table 10: Coulomb stress change value for Experiment 1 from Prague, OK showing the Coulomb stress change calculated at the hypocenter of the 2024 mainshock because of the 2011 mainshock.

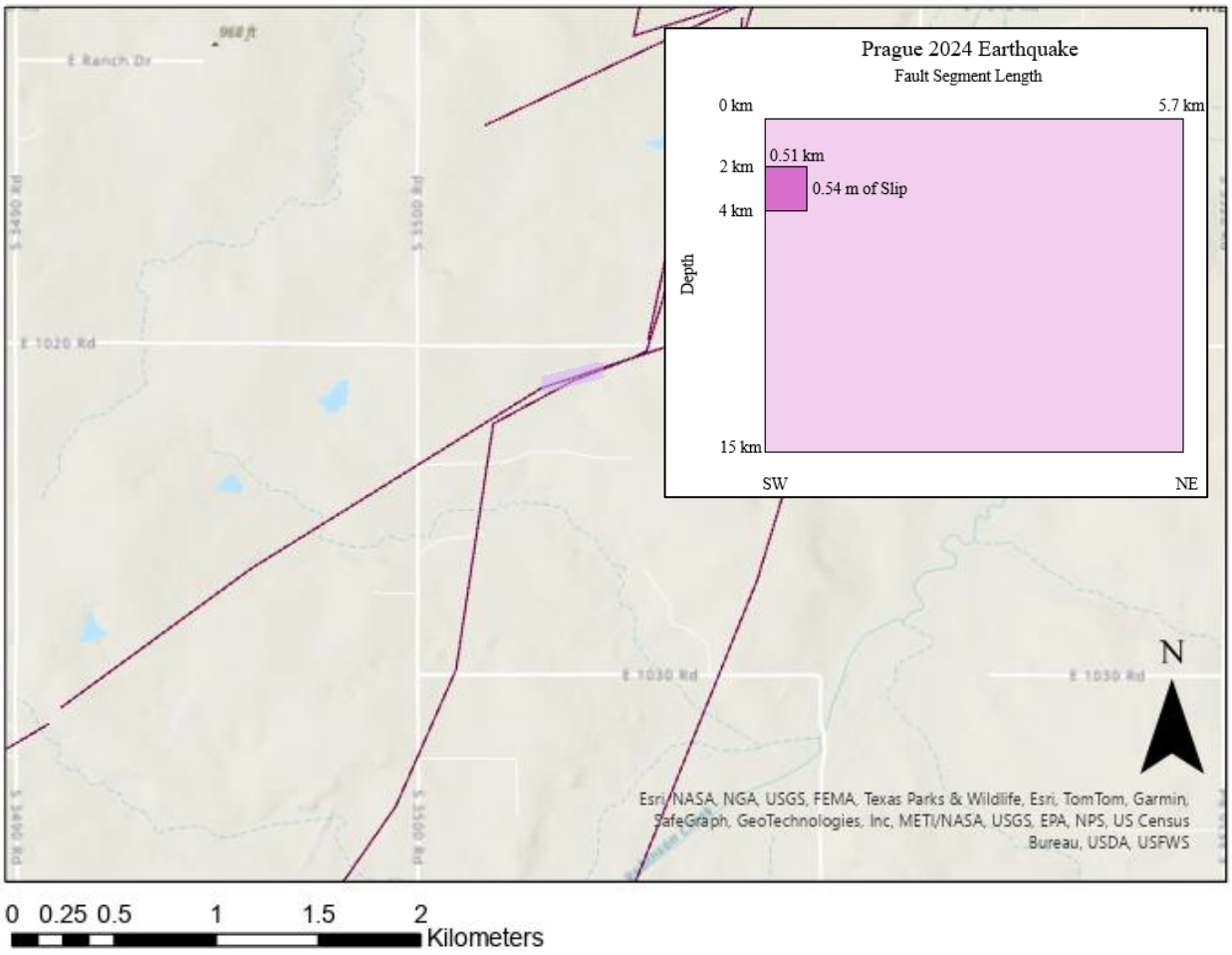

Figure 39: Prague, OK faults with light purple highlighted portion representing an added slip of 0.54m on the Wilzetta Fault System. This value was programed within Coulomb modeling software 3.4 to get the results for the reconstruction of the Prague 2024 mainshock measuring M_w 5.1. Overlain is the slip diagram at depth showing how slip was distributed into the subsurface across the length of the purple highlighted section of the Wilzetta Fault System.

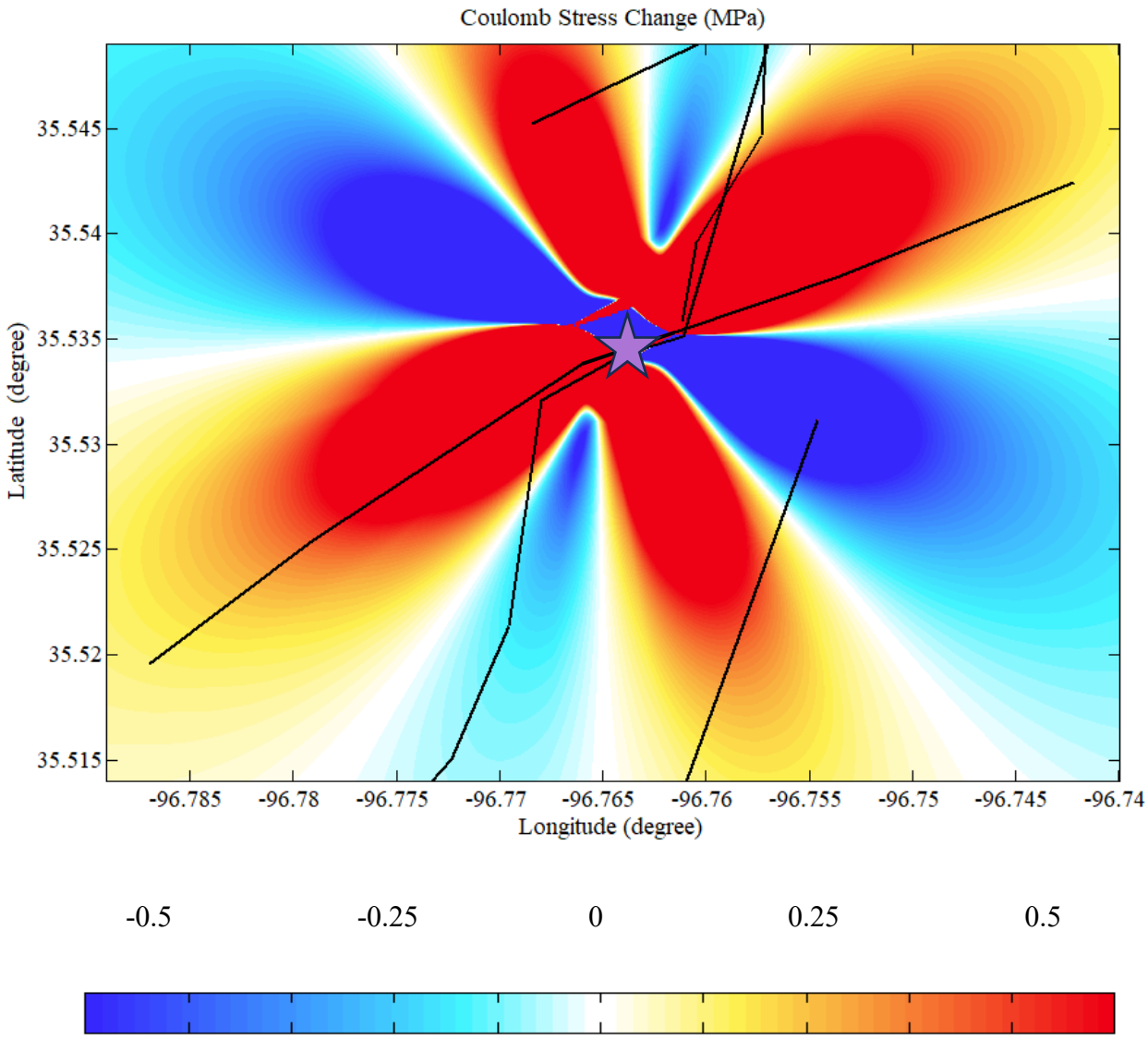

Figure 40: Coulomb stress change plot from the reconstruction of the M_w 5.1 earthquake in Prague, OK on February 3, 2024. Purple star represents the hypocenter for the main rupture event.

The results of this Coulomb stress change plot shows four negative Coulomb stress change lobes and four positive Coulomb stress change lobes. These lobes align well with aftershock patterns, which will be discussed in the discussion section in this thesis. These results are promising in

having constructed a working model since the Coulomb stress results constructed a pattern that aligns well with real work aftershock data.

DISCUSSION

5.1 Pawnee County Triple Junction

Comparing the results of this thesis to those from the Chen et al. (2017) publication, some key differences are noted. First, the slip distribution was mapped out to a higher resolution within the program Coulomb Modeling Software 3.4; however, the study done here utilized a more robust and complex fault model. These main differences in complexity were the addition of the NEFZ, removal of the OOF, extension of the SLF to the East, addition of the SLF Synthetic/Antithetic Faults, and addition of dip values to each fault strand. So, while the slip in this study was not as complex as the one in Chen et al. (2017), the results are still important for the advancement in understanding the SLF due to the increase in fault complexity. Fault locations were remapped, and dips were added, which made a more detailed fault model.

Experiments 1-3 all showed something useful about the SLF and the 2016 M_w 5.8 rupture that occurred there along the SLF. Experiment 1 was the reconstruction of the M_w 5.8 rupture along the SLF, experiment 2 was the testing of the Chen et al. (2017) NEFZ hypothesis, and experiment 3 was the testing of the Walter (2017) SLF hypothesis. All these results are discussed below, and each adds something valuable to the understanding of the Pawnee triple junction and its surrounding faults.

The results from SLF experiment 1 show a strong correlation between Coulomb stress increase and aftershock locations, while areas with Coulomb stress decrease align with the areas lacking in aftershocks (*Figure 41*). These results showed that the model did a good job at predicting the aftershock locations for the SLF M_w 5.8 rupture since the aftershock patterns aligned extremely well with the positive Coulomb stress change lobes. Additionally, this is consistent with other

studies that have shown that increases in coulomb stress result in aftershocks (Stein, 1999; King et al. 1994). These other publications show that the increased aftershocks indeed directly correlated with the positive Coulomb stress change lobes.

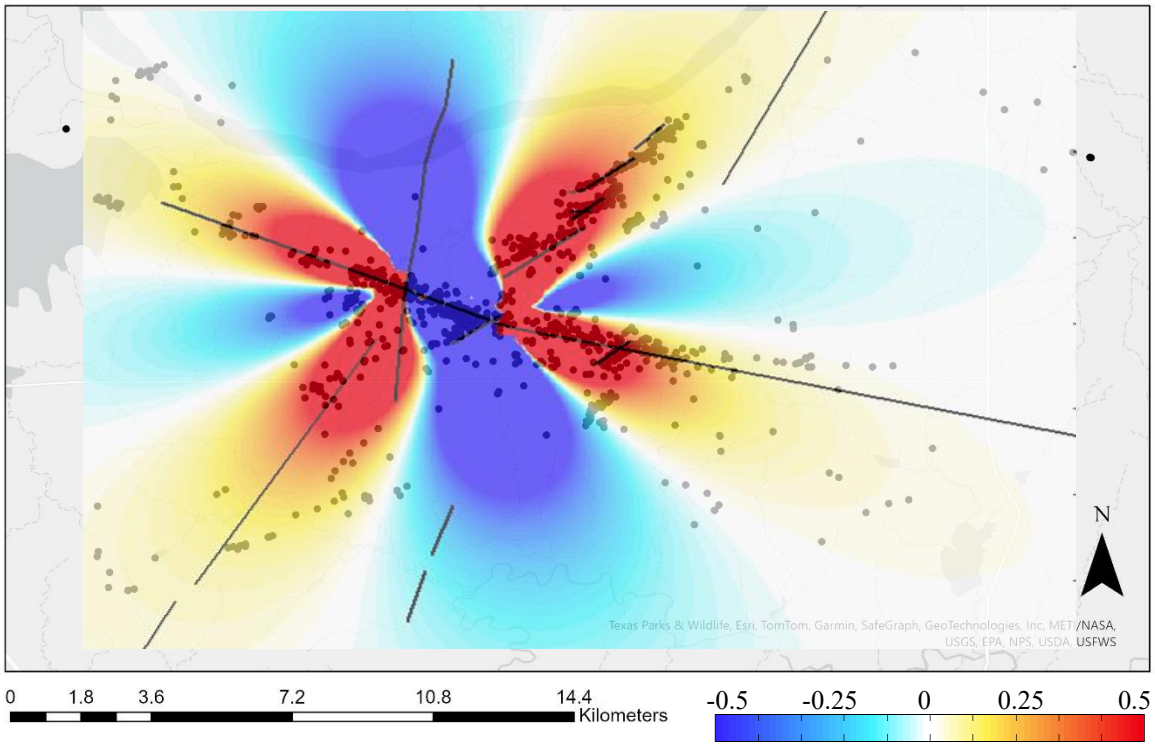

Figure 41: Comparison of the Coulomb stress change plot from the 2016 M_w 5.8 reconstruction in Coulomb Modeling Software 3.4 with the aftershock data from OGS. Seismicity dates range from September 3, 2016, to May 15, 2023.

Comparing the results of the reconstruction of the M_w 5.8 rupture in 2016 with the seismicity migration time plot a lot can be interpreted. The biggest correlation seen is that the NEFZ shows a NE migration of seismicity. A clearer zoomed-in image of this seismicity migration over the NEFZ is seen in *Figure 42*. This migration occurs very clearly from the southwest to the northeast over time. Then, more recently, some seismicity has occurred in the middle of the NEFZ. However,

even with this little bit of recent seismicity in the middle of the NEFZ, there is still a very clear migration to the northeast across this fault zone.

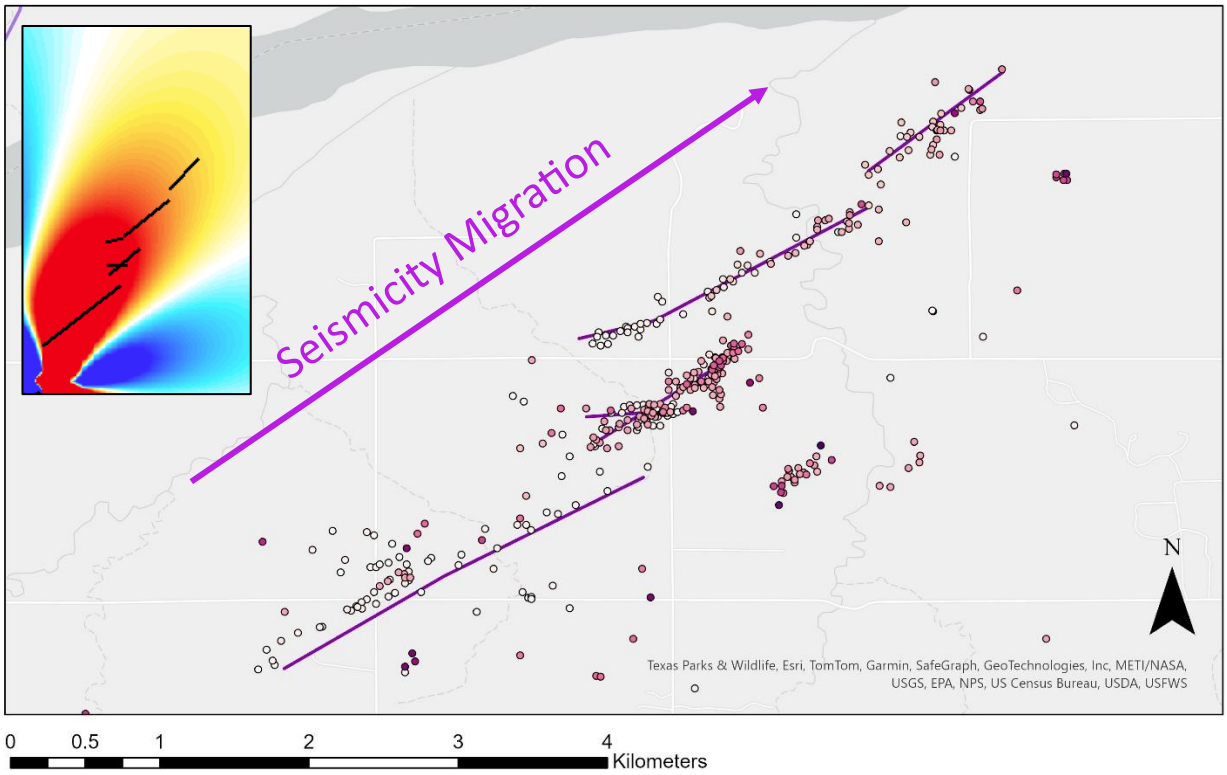

Figure 42: Seismicity with time showing how aftershocks propagated from the 2016 M_w 5.8 earthquake along the NEFZ. Lighter colors indicate earthquakes occurring first and darker ones indicate the more recent earthquakes. Dates of seismicity here range from September 3, 2016, to May 15, 2023. Inset is the Coulomb stress analysis results from Coulomb Modeling Software 3.4 to show how the Coulomb stress changes align with the aftershock migration patterns.

This migration pattern strongly aligned with the Coulomb stress change results seen in *Figure 41*. These results show a positive Coulomb stress change lobe going across the entire NEFZ.

Additionally, this positive Coulomb stress change is larger to the southwest and smaller to the northeast. This supports the first aftershocks occurring in the Southwest of the NEFZ and slowly migrating to the northeast, where the Coulomb stress change was not as highly positive.

The seismicity migration patterns seen for the SLF (*Figure 43*) are not as strong as the NEFZ but still show interesting results. These are not as strong since they do not have as clear a migration pattern. For the NEFZ there was a clear seismicity change over time with more consistent migration changes. For the SLF there is a slower migration of seismicity, and these migrations have not been to a smaller degree. The seismicity migration here shows more of a tapering effect over time. At the start of the aftershock sequence, there is seismicity across most of the SLF. This seismicity then progresses to cover less of the SLF over time. By the end of the sequence, there are two things easily seen: (1) seismicity is mostly seen towards the center of the SLF, (2) seismicity now covers the SLF conjugate faults (SLFC1 and SLFC2) (*Figure 43*). Until recently, these conjugate faults were unmappable since there was very little seismicity occurring.

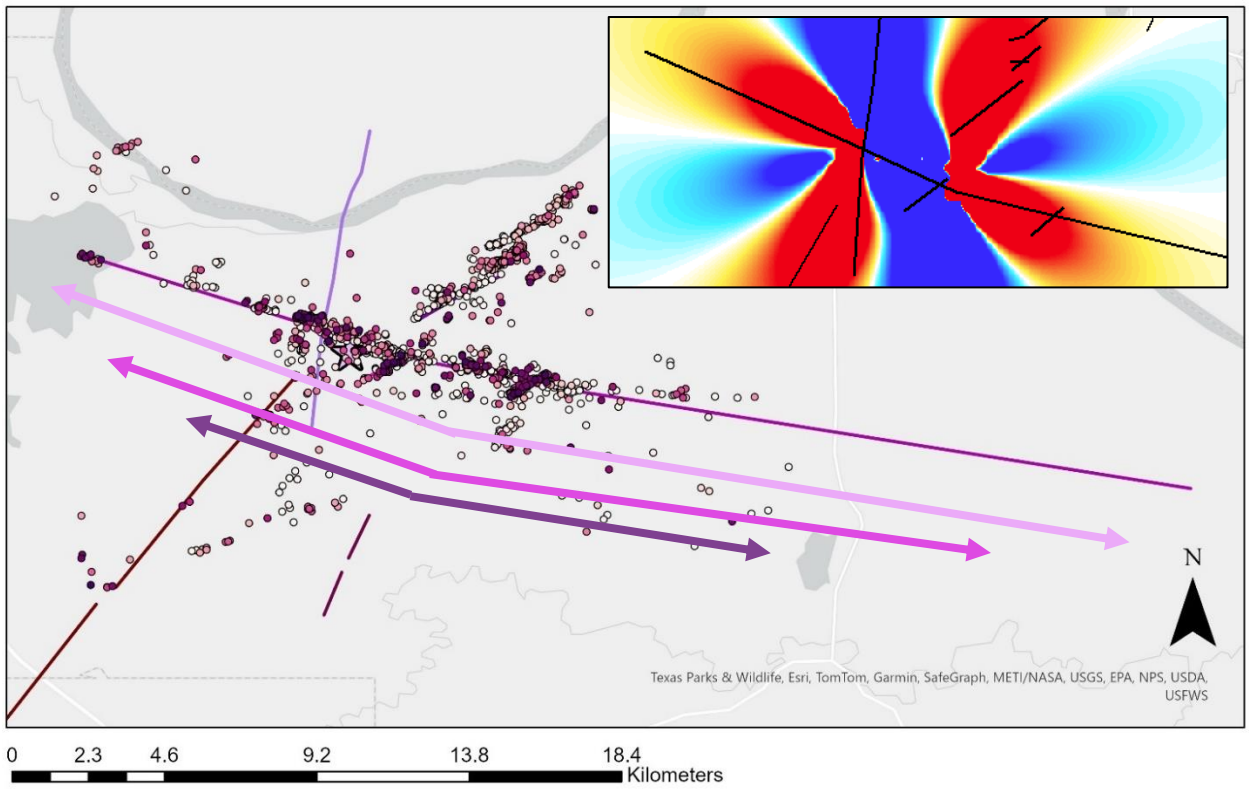

Figure 43: Seismicity with time showing how aftershocks propagated from the 2016 M_w 5.8 earthquake along the SLF. Lighter colors indicate earthquakes occurring first and darker ones indicate the more recent earthquakes. These are labeled as 1 (being the M_w 5.8 event itself) and 1,337 being the most recent earthquake in this catalog. The purple arrows indicate the tapering of seismicity migration. Light purple represents the earliest seismicity, medium purple represents the middle of the data set, and dark purple represents the latest seismicity recorded. Dates of seismicity here range from September 3, 2016, to May 15, 2023. Inset is the Coulomb stress analysis results from Coulomb Modeling Software 3.4 to show how the Coulomb stress changes align with the aftershock migration patterns.

SLF experiment 2 shows that the Chen et al. (2017) hypothesis is probable in being the driving factor of the SLF M_w 5.8 earthquake in 2016. *Figures 31* and *Tables 5 and 6* show that SLF1 is critically stressed, and any added coulomb stress would cause it to fail. Even as little as 0.007 meters of slip along NEFZ6 showed a positive Coulomb stress change, indicating it would have caused the SLF1 to fail. Additionally, the values in *Tables 5, 6, and 7* are the coulomb stress change for the exact location of the hypocenter for the 2016 M_w 5.8 rupture and since these are positive coulomb stress changes the Chen et al. (2017) hypothesis is a valid and probable causation for that earthquake to have been created. Pennington's thesis (2017) also looked into this foreshock as a potential driving factor of the M_w 5.8 rupture in 2016. His thesis found that this foreshock indeed did have an influence in promoting failure of the mainshock and even stated it was the most likely of the three looked into in his thesis (one of the others was the Walter 2017 foreshock hypothesis) (Pennington, 2017). *Figure 44* shows the foreshocks across the SLF and surrounding faults in the time prior to the mainshock on the SLF on September 3, 2016.

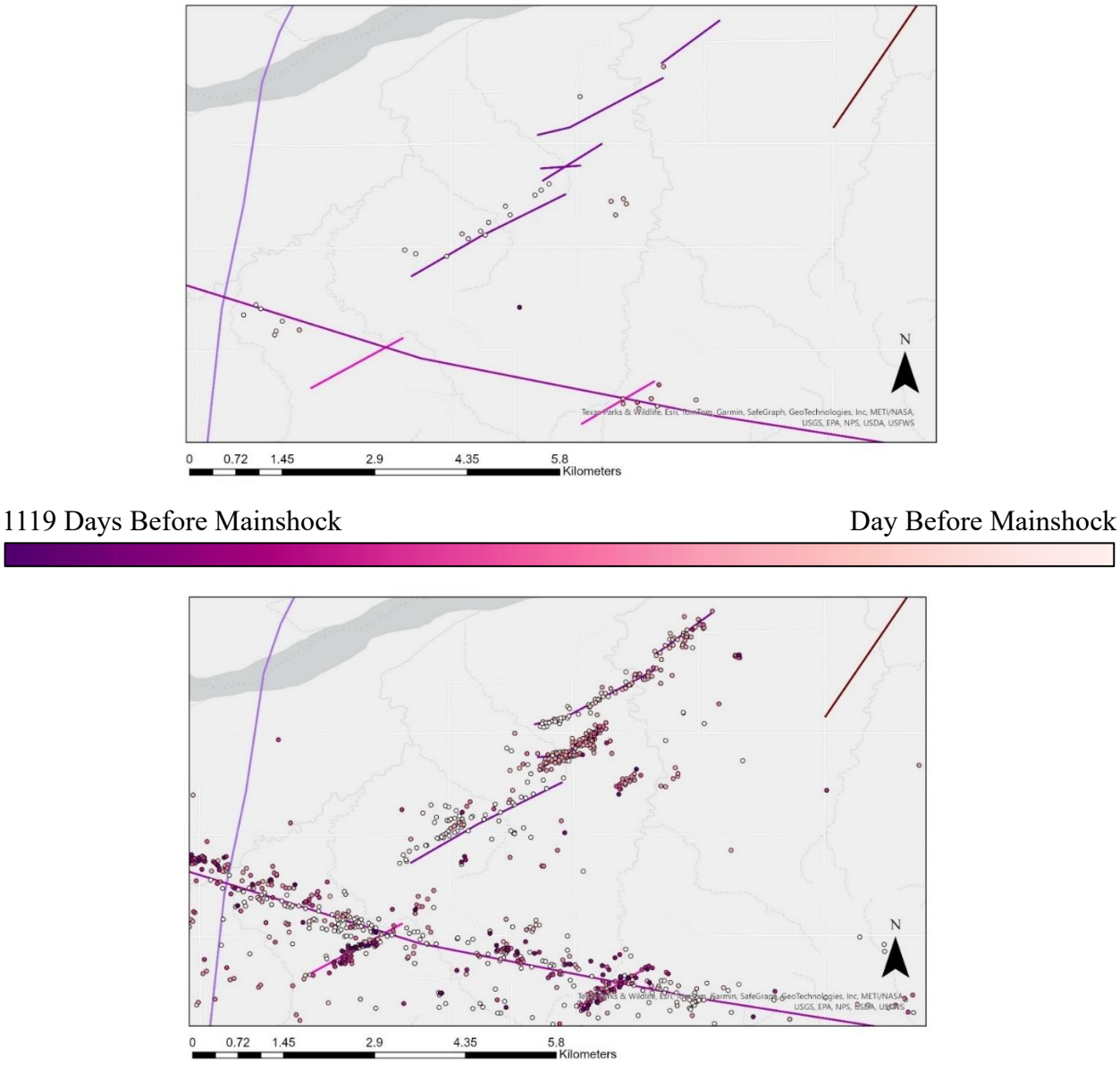

Figure 44: Seismicity with time prior to the M_w 5.8 earthquake along the SLF in 2016. This shows what seismicity prior to the main rupture looked like. Additionally, indicates which areas had the most seismicity close to the main rupture. Top photo: foreshocks of the SLF M_w 5.8 rupture on September 3, 2016, dates range from November 8, 2013, to September 1, 2016. Bottom photo: aftershocks of the SLF M_w 5.8 rupture on September 3, 2016, dates range from September 3, 2016, to May 15, 2023.

Experiment 3 for the SLF looks at the second hypothesis discussed in this thesis. This hypothesis was tested the same way experiment 2, and the results can be seen in *Figures 33* and *Tables 5 and 6*. These results show a very similar interpretation as experiment 2 in that hypothesis is also plausible and that the SLF hypothesis could have been the driving factor of the SLF M_w 5.8 earthquake in 2016. Putting even as little as 0.015 meters of slip along that section of the SLF made a positive Coulomb stress change which according to *Table 5* shows it would have caused the SLF to slip and rupture in that M_w 5.8 event. Additionally, the 0.007 meters slip added along the SLF made a barely negative Coulomb stress change. Since the 0.015 meters slip had a clear positive Coulomb stress change, showing that even putting very little slip on the hypothesized section of the SLF caused enough Coulomb stress increase for the M_w 5.8 event to occur. Pennington's thesis also looked into this foreshock as a potential driving factor of the M_w 5.8 mainshock and found that this foreshock also had a strong contribution in the promotion of the failure of the mainshock (Pennington, 2017).

Of the three foreshocks Pennington examined in his thesis, two of them were tested here in this thesis (e.g., Chen et al., 2017; Walter et al., 2017). Pennington found similar results to this thesis found in that both foreshocks played a role in the failure of the mainshock. This means that this thesis and the Pennington thesis found similar results when conducting experiments in different manners and with different data catalogs, showing that both are strongly supported by their individual research and the conclusions found in both theses. However, both Pennington's thesis and my own showed that both hypotheses are possible since they both promoted enough Coulomb stress increase for the 2016 M_w 5.8 earthquake to occur. While the NEFZ hypothesis hosted a larger Coulomb stress increase for all amounts of slip tested in this study, the SLF hypothesis still produced high enough Coulomb stress increases (for all but one of the slip values tested) to produce

that mainshock. Therefore, both are proven to be possible with the NEFZ hypothesis being more possible on its own based on the Coulomb values calculated in this thesis.

Figure 34 and *Tables 5, 6, and 7* show that combining the two foreshock hypotheses causes a greater Coulomb stress change at the hypocenter of the 2016 mainshock. Therefore, if these two foreshocks worked together, they were also likely to have driven this mainshock to rupture. The SLF1 foreshock occurred two days prior to the NEFZ6 foreshock, so these could have both loaded the SLF mainshock hypocenter together and caused the mainshock to occur that way.

5.2: Prague, OK

Prague 2011 has published papers, data, and hypotheses on it; however, Prague 2024 does not due to how recently it happened. The Oklahoma Geological Survey is working on the 2024 earthquake currently, and the information in this thesis presents a mix of data provided by them and research done by me. This means that experiments relating to the Prague 2011 result in an increase in knowledge of this area and an addition to the scientific understanding of it, while the Prague 2024 research adds to the picture as one of the first, if not the first, published data discussing the parameters of this M_w 5.1 earthquake. Therefore, the results in this thesis for both earthquakes have made a positive contribution to the scientific discussion of these two events.

Experiment 1 demonstrated a reconstruction of the M_w 5.7 earthquake that occurred on November 6, 2011. Comparing this reconstruction with the 2011 aftershock patterns seen it can be determined that this Coulomb stress model is likely accurate. These figures show that there is a strong correlation between Coulomb stress increase and aftershock locations, while areas with Coulomb stress decrease align with the areas lacking aftershocks (besides a few outliers discussed momentarily in section 5.2 of this thesis). These figures are combined in *Figure 45* below to show

the correlation. Additionally, the positive Coulomb stress change areas lacking aftershocks are areas lacking mapped faults. This lack of faults could be the reason why these areas of increased Coulomb stress change do not align with aftershocks. The pattern comparison between the Coulomb stress change plot and the real-time aftershock data catalog shown in *Figure 45* helps to further support previous studies. This is because these areas of increase in Coulomb stress hosted aftershocks, and previous studies suggest that this increase in Coulomb stress caused these aftershocks to occur where they did. This is discussed in many other research publications about Coulomb stress change, such as (Stein, 1999; King et al. 1994). These other publications show that the increased aftershocks indeed directly correlated with the positive Coulomb stress change lobes, which is supported in this thesis as well. Therefore, this thesis helps to support these studies, and these studies help to support this thesis.

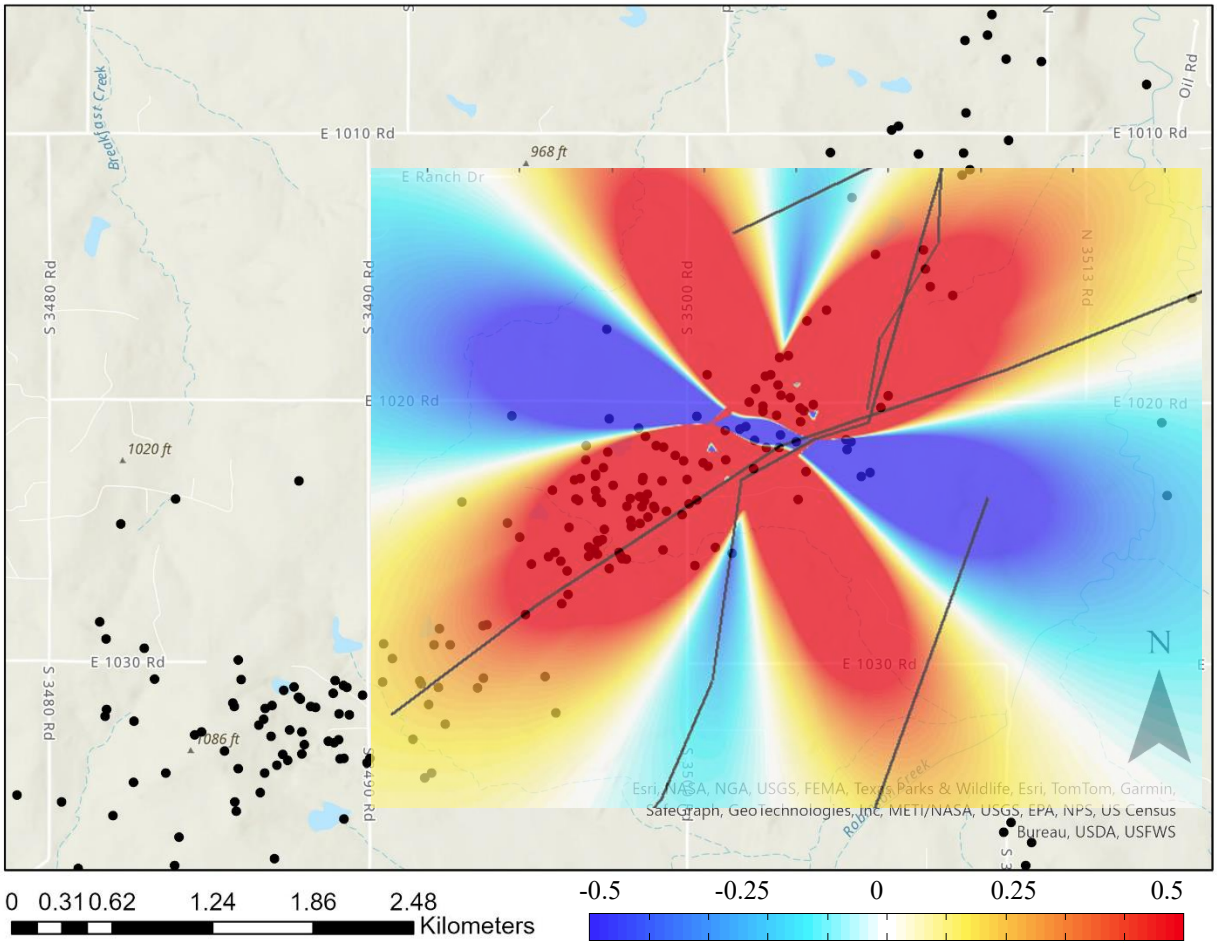

Figure 45: Comparison of the Coulomb stress change plot from the 2011 M_w 5.7 reconstruction in Coulomb Modeling Software 3.4 with the aftershock data from OGS. Seismicity dates range from November 6, 2011, to April 20, 2013.

Comparing the results of the reconstruction of the M_w 5.7 rupture in 2011 (*Figure 44*) with the seismicity migration time plot seen here (*Figure 46*) one main interpretation can be seen. This plot shows that the earthquakes along the MPF occurred quickly after the mainshock. Additionally, in the events closer to the breakoff in aftershocks there was more spacing between seismic events. These aftershocks are placed along the WFS, the MPF, and scattered in areas where there are no mapped faults. These later aftershocks show less of a distinct pattern in their rupture location.

Additionally, aftershocks in the negative Coulomb stress change lobes from *Figure 45* are produced later in the timespan this catalog recorded. This later production means these aftershocks could have been further influenced by the aftershocks around them which means that the Coulomb stress model made is still likely accurate since none of these events occurred in the negative lobes until closer to the 532-day break off of aftershocks. This pattern is interesting, and some more research into the Coulomb stress changes from each individual aftershock may help provide more insight into their location. However, from the results in this thesis, it can be inferred that their late rupture time indicates they were partly influenced by the nearby other aftershocks that occurred in the positive Coulomb stress change lobes (*Figure 45*).

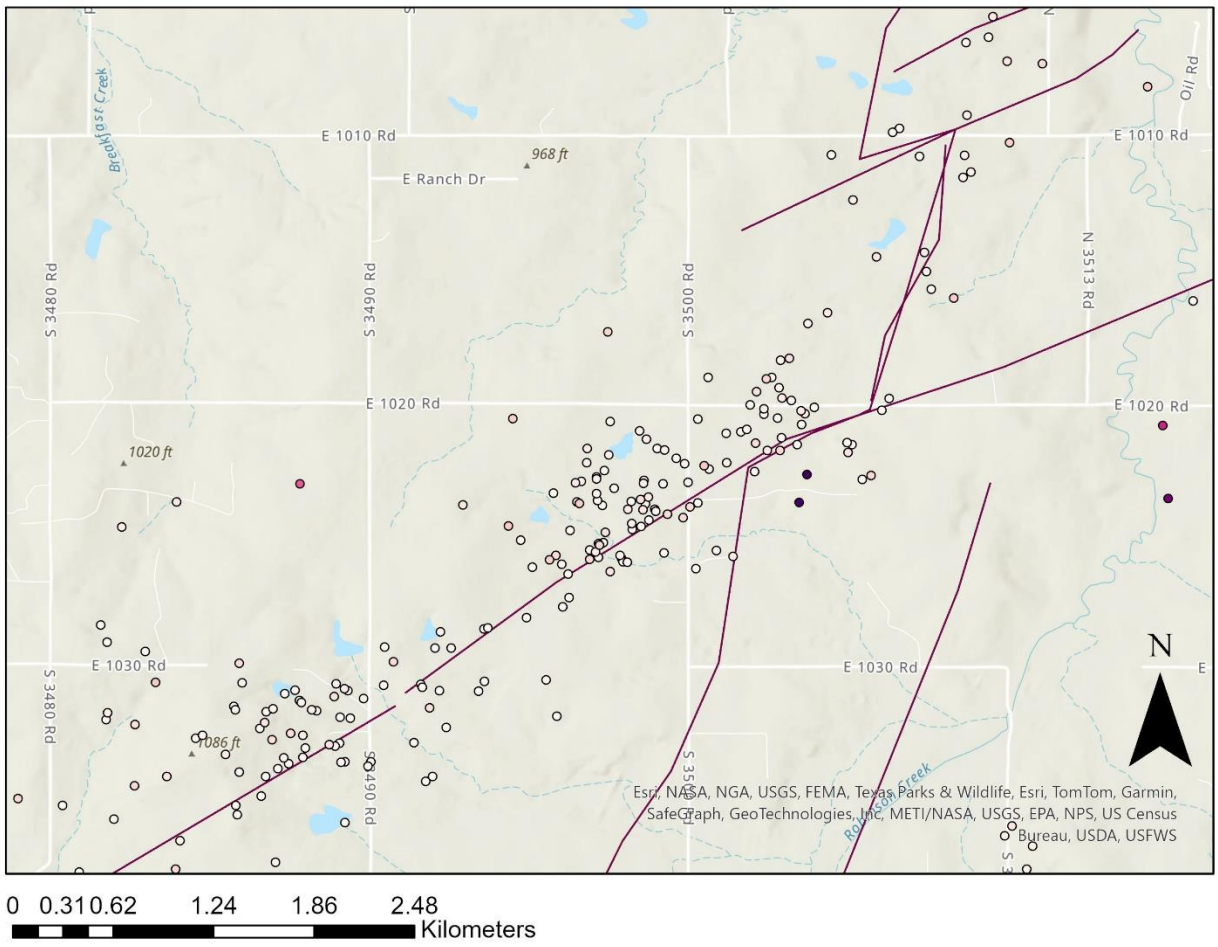

Day of Mainshock 532 Days After Mainshock

Figure 46: Seismicity by time after the M_w 5.7 earthquake along the MPF in 2011. This shows what seismicity after the main rupture looked like. Additionally, indicates which areas had the most seismicity close to the main rupture. Seismicity dates range from November 6, 2011, to April 20, 2013.

The results from the Prague experiment 2 are shown in *Table 9*. This experiment calculated the amount of Coulomb stress change on the hypocenter of the 2024 Prague earthquake from the 2011 Prague earthquake. This Coulomb stress change was a positive 0.74 MPa. *Table 10* shows that

according to FSP 2.0 WFS2 needed 0 MPa to slip. WFS2 is where the 2024 earthquake occurred, and, therefore, the Coulomb stress change from the M_w 5.7 earthquake in 2011 could be the driving factor of the M_w 5.1 earthquake in 2024. Earthquake triggering can be delayed like this for many reasons, including viscous relaxation, poroelastic rebound, and reductions in fault friction. This triggering process can take anywhere from seconds, being more of the rapid side, to years, being more on the delayed side (Freed, 2005). Therefore, due to the possibility of delayed triggering, it is possible that the 2024 Prague earthquake was produced as a result of the 2011 Prague earthquake.

Experiment 3 is shown in *Figure 47* below, which illustrates the reconstruction of the event and the resulting Coulomb stress change lobes. When comparing these lobes to the aftershock data in the same figure, it is evident that the aftershock patterns partially align with the Coulomb stress changes generated by Coulomb Modeling Software 3.4, with some outliers. Some of these outliers may be attributed to assumptions made about the slip during this event. Due to the lack of published data on the 2024 Prague earthquake and the absence of a published slip model, the slip amount was estimated using Equations 3 and 4.

Despite the number of assumptions involved, the results remain reasonably consistent with the observed aftershock patterns and support meaningful interpretations. The aftershock patterns follow through two positive Coulomb stress change lobes in *Figure 47,* and if they were slightly more north they would align even better; therefore, some assumptions involved in making the Coulomb stress change plot could be causing this slight misalignment. The positive Coulomb stress lobes suggest that aftershocks should occur along the northern portion of the WF, as well as the western and eastern portions of the MPF. Real-time aftershock data confirms the presence of

aftershocks in these regions. However, some aftershocks also appear in the areas between these zones, and one positive Coulomb stress lobe overlays faults that currently show no aftershocks.

Nevertheless, this aftershock catalog is still in its early stages, and aftershocks may eventually emerge in the currently inactive positive Coulomb stress regions. Aftershocks continue to occur in this area, and only time will reveal how these patterns develop. Based on *Figure 47*, we might expect future aftershocks along the fault located within the northwestern positive Coulomb stress change lobe.

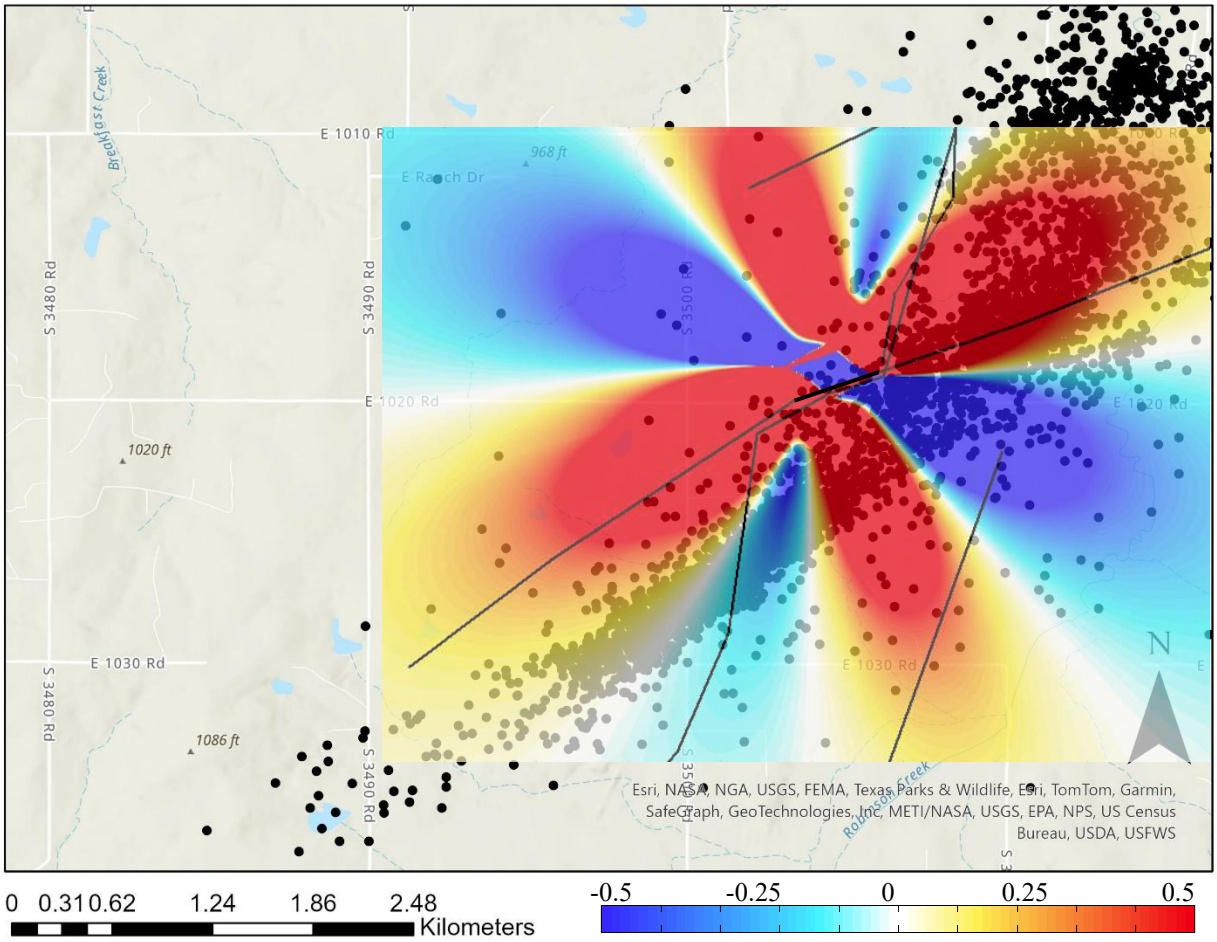

Figure 47: Comparison of the Coulomb stress change plot from the 2024 M_w 5.1 reconstruction in Coulomb Modeling Software 3.4 with aftershock data from OGS. Seismicity dates range from February 3, 2024, to February 24, 2025.

Comparing the results of the reconstruction of the M_w 5.1 rupture in 2024 (*Figure 47)* with the seismicity migration time plot seen here (*Figure 48*), no real migration pattern can be seen. However, there is not much data time-wise here since this mainshock occurred in 2024. A migration pattern may be seen when more years of aftershocks occur and are recorded, but only more time and data collection will be able to determine this. Aftershocks are still occurring in the same places they were at the time of the mainshock; however, they are tending to be less western

right now, but due to the short timespan in this catalog, this could just be a temporary lack of aftershocks to the west. As this data catalog grows in the next few years, a more in-depth analysis of this migration pattern can be conducted.

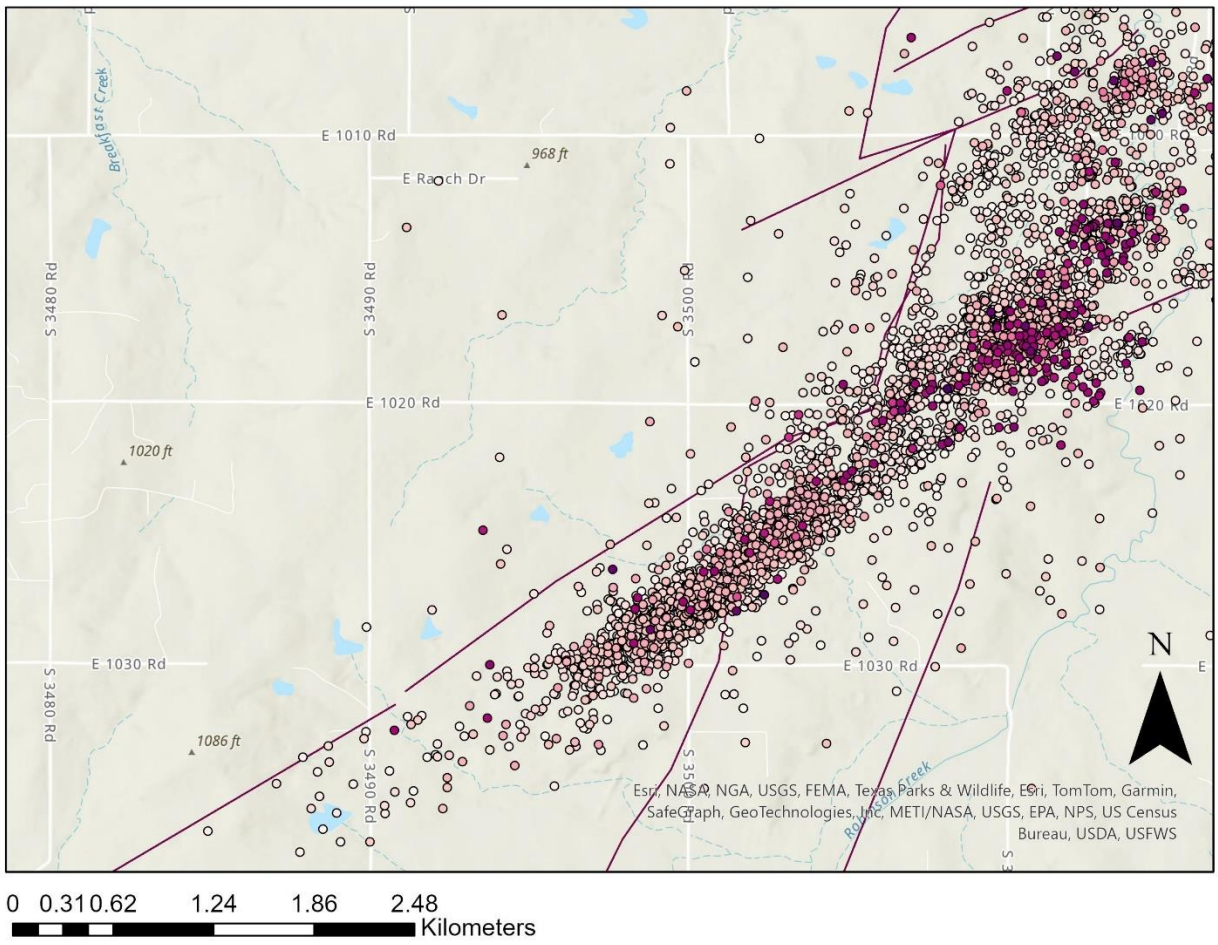

Day of Mainshock 385 Days After Mainshock

Figure 48: Seismicity with time after the M_w 5.1 earthquake along the WF in 2024. This shows what seismicity prior to the main rupture looked like. Additionally, indicates which areas had the most seismicity close to the main rupture. Seismicity dates range from February 3, 2024, to February 24, 2025.

5.3: Coulomb Stress Change

In terms of Coulomb stress change this study has helped to show that increasing fault complexity aids in increasing understanding of Coulomb stress change. By adding dips and more fault segments, this study was able to greatly reconstruct the M_w 5.8 earthquake in Pawnee, the M_w 5.7 earthquake in Prague, the M_w 5.1 earthquake in Prague, and test several hypotheses for the Pawnee area. In this successful reconstruction, this thesis was able to show that the fault complexity added to the models in Coulomb Modeling Software 3.4 aids in making accurate Coulomb stress change results.

Additionally, in comparison with other studies, the idea that increases in Coulomb stress changes is well established to increase the presence of aftershocks. This helps support the results in this thesis since the areas of Coulomb stress increase did in fact increase the presence of aftershocks, and the areas of Coulomb stress decrease did show a decrease in the presence of aftershocks. For Prague, OK, there was a M_w 5.0 earthquake in 2011 that has been of interest in some studies. One of these studies looked at the Coulomb stress changes and the resulting aftershock patterns. This M_w 5.0 earthquake caused Coulomb stress changes across many of the nearby faults, and it was found that ~60% of the aftershocks after this earthquake occurred in the regions of stress increase (>0.01 MPa) (Sumy et al., 2014). In 2016, another M_w 5.1 earthquake occurred in Oklahoma, which was also attributed to wastewater injection. This occurred in Fairview, OK and is tied with Prague 2024 for the third largest earthquake in Oklahoma history. Coulomb stress changes favored the patterns of sources, the mainshock, and an early aftershock (Lopez-Comino & Cesca, 2018). Specifically, the southwest region of this earthquake hosted the most aftershocks and this location strongly aligns within the positive Coulomb stress change lobe (Yeck et al., 2016; Lopez-Comino & Cesca, 2018).

5.4: Inducing and Triggering Earthquake Activity

Earthquake triggering and inducement were looked at from the results of the Coulomb Modeling Software 3.4 and FSP 2.0 experiments. Both rapid and delayed triggering were of great interest here since many of the aftershocks occurred instantly, but others occurred much later. Part of this could be due to aftershocks influencing the production of other aftershocks; however, for events like the 2024 Prague earthquake, it was thought that this could possibly be a delayed triggering event from the 2011 mainshock. Therefore, it is considered that there is likely a mix of this rapid and delayed earthquake triggering in this thesis research. Triggering typically occurs when stress is redistributed after an earthquake. For delayed triggering, this process can take years to complete a rupture (Freed, 2005). This is of interest due to the 2024 mainshock for Prague. Since the 2011 Prague mainshock produced a large enough positive Coulomb stress change at the hypocenter of the Prague 2024 mainshock, it is possible that the 2011 event influenced the 2024 event. Since these events were around 13 years apart, this would be considered significantly delayed triggering (Freed, 2005). Rapid triggering, however, is of interest due to the quick production of aftershocks from all three mainshocks discussed in this study. Rapid triggering is explained by the passage of dynamic seismic waves, which can induce Coulomb failure instantly or initiate other mechanisms that will induce delayed triggering (Freed, 2005). This instant Coulomb failure is seen in the production of instant aftershocks after these three mainshocks occurred.

Triggered earthquakes can take anywhere from seconds to years to complete. Delayed triggering can be explained through many mechanisms of time-dependent stress transfer. These mechanisms include viscous relaxation (Freed, 2005), poroelastic rebound (Freed, 2005; Nur & Booker, 1972; Dahm & Hainzl, 2022), pore-pressure diffusion (Miller et al., 2004; Dahm & Hainzl, 2022), and reductions in fault friction (Freed, 2005). However, rapid triggering can be explained by the

passage of dynamic seismic waves (Freed, 2005). Since earthquakes that are triggered by something can take seconds to years to complete their rupture, it is likely that the 2011 event could have caused the 2024 event, even though they were almost 13 years apart.

CONCLUSIONS, MODEL LIMITATIONS, AND FUTURE WORK

6.1 Pawnee Triple Junction

The region termed the Pawnee Triple Junction is the location of the largest earthquake in Oklahoma recorded history, a M_w 5.8 along the Sooner Lake Fault on September 3, 2016. This event produced aftershocks for years afterwards that revealed the location and extent of the Sooner Lake Fault, Northeast Trending Fault Zone, and other associated faults. Successful mapping of these faults was able to be achieved with the seismicity catalogs from the Oklahoma Geological Survey and Park et. al. (2022). This new mapping provided more accurate insights into the interplay of the faults in this region since a more accurate representation of these faults has been constructed in this thesis due to the improved seismicity catalogs. It was also determined that the NEFZ would replace the Optimally Oriented Fault (OOF) since the OOF is likely a rock contact instead of an extension of the Labette Fault. This new mapping was the biggest addition to the successful composing of a more complex and robust fault map for this area.

Coulomb modeling software was successful in reconstructing the M_w 5.8 rupture event on September 3, 2016, by adding left lateral slip along the SLF according to previous measurements made. Comparing these stress changes with the delta PP to slip calculated in FSP 2.0 showed clear indications that the stress change patterns along the SLF correspond well with the critically stressed faults from the FSP 2.0 results. Additionally, comparing these results to the aftershock data seen in the seismicity maps from the OGS and Park catalogs, it is seen that the reconstruction of the 2016 SLF rupture was likely successful since the aftershock patterns align with the areas of coulomb stress increase and the areas lacking aftershocks align with the areas of coulomb stress decrease. This shows that the aftershocks truly aligned well with areas of increased stress, and

models like this can be used to determine areas for potential future aftershocks of events like this one. Due to these results, it was determined that this experiment was accurate in recreating this rupture and is a good model for experimentation for unknown parameters.

Additionally, this model can be utilized in order to predict how variations in slip, from factors such as wastewater disposal, could impact this area in the future. This modeling can also be used in other areas that are greatly impacted by induced seismicity, as discussed in the introduction of this thesis. Induced seismicity is not an Oklahoma-specific issue, so tests and models of this nature can help humanity and companies specializing in hydrocarbons to continue to collect hydrocarbons in a safer way by modeling and determining the best and worst locations for wastewater disposal. This will help further the ability to prevent the production of massive induced seismic earthquakes as a result of wastewater disposal and other industry impacts that cause similar induced seismicity, such as subsurface CO_2 sequestration and enhanced geothermal systems.

Coulomb Modeling Software 3.4 was then used to determine how much slip along the NEFZ segment 6 was needed to bring the SLF to failure. Even as little as 0.007 meters of slip caused enough Coulomb stress increase on the hypocenter location for this 2016 event to promote its nucleation. This means that the Chen et al. (2017) hypothesis is valid and is a probable source for this rupture.

A similar conclusion can be made for the Walter et al. (2017) hypothesis along the SLF. The testing of this hypothesis showed that it is also extremely probable as the driving factor for the mainshock that occurred on September 3, 2016, due to it showing positive Coulomb stress change at 0.015 m and a barely negative Coulomb stress change at 0.007 meters. However, since the .007 meter slip showed a negative Coulomb stress change, whereas the Chen et al. (2017) hypothesis showed a

positive Coulomb stress change at 0.007 meters, these results show that the Walter et al. (2017) hypothesis is not as likely as the Chen et al. (2017) hypothesis is.

Additionally, it is possible that the foreshocks from both of these hypotheses could have worked sequentially to produce the M_w 5.8 earthquake on September 3, 2016. The order of these foreshocks was the SLF Walter (2017) hypothesis, then the NEFZ6 Chen et al. (2017) hypothesis, and then the M_w 5.8 mainshock on the SLF. The first mainshock occurred on the SLF segment 1 just east of the mainshock location on June 6, 2016. Two days later, the foreshock on the NEFZ6 ruptured on June 8, 2016. Then, the mainshock occurred on September 3, 2016, three months after these two foreshocks. It is also possible that the two foreshocks both increased stress on the SLF enough to both be the driving factors of this mainshock. While this is still an unknown the exact cause, these three ideas are all possible, and the results of this thesis help to support this.

6.2 Prague, OK

Experiment 1 from Prague, OK, shows a reconstruction of the November 6, 2011, earthquake that measured M_w 5.7 along the Meeker-Prague Fault. These results show that the model is likely an accurate one since the Coulomb stress change plot strongly aligns with the patterns of aftershocks in real life. Since these aligned so well, this was likely a successful reconstruction experiment. This showed that the model was ready to be used for experiment 2 and confirmed that the added complexity of dip measurements along each fault segment was done in a manner that still produced a realistic and accurate model for the Prague, OK faults in this study.

Experiment 2 for the Prague, OK site showed a second test for this 2011 event. This test was conducted in order to determine the amount of Coulomb stress change that was put on the hypocenter of the February 3, 2024, earthquake in Prague, OK, from the rupture of the 2011 event.

This showed that the 2011 event caused positive Coulomb stress change on the hypocenter of the 2024 event, which means it is possible the 2011 event played a role in the rupture of the 2024 event.

Experiment 3 showed similar results to experiment 1 but with less data to go off of and more assumptions being made the interpretations are not as strong. This one was done slightly differently from the SLF 2016 and Prague 2011 reconstructions since there is no published slip model for this event yet due to how recent this event occurred. Therefore, a slip calculation for this rupture was required in order to reconstruct it. Slip for the 2024 earthquake was determined to be 0.54 m from using *Equations 3* and *4* in comparison to the 2011 event. This slip value was then used along the WFS to determine what a reconstruction of this earthquake could be. The results of this experiment show four positive and four negative Coulomb stress change lobes and aftershocks partly align ell in these lobes. Areas lacking aftershocks could be due to the short timespan in the catalog and more aftershocks over the next years may fill in these gaps. Additionally, the aftershocks that align in the negative Coulomb stress change lobes are likely either due to slight imperfections in the model, due to more assumptions, or due to influences from the other earthquakes occurring in this area, since there were earthquakes occurring right before the 2024 mainshock. A more robust data catalog would be able to provide more insight into these outliers and new questions, and once more aftershocks occur in the next few years, more research can likely be done into answering these questions.

6.3: Future Work

Recommended future work includes taking a deeper dive into the northeast trend of seismicity in the NEFZ. This trend will be interesting to continue to monitor as time goes on. If the trend

continues northeastward, it will be something worth investigating further to understand more of the migration pattern trends in this area. Additionally, with a continued northeastward trend, there would be more of the fault zone visible to map out. So, further mapping as aftershocks and migrations continue will be a great addition to understanding this fault zone more.

For Prague 2024, a closer look into the aftershock alignment off of a fault would be an interesting addition to the understanding of this site. While Prague 2011 had aftershocks aligned on a fault, 2024 did not. This misalignment is very odd and would be of interest to produce a better understanding of the Prague 2024 earthquake. Additional recommended work for Prague includes performing another Coulomb stress change test in Coulomb Modeling Software 3.4 when there is a published slip model for the Prague 2024 earthquake. Building this model in order to conduct this test more accurately is something that would greatly benefit this project and the future work that can be done based on it. These additions to the understanding of the Prague 2024 earthquake would be extremely beneficial to this research area.

REFERENCES

Abbott, M. M., Runkle, D., and Rea, A., 1997, DIGITAL DATA SETS THAT DESCRIBE AQUIFER CHARACTERISTICS OF THE VAMOOSA-ADA AQUIFER IN EAST-CENTRAL OKLAHOMA, Volume 2025: Oklahoma City, Oklahoma, United States Geological Survey.

Abercrombie, E. R., 2021, Resolution and uncertainties in estimates of earthquake stress drop and energy release: Philosophical Transactions of the Royal Society A: Mathematical, Physical and Engineering Sciences, v. 379, no. 2196, p. 20200131.

Baan, D. V. M., and Calixto, J. F., 2017, Human-induced seismicity and large-scale hydrocarbon production in the <scp>USA</scp> and <scp>C</scp>anada: Geochemistry, Geophysics, Geosystems, v. 18, no. 7, p. 2467-2485.

Bai, Y., and Wierzbicki, T., 2010, Application of extended Mohr–Coulomb criterion to ductile fracture: International Journal of Fracture, v. 161, no. 1, p. 1-20.

Buchanan, C. R., 2015, Increased seismicity in Kansas: The Leading Edge, v. 34, no. 6, p. 614-617.

Buchanan, C. R., Hoffman, R., and Cochran, M., 2023a, Induced seismicity in Kansas: Events and responses, Recent Seismicity in the Southern Midcontinent, USA: Scientific, Regulatory, and Industry Responses, p. 27-35.

Buchanan, R., Peterie, S., and Miller, R., 2023b, Annual Report: Kansas Geological Survey.

Buchanan, R. C., Newell, K. D., Evans, C. S., and Miller, R. D., 2014, Induced Seismicity: The Potential for Triggered Earthquakes in Kansas.

Canada, G. o., 2025, Glossary of Seismological Terms.

Cardott, B. J., 2017, Oklahoma Shale Resource Plays.

Chase, F. B., Kolawole, F., Atekwana, A. E., Carpenter, M. B., Turko, M., Abdelsalam, M., and Finn, C., 2023, The 180-km-long Meers-Willow fault system in the Southern Oklahoma Aulacogen: A potential U.S. mid-continent seismic hazard: GSA Bulletin, v. 135, no. 3-4, p. 663-677.

Chen, X., Nakata, N., Pennington, C., Haffener, J., Chang, C. J., He, X., Zhan, Z., Ni, S., and Walter, I. J., 2017, The Pawnee earthquake as a result of the interplay among injection, faults and foreshocks: Scientific Reports, v. 7, no. 1.

Clayton P. Zalachoris, G. Rathje E. Bheemasetti, T. Caballero, S. Yu X. , and Bennett S. 2016. The Geotechnical Aspects of the September 3, 2016 M 5.8 Pawnee, Oklahoma Earthquake , GEER Association, Berkeley, California.

Cranganu, C., and Soleymani, H., 2015, Carbon dioxide sealing capacity: Textural or compositional controls? A case study from the Oklahoma Panhandle: Environmental Geosciences, v. 22, no. 2, p. 57-74.

Dahm, T., and Hainzl, S., 2022, A Coulomb Stress Response Model for Time-Dependent Earthquake Forecasts: Journal of Geophysical Research: Solid Earth, v. 127, no. 9.

Denison, R. E., 1981, Basement rocks in northeastern Oklahoma: Oklahoma Geological Survey Circular, v. 84, p. 1–84.

Dowrick, D., 2009, Earthquake Resistant Design and Risk Reduction.

Ellsworth, L. W., 2013, Injection-Induced Earthquakes: Science, v. 341, no. 6142, p. 1225942-1225942.

Ellsworth, W.L., 2013, Injection-induced earthquakes: *Science*, v. 341, no. 6142, 1225942, https://doi.org/10.1126/science.1225942.

Elst, D. V. J. N., and Savage, M. H., 2015, Frequency dependence of delayed and instantaneous triggering on laboratory and simulated faults governed by rate-state friction: Journal of Geophysical Research: Solid Earth, v. 120, no. 5, p. 3406-3429.

Fielding, E. J., Sangha, S. S., Bekaert, D. P., Samsonov, S. V., & hang, J. C. (2017). Surface deformation of north-central Oklahoma related to the 2016 M w 5.8 Pawnee earthquake from SAR interferometry time series. *Seismological Research Letters*, *88*(4), 971-982.

Foulger, R. G., Wilson, P. M., Gluyas, G. J., Julian, R. B., and Davies, J. R., 2018, Global review of human-induced earthquakes: Earth-Science Reviews, v. 178, p. 438-514.

Freed, M. A., 2005, EARTHQUAKE TRIGGERING BY STATIC, DYNAMIC, AND POSTSEISMIC STRESS TRANSFER: Annual Review of Earth and Planetary Sciences, v. 33, no. 1, p. 335-367.

Frohlich, C., Deshon, H., Stump, B., Hayward, C., Hornbach, M., and Walter, I. J., 2016, A Historical Review of Induced Earthquakes in Texas: Seismological Research Letters, v. 87, no. 4, p. 1022-1038.

Gahalaut, K., Tuan, A. T., and Rao, P. N., 2016, Rapid and Delayed Earthquake Triggering by the Song Tranh 2 Reservoir, Vietnam: Bulletin of the Seismological Society of America, v. 106, no. 5, p. 2389-2394.

Gogri, M., 2018, Investigation and real-time monitoring for safe waste-water disposal with a focus on Arbuckle Group, Oklahoma.

Grandin, R., Vallée, M., and Lacassin, R., 2017, Rupture Process of the M_w 5.8 Pawnee, Oklahoma, Earthquake from Sentinel-1 InSAR and Seismological Data: Seismological Research Letters, v. 88, no. 4, p. 994-1004.

Halkia, G., and Ludwig, G. L., 2022, Household earthquake preparedness in Oklahoma: A mixed methods study of selected municipalities: International Journal of Disaster Risk Reduction, v. 73, p. 102872.

Hardebeck, L. J., 2014, The impact of static stress change, dynamic stress change, and the background stress on aftershock focal mechanisms: Journal of Geophysical Research: Solid Earth, v. 119, no. 11, p. 8239-8266.

Hennings, P., and Smye, K. M., 2024, Knowns, questions, and implications of induced seismicity in the Permian Basin AAPG Bulletin, v. 108.

Holloway, S., Holland, A., and Keller, G.R., 2016, Oklahoma fault database contributions from the oil and gas industry: Oklahoma Geological Survey, Open-File Report OF1-2016.

Hong, Z., Moreno, A. H., and Hong, Y., 2018, Spatiotemporal Assessment of Induced Seismicity in Oklahoma: Foreseeable Fewer Earthquakes for Sustainable Oil and Gas Extraction?: Geosciences, v. 8, no. 12, p. 436.

Hough, E. S., and Page, M., 2015, A Century of Induced Earthquakes in Oklahoma?: Bulletin of the Seismological Society of America, v. 105, no. 6, p. 2863-2870.

Inc., T. T., 2025, Selected States Oil, Gas and Injection Wells Maps.

Ito, T., and Zoback, D. M., 2000, Fracture permeability and in situ stress to 7 km depth in the KTB scientific drillhole: Geophysical Research Letters, v. 27, no. 7, p. 1045-1048.

Johnson, K. S., 2008, GEOLOGIC HISTORY OF OKLAHOMA: University of Oklahom.

Jones, L. M., and P. Molnar (1979), Some characteristics of foreshocks and their possible relationship to earthquake prediction and premonitory slip on fault, *J. Geophys. Res.*, **84**, 3596–3608.

Keranen, M. K., Savage, M. H., Abers, A. G., and Cochran, S. E., 2013, Potentially induced earthquakes in Oklahoma, USA: Links between wastewater injection and the 2011 M_w 5.7 earthquake sequence: Geology, v. 41, no. 6, p. 699-702.

Keranen, M. K., Weingarten, M., Abers, A. G., Bekins, A. B., and Ge, S., 2014, Sharp increase in central Oklahoma seismicity since 2008 induced by massive wastewater injection: Science, v. 345, no. 6195, p. 448-451.

Kibikas, W., 2021, Characterizing rock properties and their impact on mechanical behavior of crystalline basement and caprocks.

Kilb, D., Gomberg, J., and Bodin, P., 2002, Aftershock triggering by complete Coulomb stress changes: Journal of Geophysical Research: Solid Earth, v. 107, no. B4, p. ESE 2-1-ESE 2-1.

King, G., Stein, S., and Lin, J., 1995, Static stress changes and the triggering of earthquakes: International Journal of Rock Mechanics and Mining Sciences & Geomechanics Abstracts, v. 32, no. 2, p. A50-A51.

Lippiello, E., Bottiglieri, M., Godano, C., and Arcangelis, D. L., 2007, Dynamical scaling and generalized Omori law: Geophysical Research Letters, v. 34, no. 23, p. n/a-n/a.

Litherland, M., 2023, History of monitoring induced seismicity in New Mexico, Recent Seismicity in the Southern Midcontinent, USA: Scientific, Regulatory, and Industry Responses, p. 43-51.

López-Comino, J. A., & Cesca, S. (2018). Source complexity of an injection induced event: The 2016 M_w 5.1 Fairview, Oklahoma earthquake. *Geophysical Research Letters*, *45*(9), 4025-4032.

Machado, L. G., Hickman, J. G., Gogri, P. M., Marfurt, J. K., Pranter, J. M., and Reza, A. Z., 2019, Characterization of Arbuckle-basement wastewater disposal system, Payne County, Northern Oklahoma: Interpretation, v. 7, no. 4, p. SL19-SL36.

Mavrouli, M., Mavroulis, S., Lekkas, E., and Tsakris, A., 2023, The Impact of Earthquakes on Public Health: A Narrative Review of Infectious Diseases in the Post-Disaster Period Aiming to Disaster Risk Reduction: Microorganisms, v. 11, no. 2, p. 419.

Mcgarr, A., Bekins, B., Burkardt, N., Dewey, J., Earle, P., Ellsworth, W., Ge, S., Hickman, S., Holland, A., Majer, E., Rubinstein, J., and Sheehan, A., 2015, Coping with earthquakes induced by fluid injection: Science, v. 347, no. 6224, p. 830-831.

Mcmahon, D. N., Aster, C. R., Yeck, L. W., Mcnamara, E. D., and Benz, M. H., 2017, Spatiotemporal evolution of the 2011 Prague, Oklahoma, aftershock sequence revealed using subspace detection and relocation: Geophysical Research Letters, v. 44, no. 14, p. 7149-7158.

Miller, A. S., Collettini, C., Chiaraluce, L., Cocco, M., Barchi, M., and Kaus, P. J. B., 2004, Aftershocks driven by a high-pressure CO2 source at depth: Nature, v. 427, no. 6976, p. 724-727.

Moschetti, P. M., Hartzell, H. S., and Herrmann, B. R., 2019, Rupture Model of the M5.8 Pawnee, Oklahoma, Earthquake From Regional and Teleseismic Waveforms: Geophysical Research Letters, v. 46, no. 5, p. 2494-2502.

Nandan, S., Ouillon, G., and Sornette, D., 2022, Are Large Earthquakes Preferentially Triggered by Other Large Events?: Journal of Geophysical Research: Solid Earth, v. 127, no. 8.

Norbeck, H. J., and Horne, N. R., 2016, Evidence for a transient hydromechanical and frictional faulting response during the 2011 M_w 5.6 Prague, Oklahoma

earthquake sequence: Journal of Geophysical Research: Solid Earth, v. 121, no. 12, p. 8688-8705.
Norris, Q. J., Turcotte, L. D., Moores, M. E., Brodsky, E. E., and Rundle, B. J., 2016, Fracking in Tight Shales: What Is It, What Does It Accomplish, and What Are Its Consequences?: Annual Review of Earth and Planetary Sciences, v. 44, no. 1, p. 321-351.
Nur, A., and Booker, R. J., 1972, Aftershocks Caused by Pore Fluid Flow?: Science, v. 175, no. 4024, p. 885-887.
Okada, Y., 1992, Internal deformation due to shear and tensile faults in a half-space: *Bulletin of the Seismological Society of America*, v. 82, p. 1018–1040.
Omori, F., 1894, One the Aftershocks of Earthquakes: Journal of the College of Science.
Papavasileiou, S., 2024, Drained Settlement Vs. Consolidation: Differences at Failure in Output, Bentley Communities.
Park, Y., Beroza, C. G., and Ellsworth, L. W., 2022, Basement Fault Activation before Larger Earthquakes in Oklahoma and Kansas: The Seismic Record, v. 2, no. 3, p. 197-206.
Peikert, J., Hampel, A., and Bagge, M., 2024, Three-dimensional finite-element modeling of Coulomb stress changes on normal and thrust faults caused by pore fluid pressure changes and postseismic viscoelastic relaxation: Geosphere, v. 20, no. 1, p. 105-128.
Peng, Z., Vidale, J.E., Ishii, M., and Helmstetter, A., 2007, Seismicity rate immediately before and after main shock rupture from high-frequency waveforms in Japan: Journal of Geophysical Research—Solid Earth, v. 112, B3, https://doi.org/10.1029/2006JB004386.
Pennington, C., 2017, INVESTIGATION OF FAULTING PROCESSES OF TWO M5 EARTHQUAKE SEQUENCES IN OKLAHOMA: University of Oklahoma.
Pennington, C., and Chen, X., 2017, Coulomb Stress Interactions during the M_w 5.8 Pawnee Sequence: Seismological Research Letters, v. 88, no. 4, p. 1024-1031.
Pickett, A., 2018, Oil and Gas Reporter, New Play Concept 'Merges' SCOOP and STACK Trends in Red-Hot Central Oklahoma.
Program, E. H., Earthquake Magnitude, Energy Release, and Shaking Intensity.
Qin, Y., Chen, X., Carpenter, M. B., and Kolawole, F., 2018, Coulomb Stress Transfer Influences Fault Reactivation in Areas of Wastewater Injection: Geophysical Research Letters, v. 45, no. 20.
Rudnicki, W. J., and Rice, R. J., 2006, Effective normal stress alteration due to pore pressure changes induced by dynamic slip propagation on a plane between dissimilar materials: Journal of Geophysical Research: Solid Earth, v. 111, no. B10.
Ryder, P. D., 1996, **GROUND WATER ATLAS of the UNITED STATES**, Hydrologic atlas 730-E, Volume 2025, United States Geological Survey.
Salazar Florez, D., 2023, Application of seismic attributes and unsupervised machine learning methods for identification of hidden faults in basement and carbonate rocks: University of Oklahoma.
Schulte, K., 2022, Fundamentals of Geology, LibreTexts.
Skoumal, J. R., Barbour, J. A., Brudzinski, R. M., Langenkamp, T., and Kaven, O. J., 2020, Induced Seismicity in the Delaware Basin, Texas: Journal of Geophysical Research: Solid Earth, v. 125, no. 1.
Skoumal, J. R., Barbour, J. A., Rubinstein, L. J., and Glasgow, E. M., 2024, Reduced Injection Rates and Shallower Depths Mitigated Induced Seismicity in Oklahoma: The Seismic Record, v. 4, no. 4, p. 279-287.

Skoumal, J. R., and Trugman, T. D., 2021, The Proliferation of Induced Seismicity in the Permian Basin, Texas: Journal of Geophysical Research: Solid Earth, v. 126, no. 6.
Smye, M. K., Ge, J., Calle, A., Morris, A., Horne, A. E., Eastwood, L. R., Darvari, R., Nicot, P. J., and Hennings, P., 2024, Role of Deep Fluid Injection in Induced Seismicity in the Delaware Basin, West Texas and Southeast New Mexico: Geochemistry, Geophysics, Geosystems, v. 25, no. 6.
Stein, S., and Wysession, M., 2003, *An Introduction to Seismology, Earthquakes, and Earth Structure*: Malden, Massachusetts, Blackwell Publishing, 498 p.
Stein, S. R., 1999, The role of stress transfer in earthquake occurrence: Nature, v. 402, no. 6762, p. 605-609.
Suckale, J., 2009, Induced Seismicity in Hydrocarbon Fields, Advances in Geophysics, p. 55-106.
Sumy, F. D., Cochran, S. E., Keranen, M. K., Wei, M., and Abers, A. G., 2014, Observations of static Coulomb stress triggering of the November 2011M5.7 Oklahoma earthquake sequence: Journal of Geophysical Research: Solid Earth, v. 119, no. 3, p. 1904-1923.
Survey, U. S. G., 1986, Geohydrology of the Vamoosa-Ada aquifer east-central Oklahoma with a section on chemical quality of water, Volume 2025.
-, 2011, M 5.7 - 8 km NW of Prague, Oklahoma, Volume 2025, USGS.
-, 2016, M 5.8 - 14 km NW of Pawnee, Oklahoma, Moment Tensor, Volume 2025, USGS.
-, 2017, Oklahoma experiences largest earthquake during ongoing regional wastewater injection hazard mitigation efforts, Volume 2025, USGS.
-, 2024, M 5.1 - 8 km NW of Prague, Oklahoma, Volume 2025, USGS.
Survey, U. S. G., 2025, The Science of Earthquakes.
Toda, S., Stein, R. S., Sevilgen, V., and Lin, J., 2011a, Coulomb 3.3 Graphic-Rich Deformation and Stress-Change Software for Earthquake, Tectonic, and Volcano Research and Teaching—User Guide, Volume 2025, USGS.
Toda, S., Stein, S. R., Sevilgen, V., and Lin, J., 2011b, Coulomb 3.3 Graphic-rich deformation and stress-change software for earthquake, tectonic, and volcano research and teaching-user guide, Open-File Report.
Townend, J., and Zoback, M., 2000, How Faulting Keeping the Crust Strong.
Utsu, T., Ogata, Y., and Matsu'ura, R.S., 1995, The centenary of the Omori formula for a decay law of aftershock activity: Journal of Physics of the Earth, v. 43, p. 1–33.
Walsh, R. F., and Zoback, D. M., 2015, Oklahoma's recent earthquakes and saltwater disposal: Science Advances, v. 1, no. 5, p. e1500195.
Walter, I. J., Chang, C. J., and Dotray, J. P., 2017, Foreshock Seismicity Suggests Gradual Differential Stress Increase in the Months Prior to the 3 September 2016 M_w 5.8 Pawnee Earthquake: Seismological Research Letters, v. 88, no. 4, p. 1032-1039.
Walter, I. J., Ogwari, P., Thiel, A., Ferrer, F., Woelfel, I., Chang, C. J., Darold, P. A., and Holland, A. A., 2020, The Oklahoma Geological Survey Statewide Seismic Network: Seismological Research Letters, v. 91, no. 2A, p. 611-621.
Wang, T., Zhang, D.-L., Yang, X.-Y., Xu, J.-Q., Matthew, C., and Tang, Y.-J., 2020, RETRACTED ARTICLE: Light hydrocarbon geochemistry: insight into oils/condensates families and inferred source rocks of the Woodford–Mississippian tight oil play in North-Central Oklahoma, USA: Petroleum Science, v. 17, no. 3, p. 582-597.
Weingarten, M., Ge, S., Godt, W. J., Bekins, A. B., and Rubinstein, L. J., 2015, High-rate injection is associated with the increase in U.S. mid-continent seismicity: Science, v. 348, no. 6241, p. 1336-1340.

White, A. J., and Foxall, W., 2016, Assessing induced seismicity risk at CO2 storage projects: Recent progress and remaining challenges: International Journal of Greenhouse Gas Control, v. 49, p. 413-424.
Witze, A., 2017, Risk of human-triggered earthquakes laid out in biggest-ever database: Nature.
Woo, S., 2020, Reliability Design of Mechanical Systems.
World, T., 2019, Oklahoma earthquakes decrease for 3rd straight year.
Yeck, W. L., Weingarten, M., Benz, H. M., McNamara, D. E., Bergman, E. A., Herrmann, R. B., ... & Earle, P. S. (2016). Far-field pressurization likely caused one of the largest injection induced earthquakes by reactivating a large preexisting basement fault structure. *Geophysical Research Letters*, *43*(19), 10-198.

Ye, Z., and Ghassemi, A., 2020, Heterogeneous Fracture Slip and Aseismic-Seismic Transition in a Triaxial Injection Test: Geophysical Research Letters, v. 47, no. 14.
Zavyalov, A., Zotov, O., Guglielmi, A., and Klain, B., 2022, On the Omori Law in the Physics of Earthquakes: Applied Sciences, v. 12, no. 19, p. 9965.
Zhang, Y., Feng, W., Xu, L., Zhou, C., and Chen, Y., 2009, Spatio-temporal rupture process of the 2008 great Wenchuan earthquake: Science in China Series D: Earth Sciences, v. 52, no. 2, p. 145-154.
Zhang, Z., Liu, M., Tan, J. Y., Walter, F., He, S., Chmiel, M., and Su, J., 2024, Landslide hazard cascades can trigger earthquakes: Nature Communications, v. 15, no. 1.
Zhao, J., Feng, X.-T., Zhang, X.-W., Zhang, Y., Zhou, Y.-Y., and Yang, C.-X., 2018, Brittle-ductile transition and failure mechanism of Jinping marble under true triaxial compression: Engineering Geology, v. 232, p. 160-170.
Zhu, S., and Miao, M., 2015, How Did the 2013 Lushan Earthquake (Ms = 7.0) Trigger its Aftershocks? Insights from Static Coulomb Stress Change Calculations: Pure and Applied Geophysics, v. 172, no. 10, p. 2481-2494.

Zoback, M. D., Apel, R., Baumgärtner, J., Brudy, M., Emmermann, R., Engeser, B., ... & Vernik, L. (1993). Upper-crustal strength inferred from stress measurements to 6 km depth in the KTB borehole. *Nature*, *365*(6447), 633-635.